Dissolution Technologies

www.dissolutiontech.com Volume 32, Issue 1 | February 2025

6 **Characterization of Apex Vessel Geometries and Irregularities**
Satish Perivillia and Mark R. Liddell

20 **Development of a Physiologically Relevant Simulated Nasal Fluid for In Vitro Dissolution Studies**
Shengnan Zhao, Tyson S. Le, Neal M. Davies, and Raimar Löbenberg

32 **Investigation of Dissolution Failures of Metformin Delayed-Release Tablets During Formulation Design**
Anumol Joseph, Sideequl Akbar Thencheeri, Rajkumar Malayandi, Subramanian Natesan, and Ravichandiran Velayutham

42 **Hypothetical Plasma Concentration-Time Profiles of Amiodarone-HCl From In Vitro Release Data**
José Raúl Medina-López and Felipe Dino Reyes-Ramírez

50 **Question & Answer Section**
Margareth Marques and Mark Liddell

JetX —
Automated
Sample Preparation.
sotax
Traditional
Sample Preparation
is slow. Complicated.
And expensive.
It is time
for a change.
JetX™
Coming in
March 2025.
Solutions for Pharmaceutical Testing
sotax.com/jetX

Table of Contents

In This Issue

Characterization of Apex Vessel Geometries and Irregularities 6

Development of a Physiologically Relevant Simulated Nasal Fluid for In Vitro Dissolution Studies .. 20

Investigation of Dissolution Failures of Metformin Delayed-Release Tablets During Formulation Design ... 32

Hypothetical Plasma Concentration-Time Profiles of Amiodarone-HCl From In Vitro Release Data 42

Question and Answer Section 50

Calendar of Events 52

Industry News 55

Advertisers

Sotax ..... Inside front cover
Hanson/Teledyne 5
Copley 19
Erweka 41
Pharma Test 47
Fourth Edition Handbook 48
USP 49
EAS 54
Distek ..... Back inside cover
Agilent Technologies ..... Back outside cover

To Submit Articles

Please check the website for instructions, the articles are peer-reviewed and are submitted through the PeerTrack™ website, https://www.editorialmanager.com/dt.

The scope of articles is limited to dissolution or disintegration topics as the major focus. Articles on formulation development where dissolution is just one test of many should not be submitted.

For inquiries and prescreening, e-mail vagray@rcn.com

***Dissolution Technologies* is indexed in:**

Science Citation Index Expanded®
Journal Citation Reports®/ Science Edition
International Pharmaceutical Abstracts
Chemical Abstracts (CAS)
SCOPUS
EMBASE
CrossRef
Google Scholar

Topics for the Next Issue

The May 2025 issue will include research articles on the apex vessel, mebendazole suspensions, dose dumping, IVIVC and accelerated dissolution method for antibiotics; highlights from the AAPS annual meeting; and the Q and A feature.

Research Editor
Vivian Gray
vagray@rcn.com

Dissolution Technologies Editorial Advisory Board

The Editorial Advisory Board of *Dissolution Technologies* is a distinguished group of scientists active in fields and/or organizations related to dissolution testing. Members of the board review manuscripts and suggest subject matters relevant to dissolution testing.

Cynthia K. Brown
Founder

William Brown
Retired

Robert G. Buice, Ph.D.
Buice & Associates, LLC

Bryan Crist
DissoAssist Consulting

Jennifer B. Dressman, Ph.D.
Fraunhofer Institute of Translational Medicine and Pharmacology

Nikoletta Fotaki, Ph.D.
University of Bath, Bath, UK

Vivian A. Gray
V. A. Gray Consulting, Inc.

Sandra Klein, Ph.D.
Ernst Moritz Arndt University of Greifswald

Johannes Krämer, Ph.D.
DISSO GmbH

Raimar Löbenberg, Ph.D.
University of Alberta

Petra Loos, Ph.D.
Sanofi-Aventis

Xujin Lu, Ph.D.
Pharmaceutical Consultant

Margareth R. C. Marques, Ph.D.
USP

Gregory P. Martin
Complectors Consulting LLC

John W. Mauger, Ph.D.
University of Utah

Aleksander Mendyk, Ph.D.
Jagiellonian University - Medical College, Cracow, Poland

Rakesh P. Patel, Ph.D.
Ganpat University, Gujarat, India

James E. Polli, Ph.D.
University of Maryland

Brian R. Rohrs, Ph.D.
Bausch & Lomb

Thomas W. Rosanske, Ph.D.
Pharmaceutical Consultant

Alger Salt, MS
Pharmaceutical Consultant

Peter Scott
Dissolution Solutions

Vinod P. Shah, Ph.D.
Pharmaceutical Consultant

David C. Sperry, Ph.D.
Eli Lilly and Company

Erika Stippler, Ph.D.
EDQM

Roderick B. Walker, Ph.D.
Rhodes University, Grahamstown, South Africa

Publisher's Information

PURPOSE: *Dissolution Technologies* is a peer-reviewed quarterly publication reporting current information on dissolution testing. It provides an international forum for open exchange of information on various dissolution topics.

CORRESPONDENCE: Send all correspondence to: *Dissolution Technologies*, Inc., 9 Yorkridge Trail, Hockessin, DE 19707. Phone (302) 235-0621, e-mail: vagray@rcn.com. Website: www.dissolutiontech.com (SSL certified).

STAFF: Founder, Cynthia Brown; Managing Director, Vivian Gray; Associate Editor, Valerie Clark; Research Editor, Vivian Gray; Research Editor, William Brown; Communications, Michael Larson; Circulation Manager, Sandra Larson; Layout, Michele Arnold; Publication, Printing, and Distribution Services, Archer Print Group, Sellersville, Pennsylvania.

All articles represent the view of the authors and not necessarily those of *Dissolution Technologies*. Advertising content does not signify endorsement of products or services by *Dissolution Technologies*. Unless otherwise specified, letters sent to *Dissolution Technologies* are assumed for publication. Copyright 2025 by Dissolution Technologies, Inc. All rights reserved.

ISSN 1521-298X

Dissolution Technologies is indexed in:
Science Citation Index Expanded®
Journal Citation Reports®/ Science Edition
International Pharmaceutical Abstracts
Chemical Abstracts (CAS)
SCOPUS
EMBASE
CrossRef
Google Scholar

Go Configure

Easily find the perfect solution to your Dissolution or Diffusion testing needs with our online, interactive configurators. Answer a few targeted questions to quickly discover the Hanson brand system of your dreams and receive a price quote fast.

First in design, first in performance, first in service.
That's Teledyne LABS.

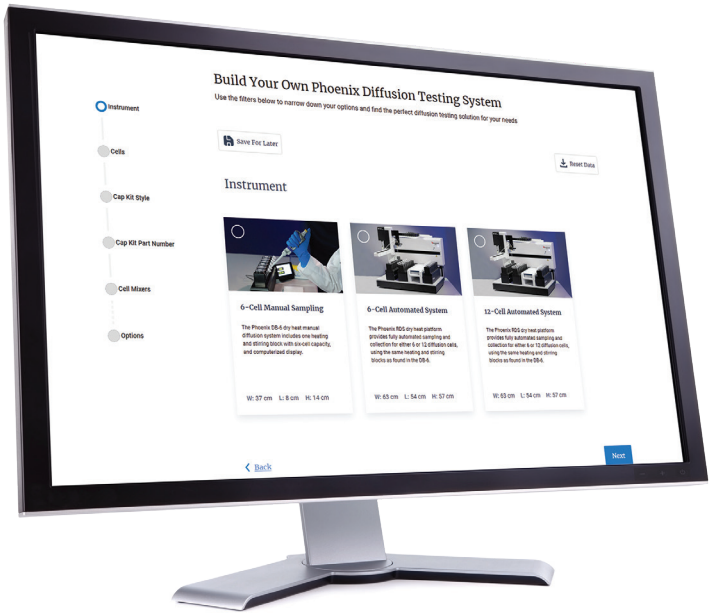

https://diffusion-configurator.teledynehanson.com/

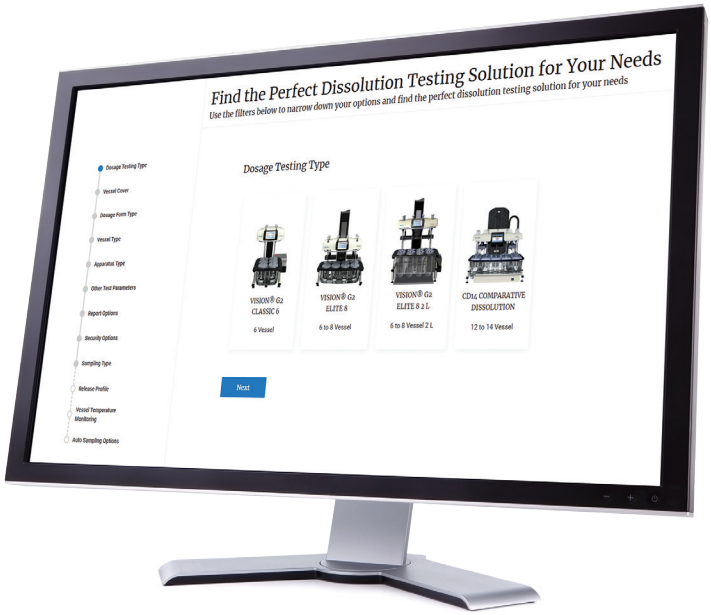

https://dissolution-configurator.teledynehanson.com/

TELEDYNE | Teledyne LABS

teledynelabs.com

dx.doi.org/10.14227/DT320125P6

Reprinted with permission. © 2025 The United States Pharmacopeial Convention. All rights reserved.

STIMULI TO THE REVISION PROCESS

Stimuli articles do not necessarily reflect the policies of the USPC or the USP Council of Experts

Characterization of Apex Vessel Geometries and Irregularities

Satish Perivilli[1] and Mark R. Liddell[1]
[1]*United States Pharmacopeia, 12601 Twinbrook Parkway, Rockville, MD, USA.*

Correspondence should be addressed to:
Margareth R.C. Marques, Senior Principal Scientist
US Pharmacopeia
12601 Twinbrook Parkway
Rockville, MD 20852-1790
email: mrm@usp.org

This article was originally published as a stimuli article in issue 51(1) of the United States Pharmacopeia's (USP) *Pharmacopeial Forum* (PF). PF is a free bimonthly online journal in which USP publishes items for public review and comment. The commenting period for this stimuli article in PF is open until March 31, 2025. Please visit the following website to comment on the stimuli article: https://doi.org/10.31003/USPNF_S203304_10101_01. All other correspondence on this article should be addressed to Margareth R. C. Marques as noted above.

ABSTRACT

Apex vessels, previously referred to as PEAK vessels, are commonly used in dissolution experiments with Apparatus 2. They are mentioned in *The Dissolution Procedure: Development and Validation* <1092> for their utility in the possible elimination of coning associated with using standard vessels. A *Stimuli* article, *The Case for Apex Vessels*, discussing the benefits of including apex vessels in *USP–NF* general chapters was published in *PF* 47(6) (Nov–Dec 2021). The objective of the study discussed in the new Stimuli article below was to characterize apex vessels, available from different manufacturers, more comprehensively with the objective of understanding their geometries and associated variabilities. A coordinate measuring machine (CMM) was used to evaluate 37 selected characterization parameters associated with the apex vessel geometries and inherent geometric irregularities. Six vessels, each from seven manufacturers, were characterized. Measurement data was analyzed using skewness plots and statistical tools to understand the variability in all parameters considered. Upon analysis, the apex characterization parameters were found to exhibit intra- and inter-manufacturer variability, indicating variability in the geometries of apex vessels available commercially. Measurements of the geometric irregularities associated with the apexes also presented similar variability across all vessels considered. Results from this study indicate that end-users of apex vessels should be aware of the variabilities in commercially available vessels and should consider controlling the source of apex vessels used with dissolution testing.

INTRODUCTION

Apex vessels are noncompendial glass vessels typically used with *Dissolution* <711> Apparatus 2. There are currently several manufacturers of apex vessels. *The Dissolution Procedure: Development and Validation* <1092> mentions the utility of using apex vessels to possibly eliminate coning usually observed towards the lowest point of the vessel bottom (directly underneath the rotating paddle) with a disintegrating dosage form. A *Stimuli* article, *The Case for Apex Vessels*, discussing the benefits of including apex vessels in *USP–NF* general chapters was published in *PF* 47(6) (Nov–Dec 2021). The article proposed the apex height, the apex external angle, and the deviation of the apex from the vessel centerline as three possible parameter choices for providing specifications specific to apex vessels. While these can be useful, many other geometric parameters characterize the vessels and can thus be used for a similar purpose. Hence, it was of substantial interest to gain a comprehensive understanding of the ranges and variabilities in measurements of these (i.e., both proposed and additional) parameters and associated geometric irregularities. For this purpose, five sets of six vessels each were procured on loan (or as donations) from the

different manufacturers who provided vessels for the *2021 Stimuli article*, namely Agilent, Distek, Erweka, Hanson, and Sotax. Additionally, two sets of apex vessels purchased previously from Quality Lab Accessories and Vankel were also included in the study.

A review of available literature indicates that apex (previously known as PEAK) vessels have been an area of substantial interest over the past several years. Studies that focused on the comparison of dissolution results obtained while using PEAK and standard vessels are readily available. For example, an early study by Beckett et al. (*1*) showed that the effect of deaeration on dissolution was not as marked as with standard vessels when PEAK vessels were used by comparing the dissolution behaviors of FDA Prednisone NCDA#2 10 mg, USP Prednisone Calibrator 50 mg, and USP Salicylic Acid Calibrator 300 mg tablets. Similar outcomes were also exemplified with changes to the paddle rotational speed for the first two formulations. Collins and Nair (*2*), in another study, compared the dissolution results of acetaminophen and naproxen sodium tablets at four different paddle rotation speeds with three different dissolution media under deaerated and nondeaerated conditions. For acetaminophen, at the lowest rpm investigated, it was shown that a substantially higher percentage (about 100%) of the drug was released while using PEAK vessels in about half the time (15 min) compared to about 55% in 30 min with standard vessels using Apparatus 2. Higher rpm results indicated faster rates of dissolution with PEAK vessels initially, even though the release profiles showed no difference with standard vessels towards later time points. Naproxen tablets, on the other hand, were shown to have relatively similar release rates throughout the runs, with both vessels at the lowest rpm. However, increasing rpm indicated faster dissolution rates initially with the PEAK vessels with the differences decreasing with time. Rotational speed and deaeration were found to influence dissolution results with both vessels.

Mirza et al. (*3*) compared the percentage of releases with both a “low solubility drug” and a “high solubility drug” while using standard, PEAK and flat-bottom vessels. It was shown that the PEAK vessels generated the highest percent release for both drugs. Furthermore, Baxter et al. (*4*) conducted flow visualization studies and ran computational fluid dynamics (CFD) simulations to understand the hydrodynamics associated with PEAK vessels. It was shown that a dosage form would be subjected to only high shear rates with PEAK vessels as opposed to low shear rates surrounded by higher shear rates with standard vessels. In a more recent article, Yoshida et al. (*5*) investigated the effects of using five different apex vessels with varying apex diameters and heights (and, in the case of the fifth vessel, with a 3-mm offset of the apex from the center axis) on the dissolution profiles of disintegrating tablets (USP Prednisone Tablet RS, lot No. R132B0 and amlodipine besylate tablets), sticking tablets (atorvastatin calcium hydrate tablets 10 mg), and large volume excipient formulations (levofloxacin fine granules 10%) and compared them with data using standard vessels. It should be noted that three of the vessels were custom-made for the study and are not available commercially. Dissolution profiles were evaluated for similarity using the FDA guidelines' similarity factor, f_2. It was shown that the dissolution behavior of the disintegrating and sticking tablets obtained with vessels with high apexes (with the paddle rotating at 50 rpm) was similar to that of using compendial vessels at 75 rpm. The apex centering was shown to have no effect on the dissolution of prednisone tablets and levofloxacin formulation at varying paddle rotation speeds from 30 to 100 rpm. All formulations, in general, were shown to dissolve faster at 50 rpm with the apex vessels in comparison to standard vessels. The effect on the "mount" at the bottom of the apex vessels was found to vary with formulation.

Even with the availability of dissolution results that show *improved* performance with apex vessels, such as from some studies mentioned above, there is still a lack of comprehensive understanding of the vessels themselves. Some of the key missing pieces of information include knowledge of geometric variabilities in commercially available apex vessels, the influence of any inherent variabilities on the resultant hydrodynamics and/or associated dissolution results, a standardized procedure for mechanical calibration and/or a performance verification test (PVT), etc. Some of these concerns have been highlighted in expert reviews/perspectives published previously. For example, Gray et al. (*6*), in their expert review, while acknowledging some of the aforementioned work and the impact on dissolution data of changing vessel geometries (such as with apex vessels), suggested caution in balancing the overall objectives of the test itself (for example, its discriminating capability) with changes to dissolution rate and variance. In another perspective article, Grady et al. (*7*) pointed out the limitations of using PEAK vessels: their noncompendial status and nonexistence of a “mechanical calibration procedure”. Additionally, Baxter et al. (*4*) also indicated that the high shear rates observed around the dosage form might affect the discriminating ability of the apparatus. Concerns about sufficient discriminative

ability with the usage of apex vessels were also raised by Yoshida et al. (*5*).

The current study on apex vessel characterization focused on the first piece of missing information, i.e., a complete characterization of apex vessels available commercially with the objective of identifying ranges and variabilities in values of key geometric parameters. The results of this characterization would assist towards anticipated CFD simulation project(s). The CFD projects (parametric studies) would help understand the impact of changing geometries (for example, various apex definitions) on the associated hydrodynamics—the second piece of missing information. Anticipated in-tandem dissolution experiments with various commercially available apex vessels will provide additional insights into understanding apex vessels. Results from the current and planned studies would aid in establishing specifications based on a robust scientific foundation for apex vessel geometries. For this current study, an approach similar to that previously used by Liddell et al. (*8*) for the characterization of standard vessels was followed. Liddell et al. mapped the coordinates of discrete points using a three-dimensional coordinate measuring machine (CMM) and measured several geometric dimensions and irregularities across vessels. Results were analyzed to highlight differences between vessels from not only different manufacturers but also among vessels from the same manufacturer. As with the measurements in Liddell et al., services of Brandywine Metrology Associates, Inc. (BMA; West Chester, Pennsylvania) were retained for performing the CMM measurements for this study too. The seven sets of vessels were shipped to BMA at convenient intervals for data collection. In this article, comparisons of results obtained from the current study were made with those available in the previous publication (*8*) wherever possible.

CHARACTERIZATION PARAMETERS

Several sizing dimensions and irregularities of interest were identified to help characterize apex vessels comprehensively. For this study, the characterization was broken down into three main elements: the vessel geometry (i.e., the geometry that does not include the apex), the apex geometry, and irregularities associated with both the vessel and apex geometries. Basic definitions associated with the geometry of the vessels and the apex—such as diameters, radii, heights, and, as applicable, width, thickness, and angles—are referred to as "sizing parameters" in this article. Other parameters that represent geometric characteristics, such as circularities and perpendicularities associated with both the vessel and apex geometries, are presented as geometric irregularities.

Analysis of the measurements is presented through skewness plots (i.e., plots of raw data categorized by manufacturer) and data tables that show averages of values and standard deviations within a manufacturer set. The tables also include ranges, averages, and standard deviations across all 42 vessels. Additionally, three specific approaches, i.e., evaluations for intra-manufacturer variability (ratio of standard deviation to average values within a manufacturer set of vessels), inter-manufacturer variability (ratio of standard deviation to average values within all 42 vessels), and range variation (change from minimum to maximum values expressed as a relative percentage of the minimum value), were used to quantify and compare differences in the characterization parameters. It should be noted that individual outliers affect the values of the range variation differently than either the intra- or inter-manufacturer variability values.

Sizing Parameters—Vessel Geometry

Cylinder Diameter

The diameter of the cylindrical part of each vessel was measured at five distinct elevations along its height (locations might have differed based on vessel height), as depicted in Figure 1a. At each of the five elevations (i.e., along horizontal planes at locations 1–5), the diameter was calculated as the average of 50 evenly distributed measurement points taken around the circumference of the vessel at that specific elevation. The cylinder diameter, corresponding to each vessel, was determined by averaging values from the 250 points that made up the five locations for that vessel. For the sake of brevity, only data for the cylinder diameter is presented in Figure 2a.

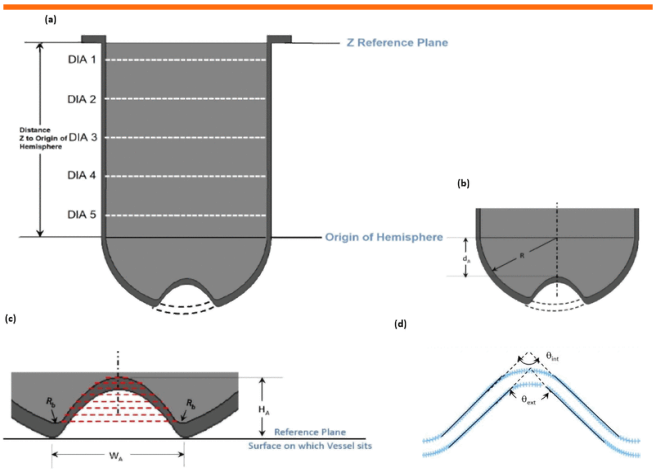

Figure 1. Schematic representations of (a) cylinder diameter locations and cylinder height, (b) hemisphere radius and distance of apex to hemisphere origin, (c) apex diameter locations, height, width, and blend radius and (d) apex internal and external surface angles.

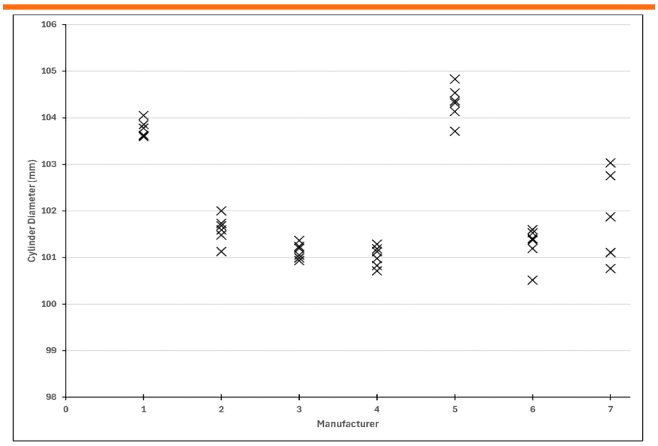

a

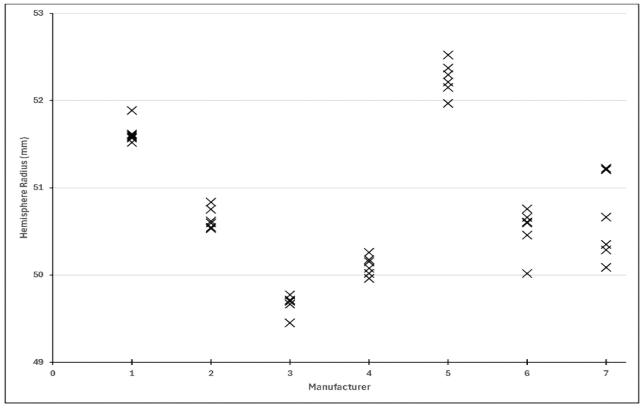

b

*Figure 2. Skewness plots for cylinder diameter (**a**) and hemisphere radius (**b**).*

Hemisphere Radius

The hemisphere radius, denoted by *R* in Figure 1b, was defined to be the average value evaluated from 100 evenly distributed points on the hemisphere's inner surface, i.e., from the top of the hemisphere to the apex transition region. Data for the hemisphere radius is shown in Figure 2b. While the hemisphere radius compares favorably with half of the cylinder diameter values for most manufacturers, data from certain manufacturers indicate slight differences. This observation is important as it indicates that the vessel diameter might not be characterized by a single value (i.e., either the cylinder or hemisphere diameter) for all vessels.

Compiled numerical values for the sizing parameters associated with the vessel geometries are presented in Table 1. Analysis of Table 1 for intra-manufacturer variability of the cylinder diameter shows that the standard deviation, within any manufacturer, was typically < 1% of the associated average value while comparing the data for inter-manufacturer variability (i.e., variability across manufacturers) shows that the standard deviation was about 1.3% of its associated average value. The variation from the minimum cylinder diameter value to its maximum across all 42 vessels considered in this study is limited to only about 4%. Moreover, an examination of the ranges indicates that all values fall well within the specifications of <711> (i.e., 98–106 mm). Thus, it can be reasonably concluded that the cylinder diameters with available apex vessels are well-controlled, and that the specifications provided in <711> are likely sufficient for this parameter. Table 1 also shows that, within each manufacturer, the hemisphere radius by itself is well controlled to be within the specifications of <711>, in that all values were within one-half of the specifications for the diameter of standard vessels, i.e., 98–106 mm.

Vessel Height

The vessel height, H_V, (i.e., the distance between the top of the vessel and the surface on which the vessel sits) can be calculated as:

$$H_V = d_{Z,hs} + d_A + H_A$$

where $d_{Z,hs}$, d_A, and H_A are, respectively, the distance *Z* to the origin of the hemisphere, the distance of the apex to the origin of the hemisphere, and the apex height, as shown in Figure 1a, Figure 1b, and Figure 1c. The distance *Z* to the origin of the hemisphere was determined as the distance between two points — one at the top of the vessel and another point determined to be the center of a theoretical sphere created by the data points taken on the hemisphere.

Data for the vessel height, H_V, across all 42 vessels considered in this study indicates a range of values from approximately 156.106 to 197.944 mm. It should be noted that these values are smaller in comparison to the standard vessel heights specified in <711> due to the apex "cuts" during manufacturing of the apex vessels. The height of the *missing* portion of the vessels, when compared to standard vessels, was limited to as much as 6.8 mm across all 42 vessels considered in the study.

Sizing Parameters—Apex Geometry

Distance of Apex to Hemisphere, Apex Diameters, and Top of Apex Radius

The distance of the apex to the origin of the hemisphere, d_A in Figure 1b, was evaluated to be the distance between two points — one at the top of the apex and another at the theoretical center point of the sphere previously described with the measurements of $d_{Z,hs}$. Measurement values for the distance of the apex to the hemisphere origin are depicted in Figure 3a. These values are indications of the difference between the hemisphere

Table 1. Selected Statistics of Sizing Parameters for Vessel Geometries

Characterization Parameter	Individual Manufacturer (Mfr) Data, Average ± SD							All Vessels	
	Mfr. 1	Mfr. 2	Mfr. 3	Mfr. 4	Mfr. 5	Mfr. 6	Mfr. 7	Range	Average ± SD
Cylinder diameter (mm)	103.750 ± 0.181	101.603 ± 0.290	101.130 ± 0.165	101.020 ± 0.220	104.315 ± 0.379	101.269 ± 0.395	101.772 ± 0.945	100.515–104.831	102.123 ± 1.321
Hemisphere radius, *R* (mm)	51.630 ± 0.130	50.646 ± 0.122	49.668 ± 0.112	50.106 ± 0.110	52.253 ± 0.191	50.516 ± 0.264	50.635 ± 0.485	49.451–52.522	50.779 ± 0.857

radius, presented previously in Figure 1b, and the apex height for each vessel (data of which follow) and thus are a function of both parameters.

Diameters at the apex were evaluated at different elevations, using an approach similar to that used with the cylinder diameter. However, due to the apex curvature, nine locations (instead of five, as with the vessel cylinder) were used to obtain a more detailed description of the apexes. An illustration of the diameter locations or elevations used to characterize the apexes is shown in Figure 1c. Starting with 20 evenly distributed data points at the bottommost location (location 1 for apexes), the number of data points was decreased by one for each subsequent location due to the decreasing diameter of apexes going from bottom to top. The diameter at each location was evaluated as an average value from the associated data points along the circle corresponding to that specific location.

It should be noted that the locations of measurement varied from one manufacturer to another, due to differences in apex heights between manufacturers. However, for consistency, each apex diameter location was separated by 1 mm, and the distance within which all the nine locations fell was retained to be 8 mm across all manufacturer vessels. There was no discrepancy in locations within a single manufacturer's set of vessels. The distribution of apex diameter values at location 1 is shown in Figure 3b.

The top of the apex radius was evaluated from 30 data points and is defined as the radius of curvature at the top of the apex inside the vessel. The center of the apex radius at the top, for this evaluation, was based on the center axis of the apex at the smallest diameter measured at the top of the apex. It was thus assumed that there is only minimal deviation between the actual center at the top of the apex compared to the center obtained from the lowest diameter elevation directly adjacent to the topmost measurements.

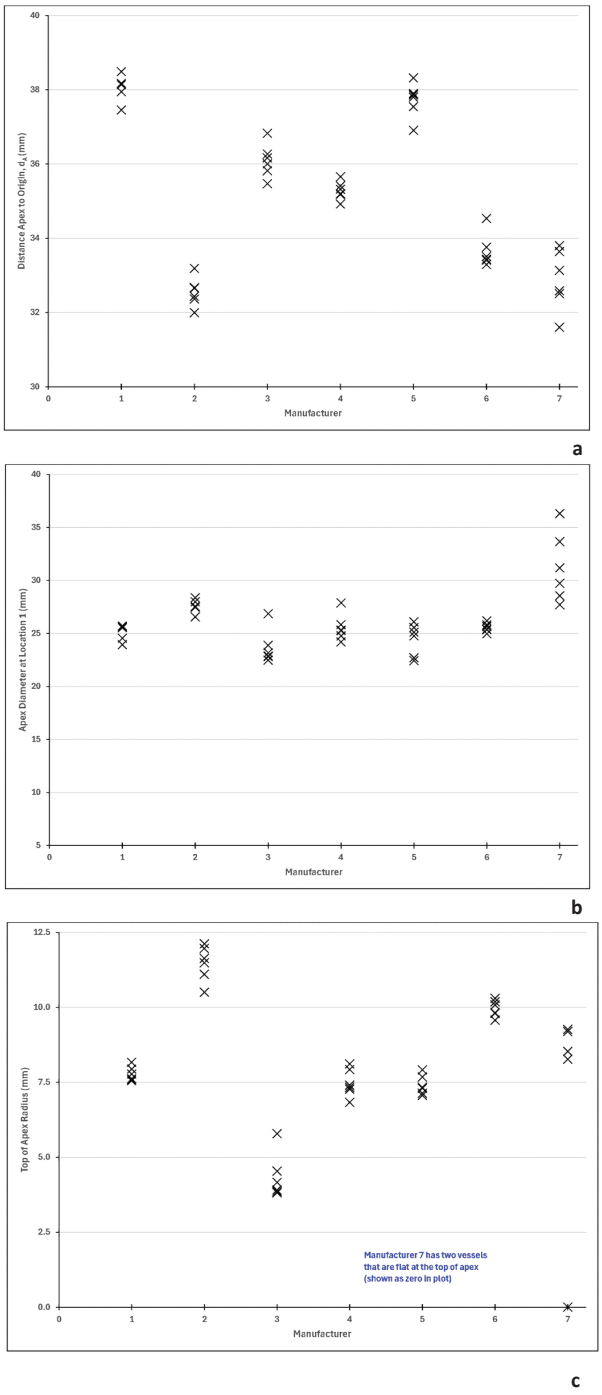

*Figure 3. Skewness plots for apex distance to hemisphere origin (**a**), apex diameters at location 1 (**b**), and top of the apex radius (**c**).*

Data for the top of the apex radius is presented in Figure 3c. As can be seen from the figure, the radius at the top of the apex varied considerably from one manufacturer to another. Additionally, within the manufacturer 7 data, two vessels were observed to have flat surfaces at the top (instead of the usual curved surfaces). These vessels were depicted as having a radius of 0 in the data set. This observation of flat surfaces at the apex top was not associated with vessels from any of the other manufacturers.

Table 2 presents statistical data for the sizing parameters associated with the apex geometries. The intra-manufacturer variability associated with the distance of apex to the hemisphere origin, d_A, varied from 0.70% to 2.49% for each manufacturer considered. When all 42 vessels were considered together, the inter-manufacturer variability was within about 6.11% of the average value. Evaluation of the range in values across all vessels indicated a variation of about 22% when compared to the minimum value measured.

The decrease in apex diameter going from location 1 to location 9 within a vessel is evident from Table 2. Because of the retention of the locations within a manufacturer, an intra-manufacturer variability analysis would be similar to that of any other parameter. An analysis of ranges of intra-manufacturer variability at each location indicated that the lowest and highest values (of 1.64% and 18.41%, respectively) were associated with the bottommost and topmost locations. It should, however, be noted that there was no relationship between the location and maxima or

Table 2. Selected Statistics of Sizing Parameters for Apex Geometries

Characterization Parameter	Individual Manufacturer (Mfr) Data, Average ± SD							All Vessels	
	Mfr. 1	Mfr. 2	Mfr. 3	Mfr. 4	Mfr. 5	Mfr. 6	Mfr. 7	Range	Average ± SD
Distance of apex to hemisphere origin, d_A (mm)	38.063 ± 0.344	32.549 ± 0.397	36.091 ± 0.458	35.280 ± 0.247	37.722 ± 0.472	33.655 ± 0.455	32.879 ± 0.819	31.605–38.489	35.177 ± 2.148
Apex diameter at location 1 (mm)	25.148 ± 0.736	27.571 ± 0.607	23.675 ± 1.629	25.539 ± 1.270	24.440 ± 1.523	25.555 ± 0.419	31.180 ± 3.272	22.427–36.295	26.158 ± 2.796
Apex diameter at location 2 (mm)	22.694 ± 0.685	25.536 ± 0.562	20.686 ± 1.490	23.199 ± 1.111	22.364 ± 1.456	23.527 ± 0.430	27.939 ± 2.494	19.599–32.217	23.706 ± 2.542
Apex diameter at location 3 (mm)	20.646 ± 0.737	23.595 ± 0.548	17.894 ± 1.331	21.099 ± 1.009	20.598 ± 1.433	21.643 ± 0.416	25.007 ± 1.861	16.964–28.453	21.497 ± 2.395
Apex diameter at location 4 (mm)	18.717 ± 0.779	21.711 ± 0.561	15.283 ± 1.084	19.152 ± 0.952	18.910 ± 1.398	19.882 ± 0.407	21.916 ± 1.045	14.272–23.800	19.367 ± 2.257
Apex diameter at location 5 (mm)	16.835 ± 0.804	19.849 ± 0.587	13.033 ± 0.909	17.278 ± 0.936	17.184 ± 1.335	18.192 ± 0.384	19.848 ± 1.211	11.885–22.006	17.460 ± 2.331
Apex diameter at location 6 (mm)	14.957 ± 0.783	17.975 ± 0.610	11.261 ± 0.812	15.395 ± 0.951	15.336 ± 1.240	16.493 ± 0.347	17.528 ± 1.181	10.242–19.260	15.564 ± 2.236
Apex diameter at location 7 (mm)	13.020 ± 0.710	16.014 ± 0.615	9.722 ± 0.732	13.412 ± 0.991	13.282 ± 1.106	14.672 ± 0.304	15.292 ± 1.299	8.915–16.787	13.630 ± 2.090
Apex diameter at location 8 (mm)	10.960 ± 0.634	13.808 ± 0.598	8.084 ± 0.654	11.211 ± 1.071	10.907 ± 0.942	12.515 ± 0.262	13.465 ± 1.462	7.465–15.030	11.564 ± 1.992
Apex diameter at location 9 (mm)	8.610 ± 0.637	11.052 ± 0.590	6.039 ± 0.550	8.552 ± 1.302	7.997 ± 0.734	9.649 ± 0.207	10.326 ± 1.901	5.587–12.586	8.889 ± 1.803
Top of apex radius (mm)	7.773 ± 0.240	11.467 ± 0.593	4.343 ± 0.756	7.479 ± 0.465	7.401 ± 0.328	9.957 ± 0.277	8.813 ± 0.491	3.816–12.117	8.144 ± 2.201
Apex height, H_A (mm)	13.298 ± 0.639	15.430 ± 0.509	13.250 ± 0.155	14.335 ± 0.380	15.023 ± 0.431	15.269 ± 0.250	13.640 ± 0.781	12.293–15.802	14.321 ± 0.989
Apex width, W_A (mm)	32.853 ± 0.721	39.417 ± 0.499	31.887 ± 1.049	35.138 ± 0.070	33.867 ± 1.022	35.890 ± 1.297	42.489 ± 3.886	30.125–47.222	35.934 ± 3.869
Apex thickness (mm)	2.133 ± 0.273	2.763 ± 0.344	2.006 ± 0.301	2.374 ± 0.186	3.230 ± 0.228	2.825 ± 0.103	1.820 ± 0.355	1.420–3.486	2.450 ± 0.537
Apex internal angle, θ_{int} (°)	88.138 ± 2.266	90.972 ± 4.385	93.466 ± 5.647	87.509 ± 1.338	91.935 ± 1.224	92.822 ± 0.743	99.001 ± 6.831	83.422–107.671	91.978 ± 5.089
Apex external angle, θ_{ext} (°)	90.041 ± 1.261	92.776 ± 1.466	84.842 ± 6.248	93.912 ± 1.912	90.079 ± 1.000	88.305 ± 1.322	99.767 ± 6.715	75.087–108.058	91.389 ± 5.582
Blend radius, R_b (mm)	5.616 ± 0.933	6.246 ± 0.357	5.952 ± 0.552	4.411 ± 0.136	5.527 ± 0.290	4.897 ± 0.740	6.320 ± 1.028	4.012–7.672	5.567 ± 0.895

minima of the variabilities, i.e., the intra-manufacturer variabilities did not change in any particular order with the location.

An inter-manufacturer variability analysis was also performed because the locations were at similar relative positions across all manufacturers. The variabilities increased from 10.69% to 20.29% from location 1 to location 9, progressively, in that order. This indicates that measurements are closer to each other towards the bottom of the apex (i.e., location 1) than towards the top (i.e., location 9). This increasing variability is also shown in how the location maxima varied with the associated minima. The maxima were found to be from 61.8% to 125% of the corresponding minima for locations 1 through 9. Whether this is because of the geometry of the apex (and the associated variability in the manufacturing process) or the decreasing resolution in measurement points (with the number of measurement points decreasing by 1 with each changing location) is a point of consideration. Regardless, and especially because the number of measurement points at each location was dictated by the available geometry (i.e., region), it can be concluded that apex geometries are not well controlled from one manufacturer to another or even within a single manufacturer's set of vessels.

Apex Height, Width, Thickness, and Blend Radii

Representations for the height and width of the apex and blend radius are shown in Figure 1c. The apex height, H_A, was evaluated as the perpendicular distance from a point at the top of the apex to the horizontal surface along which the vessels rest. The horizontal distance between the two points on which the vessels sat was defined to be the apex width, W_A. The apex thickness was evaluated as a least squares fit gap based on 100 data points each on the cross-sections of the internal and external surfaces of the apex through a selected axis. The blend radius, R_b, was also evaluated as a least squares fit value based on 30 points around the blend collected on the internal surface of the hemisphere of the vessel.

Data corresponding to the apex height, width, and thickness are presented in Figure 4a, Figure 4b, and Figure 4c, while that associated with the blend radii of

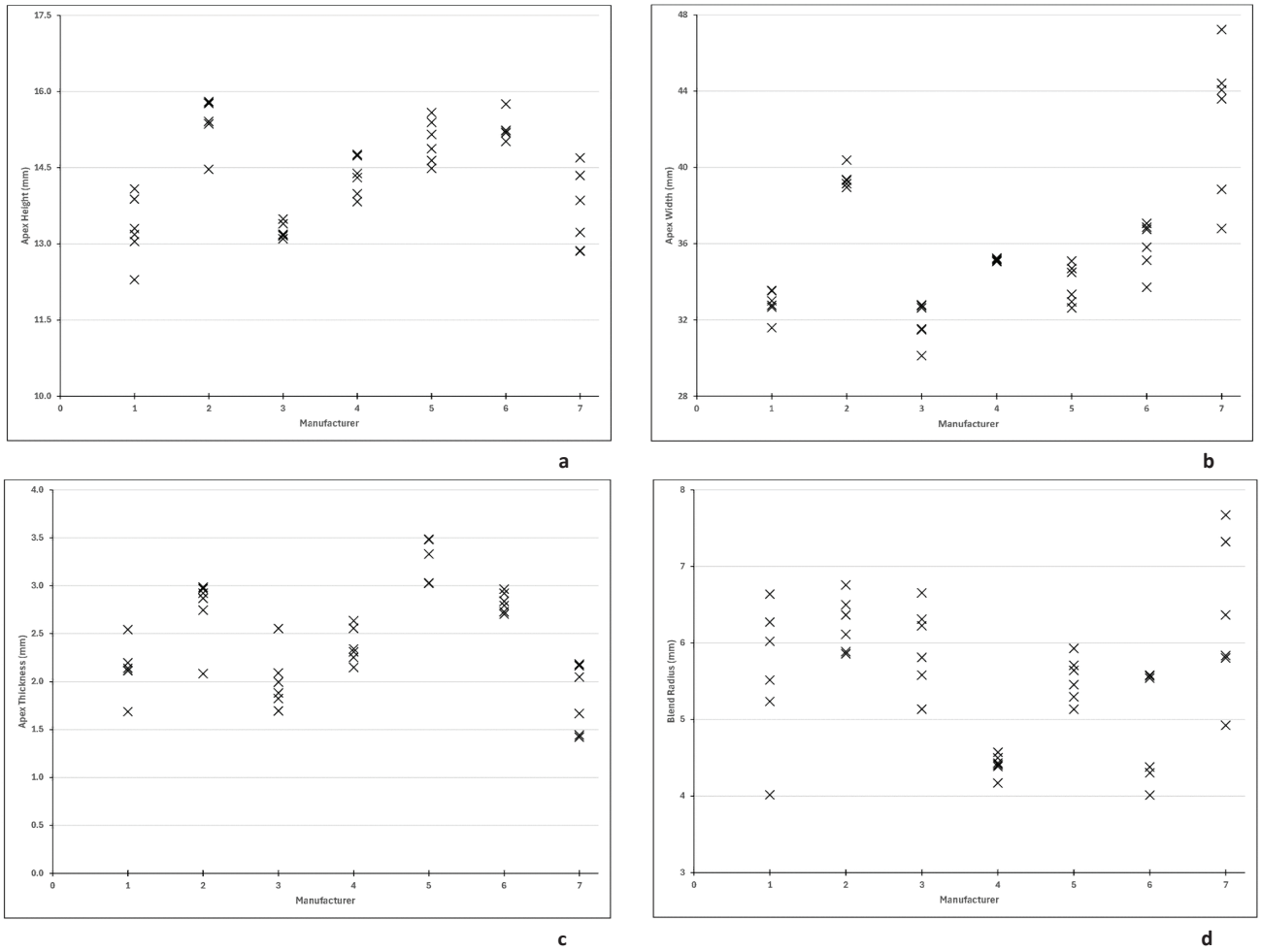

*Figure 4. Skewness plots for apex height (**a**), apex width (**b**), apex thickness (**c**), and blend radius (**d**).*

the apexes to the adjoining hemispherical parts of the vessels is shown in Figure 4d. Possibly due to the difficulty of standardizing the manufacturing process associated with the apex, considerable intra- and inter-manufacturer variabilities were observed in these values (most notably with the blend radius data).

The apex height is one of the parameters whose specifications were proposed in the 2021 *Stimuli* article as a means of characterizing the apex vessels. The article proposed 15 ± 2.5 mm as possible specifications for this measurement. Analysis of the measurements taken for this study indicates that the values range from 12.293 to 15.802 mm, as shown in Table 2. Thus, the proposed specifications in the 2021 *Stimuli* article do not encompass data from all of the vessels evaluated and, therefore, may need to be modified. Additionally, the intra-manufacturer variability associated with the apex height ranged from 1.17% to 5.72%, while the inter-manufacturer variability was 6.91%. The variation from the minimum value observed across all vessels was 29%.

The intra-manufacturer variabilities associated with apex width and apex thickness were observed to be from 0.199% to 9.15% and from 3.66% to 19.5%, respectively. The corresponding inter-manufacturer variabilities were found to be 10.77% and 21.91%. The ranges also show considerable variability in measurements of these values across manufacturers. This might imply that in some dissolution equipment, specifically where the vertical position of the paddle-shaft assembly is fixed, any variability in apex height will also be reflected as variability of distance between the bottom of the paddle and the top of the apex. The impact that the variability in this distance may have on dissolution requires further investigation.

Apex Internal and External Surface Angles

To determine the internal and external surface angles shown in Figure 1d, 60 data points that best fit a straight line along the curvature of the apex on one side of a central axis of the apex were used. The central axis was derived from the 144 data points corresponding to the nine apex diameter locations described above. The angle between the axis and the best-fit lines created from the 60 data points was measured. Doubling the measured angle resulted in the total apex angle. This approach was adopted for both the apex internal surface angles and the external surface angles. Skewness plots associated with the apex internal and external angles are shown in Figure 5a and Figure 5b. As with the other parameters associated with the apex, data for both internal and external angles showed high intra- and inter-manufacturer variabilities.

The 2021 *Stimuli* article provides a specification for the apex external angle as 90 ± 3°. The range of measured values obtained from this study indicates that the external surface angles vary from about 75° to about 108° (a variation of 44% from the minimum), as shown in Table 2. Thus, there is a need to either revise the specifications proposed in the article to encompass vessels from all manufacturers or to modify the manufacturing process to obtain more consistent internal and external angles for the vessel apex. Additionally, the intra-manufacturer variabilities associated with the apex external surface angle were found to be from 1.11% to 7.36%. The inter-manufacturer variability was evaluated to be 6.11% across all manufacturers.

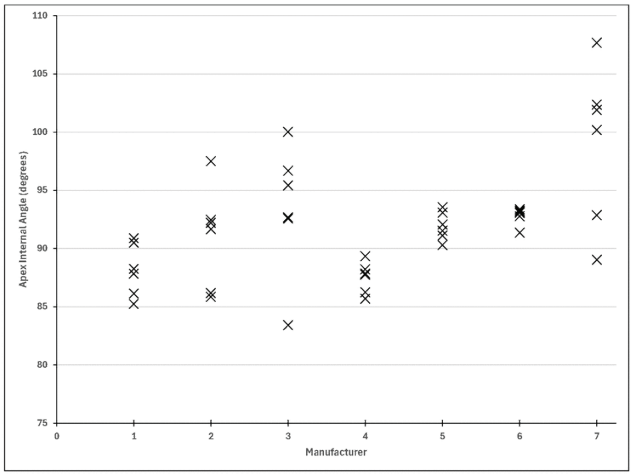

*Figure 5. Skewness plots for apex internal (**a**) and external (**b**) surface angles.*

In general, the apex internal surface angle could be assumed to be equal to the external surface angle if the two surfaces making up the apex thickness were parallel to each other. However, this was not found to be the case with apex vessels considered in this study. Analysis of

Figure 5a and Figure 5b show that while the values for external and internal surface angles compared favorably with each other for each vessel, the angles were rarely equal. Thus, it might be important to consider analyzing the apex internal surface angle separately in order to provide an apex angle specification for the vessels.

Geometric Irregularities

Cylinder Circularity And Cylindricity

The values of cylinder circularity and cylindricity are indicative of a separation distance, respectively, between two circles or two cylinders within which all measurements fell. Cylinder circularities at each of the five locations, along the cylinder height, were evaluated from the associated 50 data points. Similarly, the cylindricity of the cylindrical parts of the vessels was determined from all the associated 250 points. Analysis of the cylinder circularities at locations 1–5 showed that, in general, within a manufacturer set, all vessels tended to have similar circularities. However, some manufacturers' data indicated higher circularities when compared to others. The maxima for the cylinder circularities and cylindricity, as shown in Table 3, were 0.812 and 0.952 mm, respectively, across all manufacturer vessels. In ideal situations, where there are no imperfections in geometry, the values for these and most of the other following geometric irregularities should be equal to 0. More practically, values close to 0 indicate small deviations from the ideal setup and are considered acceptable as being a consequence of manufacturing processes.

Hemisphere Circularity

Similar to the cylinder circularity, the hemisphere circularity of a vessel is defined as the difference between the maximum and minimum values evaluated from the corresponding 100 data points previously used for the evaluation of the hemisphere radius. The hemisphere circularity values for all vessels are shown in Figure 6a. It can be observed that the hemispherical circularity values are comparatively higher than the cylinder cylindricity or circularity values. As shown in Table 3, in comparison across all 42 vessels, while the average value was 0.719 mm, the highest value was 1.535 mm. The average values for hemispherical circularity within a manufacturer's set of

Table 3. Selected Statistics of Geometric Irregularities in Apex Vessels

Characterization Parameter	Individual Manufacturer (Mfr) Data, Average ± SD							All Vessels	
	Mfr. 1	Mfr. 2	Mfr. 3	Mfr. 4	Mfr. 5	Mfr. 6	Mfr. 7	Range	Average ± SD
Cylinder circularity at location 1 (mm)	0.121 ± 0.060	0.276 ± 0.105	0.160 ± 0.111	0.153 ± 0.033	0.101 ± 0.039	0.134 ± 0.058	0.446 ± 0.072	0.056–0.569	0.199 ± 0.134
Cylinder circularity at location 2 (mm)	0.118 ± 0.064	0.298 ± 0.119	0.162 ± 0.112	0.152 ± 0.022	0.097 ± 0.043	0.138 ± 0.057	0.480 ± 0.085	0.045–0.600	0.206 ± 0.148
Cylinder circularity at location 3 (mm)	0.118 ± 0.058	0.309 ± 0.133	0.166 ± 0.105	0.160 ± 0.015	0.102 ± 0.044	0.139 ± 0.057	0.498 ± 0.112	0.050–0.624	0.213 ± 0.155
Cylinder circularity at location 4 (mm)	0.134 ± 0.055	0.321 ± 0.151	0.165 ± 0.096	0.182 ± 0.025	0.143 ± 0.094	0.144 ± 0.056	0.534 ± 0.139	0.051–0.684	0.232 ± 0.166
Cylinder circularity at location 5 (mm)	0.128 ± 0.052	0.331 ± 0.161	0.155 ± 0.084	0.221 ± 0.023	0.098 ± 0.081	0.149 ± 0.052	0.602 ± 0.170	0.031–0.812	0.241 ± 0.191
Cylinder cylindricity (mm)	0.313 ± 0.070	0.466 ± 0.192	0.253 ± 0.087	0.322 ± 0.064	0.312 ± 0.152	0.251 ± 0.046	0.732 ± 0.131	0.137–0.952	0.378 ± 0.194
Cylinder perpendicularity (mm)	0.053 ± 0.041	0.173 ± 0.136	0.134 ± 0.047	0.274 ± 0.082	0.152 ± 0.031	0.151 ± 0.084	0.489 ± 0.276	0.008–0.912	0.204 ± 0.177
Hemisphere circularity (mm)	0.548 ± 0.082	0.707 ± 0.045	0.970 ± 0.129	0.462 ± 0.086	1.042 ± 0.281	0.449 ± 0.074	0.852 ± 0.141	0.355–1.535	0.719 ± 0.262
Axis-cylinder and -hemisphere perpendicularity (mm)	0.107 ± 0.043	0.253 ± 0.165	0.199 ± 0.081	0.334 ± 0.057	0.332 ± 0.099	0.287 ± 0.099	0.442 ± 0.120	0.052–0.580	0.279 ± 0.138
Apex circularity (mm)	0.013 ± 0.007	0.032 ± 0.028	0.072 ± 0.036	0.007 ± 0.005	0.062 ± 0.069	0.052 ± 0.030	0.052 ± 0.038	0.001–0.202	0.041 ± 0.041
Apex perpendicularity (mm)	0.165 ± 0.093	0.176 ± 0.171	0.399 ± 0.132	0.158 ± 0.105	0.153 ± 0.056	0.176 ± 0.077	0.213 ± 0.116	0.051–0.597	0.206 ± 0.132
Axis-cylinder, -hemisphere, and -apex perpendicularity (mm)	0.708 ± 0.477	0.603 ± 0.221	0.411 ± 0.147	0.466 ± 0.042	0.477 ± 0.073	0.377 ± 0.169	0.606 ± 0.290	0.197–1.321	0.521 ± 0.252

vessels varied from 0.449 to 1.04 mm. In comparison, the average values for hemisphere roundness for standard vessels, as presented by Liddell et al. (*8*), varied from 0.10 to 1.9 mm.

Cylinder Perpendicularity

The cylinder perpendicularity, defined as the distance between two parallel planes that are perpendicular to the horizontal surfaces on which the vessel rests, was evaluated using five data points for each vessel. The five data points consisted of a representative point from each of the five diameter locations along the cylinder height. The cylinder perpendicularity is thus an indication of how the vertical surface of the cylinder lines up with the horizontal surface and is not connected to the axis perpendicularity defined below. Figure 6b presents the skewness plot for the cylinder perpendicularity. Data ranged from low to medium to high values (with changing variabilities) across manufacturers. Evaluation of the average and associated range indicates that while the average (of 0.204 mm) is lower in comparison, the maximum value extended to as much as 0.912 mm, as shown in Table 3. The average values for cylinder perpendicularity within a manufacturer's set of vessels varied from 0.053 to 0.49 mm. In comparison, the average values for cylinder perpendicularity for standard vessels, as presented by Liddell et al. (*8*), varied from 0.07 to 0.36 mm.

Axis-Cylinder and -Hemisphere Perpendicularity

Six data points were used to evaluate the axis-cylinder and -hemisphere perpendicularity. This perpendicularity, which covers only the perpendicularity between the cylinder and hemisphere for a vessel (i.e., not the apex), is defined as the diameter of an imaginary cylinder that is perpendicular to the horizontal surface on which the vessel rests, within which the data from the six points fell. A non-zero value for this geometric characteristic would indicate that the axes for the cylinder and hemisphere are not coincident. The skewness plots for axis-cylinder and -hemisphere perpendicularity are shown in Figure 6c. Analysis of the axis-cylinder and -hemisphere perpendicularity indicates that the offsets between the axes of the cylindrical and hemispherical parts of the vessel also varied both within a manufacturer set of vessels and from manufacturer to manufacturer. Across all manufacturers, the lowest, highest, and average values were 0.052, 0.580, and 0.279 mm, respectively (as presented in Table 3), which possibly indicates that the distribution of values across vessels is centered around the average value. This implies that the cylinder and hemisphere axes are offset, at least to some degree, in apex vessels. The average values for axis-cylinder and -hemisphere perpendicularity within a manufacturer's set of vessels varied from 0.107 to 0.442 mm. In comparison, the average values of cylinder–hemisphere concentricity for standard vessels, as presented by Liddell et al. (*8*), varied from 0.55 to 1.3 mm.

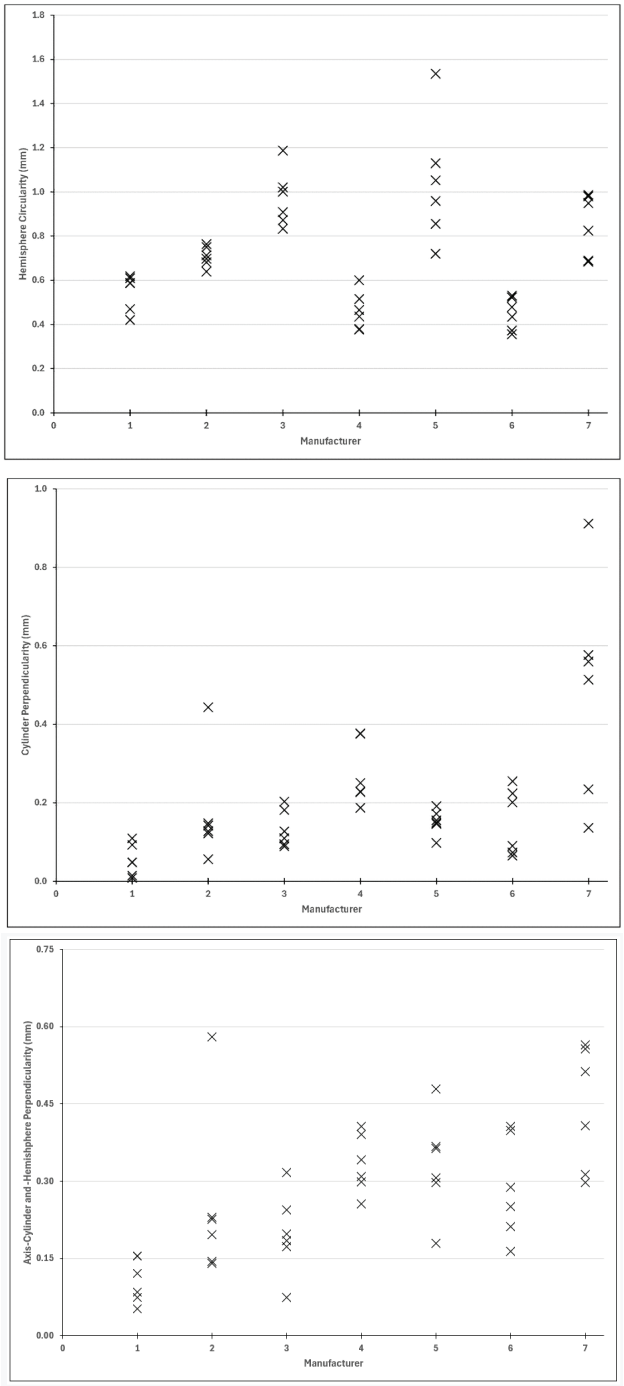

*Figure 6. Skewness plots for hemisphere circularity (**a**), cylinder perpendicularity (**b**), and axis-cylinder and -hemisphere perpendicularity (**c**).*
Note: Fig. 6c was printed incorrectly in PF 51(1) and corrected in a subsequently published Compendial Notice (https://www.uspnf.com/notices/stim-article-figure-correction-20250117).

Apex Circularity

The 144 points previously used for determining the apex diameters (i.e., concentric circles) at various locations along the apex height were used to evaluate the apex circularity as the difference in the maximum and minimum radii obtained from those points. This meant that the 144 points associated with an apex would fall within two concentric circles separated by the circularity for that apex. Also, the circularity consequently is a value that captures the greatest difference in points along the apex height and could be representative of differences in diameter values at two different axial locations within the same apex.

Skewness plots for the apex circularity are shown in Figure 7a. In general, except for certain manufacturers, data showed that the variability was observable within a manufacturer set of vessels. The values of apex circularities were, however, lower in comparison to the previously discussed cylinder and hemisphere circularities. Within a manufacturer set, as shown in Table 3, the average values were found to be typically low (and close to 0), which is possibly an indication of the fact that all points associated with the definition of this irregularity fell within two circles that are very close to each other. Across all 42 vessels, the highest apex circularity value was limited to 0.202 mm, while the average value was only 0.041 mm.

Apex Perpendicularity

As with the cylinder perpendicularity, the apex perpendicularity was evaluated from nine points, i.e., one each from the corresponding apex diameter evaluations along the apex height, as previously described. Skewness plots of the apex perpendicularity, shown in Figure 7b, indicated high intra-manufacturer variabilities. From Table 3, it can be seen that the apex perpendicularity values are typically non-zero and are more controlled with certain manufacturers than with others (as evidenced by the standard deviation values).

Axis-Cylinder, -Hemisphere, and -Apex Perpendicularity

The axis-cylinder, -hemisphere, and -apex perpendicularity is defined as the diameter of an imaginary cylinder perpendicular to the horizontal surface on which the associated vessel rests. For the evaluation of this characteristic, 15 data points were considered and thus, all points would fall within the imaginary cylinder with a diameter equal to the value of the axis-cylinder, -hemisphere, and -apex perpendicularity for that vessel. This perpendicularity covers all three geometric features of a vessel — the cylinder, the hemisphere, and the apex. Differences from the axis-cylinder and -hemisphere perpendicularity, described previously, would indicate offsets (i.e., off-centered positions) of the apex with the other parts of the vessel (i.e., cylinder and hemisphere). The axis-cylinder, -hemisphere, and -apex perpendicularity values were high, with a substantial amount of data points showing values between 0.5 and 1.5 mm regardless of the manufacturer, as shown in Figure 7c.

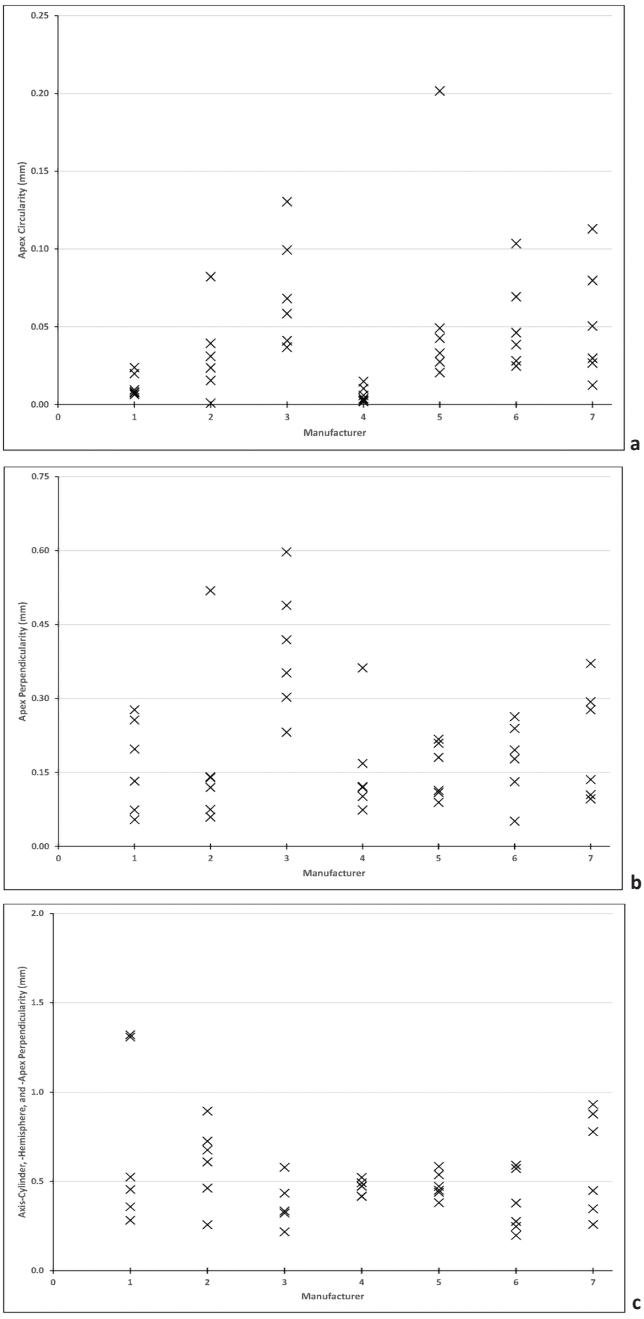

*Figure 7. Skewness plots for apex circularity (**a**), apex perpendicularity (**b**), and axis-cylinder, -hemisphere, and -apex perpendicularity (**c**).*

The axis-cylinder, -hemisphere, and -apex perpendicularity aligns with the proposed specification of apex centering (i.e., the deviation of apex from the vessel

centerline) in the 2021 *Stimuli* article. The proposed specification value for the irregularity is to be ≤ 2 mm. Analysis of Table 3 indicates that the average values for any manufacturer and the range (and average values) across all manufacturers lie within the proposed specification. Given that the axis-cylinder and hemispherical perpendicularities are also non-zero, differences between the cylinder and hemisphere centering should additionally be considered when determining a specification for the apex centering. Furthermore, any additional offset in the impeller location (from the apparatus setup), depending on its direction, would also need to be considered in defining any specification for this axis-cylinder, -hemisphere, and -apex perpendicularity. For standard dissolution apparatuses, the impeller offset is defined to be ≤ 2 mm, i.e., the same value (see <711>). Thus, if it is desired to limit the total offset of the apex and impeller to a maximum of 2 mm, care should be taken to set specifications for impeller offsets with apex vessels. Additionally, the effect of impeller and apex offsets on hydrodynamics in apex vessels should be considered from both individual and combinational perspectives.

CONCLUSION

As a first step aimed toward understanding commercially available apex vessels, a geometry characterization study was completed. Seven sets of six apex vessels, each from different manufacturers, were characterized using a CMM. A total of 37 characterization parameters (associated with either the vessel geometry, the apex geometry, or geometric irregularities) that aid in the complete definition of the apex vessel geometries were identified. Measurement data was obtained individually for each vessel, and data from all vessels were compiled to obtain an understanding of both intra- and inter-manufacturer distributions using skewness plots. Additional information about the intra- and inter-manufacturer variabilities associated with these parameters was extracted by analyzing the associated averages, standard deviations, and ranges.

All sizing parameters pertaining to the vessel geometries considered in this study, i.e., without including the apexes, fall within the specifications set in <711> and exhibited low intra- and inter-manufacturer variability. Thus, the corresponding specifications for standard vessels can be applied to apex vessels as far as the vessel parameters are considered. However, data shows that certain parameters, for example hemisphere radius, fall within much narrower ranges. Hence, there is a possibility of providing tighter specifications for apex vessels if such a need arises.

On the other hand, all apex characterization parameters considered in this study were found to vary considerably both within a manufacturer set of vessels and between manufacturers. These variations were found with the diameters at various locations, height, width, thickness, and (internal and external) angles — thus indicating a wide variety of apex geometries available commercially. Measurements of geometric irregularities also presented similar variations across all apex vessels considered. Therefore, it is crucial for end-users of apex vessels to understand that these vessels can vary in geometry (across multiple parameters) even within a single manufacturer's set and to be aware of their potential impact on dissolution results. Consequently, it is advisable to control the source of apex vessels used in testing or at least use vessels with parameters that fall within a certain acceptable tolerance.

The measurements from this study were additionally compared against the three specifications proposed for apex vessels in the 2021 *Stimuli* article. Measurements for the apex height and the apex external angle indicated that there are values for each of these parameters outside the proposed specifications. On the other hand, measurements of axis-cylinder, -hemisphere, and -apex perpendicularity were within the proposed specification for apex centering. However, additional considerations, such as its association with the axis-cylinder and -hemisphere perpendicularity and any possible impeller offsets during operation of the apparatus, need to be evaluated before setting a specification for the apex centering.

Following the conclusion of this study, it is understood that there are variabilities associated with the defining parameters of apex vessel geometries and that there is a possible need to modify certain proposed specifications provided in the 2021 *Stimuli* article. Results from the proposed CFD and dissolution studies will provide more insights into a complete understanding of the apex vessels. Upon completion of these studies, a more comprehensive understanding of the specifications required to standardize the apex vessels can be achieved. We expect that a combination of direct and/or indirect measurements may be required to assess the geometric parameters detailed herein for use of the apex vessels in dissolution labs, as the expectation is not to conduct a detailed characterization by using CMM as discussed here.

GLOSSARY

d_A: Distance of apex to the origin of hemisphere (mm).

$d_{Z,hs}$: Distance Z to the origin of hemisphere (mm).

H_A: Apex height (mm).

H_V: Vessel height (mm).

R: Hemisphere radius (mm).

R_b: Blend radius between apex and adjoining vessel surfaces (mm).

W_A: Apex width (mm).

Z: Axial coordinate along vessel/apex heights (mm); $Z = 0$ at vessel top.

θ_{ext}: Apex external surface angle (degrees).

θ_{int}: Apex internal surface angle (degrees).

ACKNOWLEDGEMENTS

The authors thank Dr. James Mann and Dr. Gavin Reynolds of AstraZeneca for discussions on their 2021 *Stimuli* article, *The Case for Apex Vessels*, which took place prior to the study presented in this current article. The authors would also like to acknowledge the contributions of Naiffer Romero of USP in initiating and facilitating the conversations with AstraZeneca that led to this study. Specific thanks are also due to Dr. Mann for his support in the procurement of vessels used in this study from various vendors and to the vendors themselves for providing us with their vessels.

The authors would additionally like to acknowledge the significant contributions of Karl Barth, BMA, Inc., in carrying out the CMM data collection efforts, providing initial summaries of results and contributing to a more comprehensive understanding of the definitions and variations in some of the geometric parameters discussed in this article.

CONFLICT OF INTEREST STATEMENT

The authors are employees of the US Pharmacopeial Convention. USP offers documentary and physical reference standards for sale as part of its activities.

USP IDENTIFICATION OF BRANDED INSTRUMENTS OR EQUIPMENT DISCLAIMER

Certain commercial equipment, instruments, vendors, or materials may be identified in this article to specify adequately the experimental procedure. Such identification does not imply approval, endorsement, or certification by USP of a particular brand or product, nor does it imply that the equipment, instrument, vendor, or material is necessarily the best available for the purpose or that any other brand or product was judged to be unsatisfactory or inadequate.

REFERENCES

1. Beckett, A. H.; Quach, T. T.; Kurs, G. S. Improved hydrodynamics for USP apparatus 2. *Dissolut. Technol*. **1996**, *3* (2), 7–18. DOI: 10.14227/DT030296P7.
2. Collins, C. C.; Nair, R. R. Comparative evaluation of mixing dynamics in USP apparatus 2 using standard USP vessels and PEAK vessels. *Dissolut. Technol*. **1998**, *5* (2), 17–21. DOI: 10.14227/DT050298P17.
3. Mirza, T.; Joshi, Y.; Liu, Q.; Vivilecchia, R. Evaluation of dissolution hydrodynamics in the USP, PEAK and flat-bottom vessels using different solubility drugs. *Dissolut. Technol*. **2005**, *12* (1), 11–16. DOI: 10.14227/DT120105P11.
4. Baxter, J. L.; Kukura, J.; Muzzio, F. J. Shear-induced variability in the United States Pharmacopeia apparatus 2: modifications to the existing system. *AAPS J*. **2005**, *7*. DOI: 10.1208/aapsj070483.
5. Yoshida, H.; Morita, T.; Abe, Y.; et al. Effects of apex size on dissolution profiles in the USP II paddle apparatus. *AAPS PharmSciTech*. **2023**, *25* (1), 9. DOI: 10.1208/s12249-023-02722-5.
6. Gray, V.; Kelly, G.; Xia, M.; Butler, C.; Thomas, S.; Mayock, S. The science of USP 1 and 2 dissolution: present challenges and future relevance. *Pharm. Res*. **2009**, *26* (6), 1289–1302. DOI: 10.1007/s11095-008-9822-x.
7. Grady, H.; Elder, D.; Webster, G. K.; et al. Industry's view on using quality control, biorelevant, and clinically relevant dissolution tests for pharmaceutical development, registration, and commercialization. *J. Pharm. Sci*. **2018**, *107*, 34–41. DOI: 10.1016/j.xphs.2017.10.019.
8. Liddell, M. R.; Deng, G.; Hauck, W. W.; Brown, W. E.; Wahab, S. Z.; Manning, R. G. Evaluation of glass dissolution vessel dimensions and irregularities. *Dissolut. Technol*. **2007**, *14* (1), 28–33. DOI: 10.14227/DT140107P28.

Test right. Dose right.

Trusted providers of pharmaceutical testing solutions for over 75 years.

Pharmaceutical dosage form testing specialists:

- Disintegration
- Dissolution
- Powder Flowability
- Friability
- Hardness
- Diffusion

COPLEY

INNOVATIVE
COMPLIANT
TRUSTED

+44 (0)115 961 6229 | copleyscientific.com | sales@copleyscientific.co.uk

dx.doi.org/10.14227/DT320125P20

Development of a Physiologically Relevant Simulated Nasal Fluid for In Vitro Dissolution Studies

Shengnan Zhao[1,2], Tyson S. Le[1], Neal M. Davies[1], and Raimar Löbenberg[1*]
[1]*Faculty of Pharmacy and Pharmaceutical Sciences, University of Alberta, Edmonton, AB, Canada.*
[2]*China Z, Pharmaceutical Productivity Centre, Beijing, China.*

e-mail: raimar@ualberta.ca

ABSTRACT

Introduction: Nasal drug delivery systems offer unique advantages, including rapid absorption, bypassing first-pass metabolism, and effectively targeting the central nervous system. However, the complex composition of natural nasal mucus poses challenges in replicating its properties for in vitro studies. Existing simulated nasal fluid (SNF) often lacks critical components, limiting the effectiveness in mimicking the natural nasal mucus under a physiological environment. **Methods:** Three novel SNF solutions were developed with a composition that includes key components (sodium, potassium, calcium, chloride, lipids, and mucin) at concentrations like those found in human nasal fluid. This study compared the developed SNFs with commercial products and human nasal fluids to assess its ability to simulate ionic strength, lipid, and protein content, all of which affect drug solubility and mucosal adhesion. Additionally, this study examined the impact of lipids and mucin on SNF properties including pH, conductivity, density, viscosity, surface tension, and zeta potential, as well as the solubility of model drugs (i.e., melatonin and triamcinolone acetonide) in different SNF solutions. **Results:** The developed SNFs more accurately replicated the composition of human nasal fluid compared to commercial products. The inclusion of lipids and mucin in the SNF improved its ability to simulate mucosal adhesion and drug solubility, evaluating the potential to enhance the accuracy of nasal drug delivery system assessments. Cost analysis demonstrated that developed SNF could be produced at a significantly lower cost than current commercial options, providing a cost-effective and adjustable solution for research applications. **Conclusion:** The developed SNFs provide a physiologically relevant and standardized medium for in vitro nasal dissolution studies. Accurate replication of human nasal mucus enhances the reliability of drug formulation and evaluation, offering a cost-effective alternative to current commercial products.

KEYWORDS: Nasal fluid, simulated nasal fluid, nasal drug development, nasal drug delivery, solubility, dissolution

INTRODUCTION

Nasal drug delivery systems offer significant advantages over traditional routes by providing faster systemic absorption, bypassing the gastrointestinal tract and first-pass metabolism, and offering noninvasive administration, which can increase patient compliance. These systems are particularly beneficial for targeting central nervous system disorders due to the direct connection between the nasal cavity and brain, bypassing the blood-brain barrier. Despite these advantages, the development and evaluation of nasal delivery systems are often constrained by the complexity of the nasal environment, particularly the nasal mucus.

Human nasal fluid (HNF) is a complex mixture, predominantly consisting of water (≈ 95% w/w), mucins (≈ 0.2–5.0% w/v), globular proteins (≈ 0.5% w/v), salts (≈ 0.5–1.0% w/w), lipids (≈ 1–2% w/w), and other components (*1*). The physicochemical properties of nasal mucus, such as pH, typically ranges from 5.5–6.5 in adults, making it slightly acidic compared to the pH of plasma (7.4) (2–5). Baseline pH of HNF is approximately 6.3, with a slightly higher pH of 6.4 in the anterior part, which is more easily influenced by buffer solutions compared with the posterior pH (3). Nasal pH does not differ significantly between patients with and without cystic fibrosis or chronic sinusitis when technical factors are considered, though it shows slight acidity (pH 5.7) after endoscopic sinus surgery (4, 5). Under normal physiological conditions, the nasal mucus layer has a thickness of approximately 10–15 µm and is continuously

*Corresponding author

refreshed by mucociliary clearance, which propels about 2 L of mucus per day from the nasal cavity towards the nasopharynx (*6*). This process ensures the effective removal of particulate matter and pathogens, providing protection for the respiratory tract. The anatomical structure of the nasal cavity and nasal epithelium are illustrated in Figure 1. The unique composition of mucins and lipids in nasal mucus affects its protective and rheological properties, which significantly influence drug solubility, retention, and absorption, posing unique challenges for drug formulation and delivery studies.

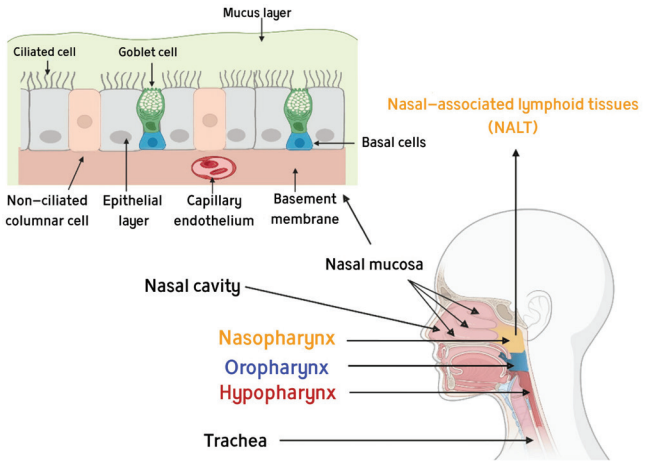

Figure 1. Anatomical structure and function of nasal mucus secretion in the nasal cavity.
Reprinted under the terms of a Creative Commons Attribution (CC BY) license from Tai et al. Different Methods and Formulations of Drugs and Vaccines for Nasal Administration. Pharmaceutics 2022, 14 (5), 1073.
DOI: 10.3390/pharmaceutics14051073.

The variability, scarcity, presence of pathogens, and ethical concerns associated with collecting HNF restrict its use in research. Current compositions of nasal fluid often lack crucial biochemical components or do not accurately replicate the ionic strength and pH of natural nasal fluids. The aim of this study was to develop a new biorelevant SNF composition that more accurately mimics the physicochemical and rheological properties of human nasal mucus, integrating robust literature data with practical composition considerations. This approach not only enhances the physiological relevance of in vitro studies but also supports more accurate assessment and development of nasal drug delivery systems.

Composition Analysis of Human Nasal Fluid (HNF)

The limited volume of mucus available in the nasal cavity presents a significant obstacle for compositional analysis. Typically, natural mucus secretion does not yield enough for such studies, necessitating the adoption of specialized collection techniques. Various methods have been documented in the literature for effectively collecting nasal mucus. These include filter paper adsorption, which directly absorbs mucus from the nasal cavity, and the use of small spoons to carefully extract the mucus (*7–9*). Techniques such as induced sneezing and cryo-stimulation are employed to enhance mucus production, facilitating collection. Additionally, x-ray microanalysis has been utilized to analyze the distribution and quantity of mucus, offering a noninvasive approach to study its composition (*10*, *11*). The considerable variation in ion concentrations observed in mucus samples obtained by different collection techniques may be due to the inherent variations introduced by the distinct collection techniques employed.

The ion composition of HNF has been comprehensively studied (Table 1) (*6–12*). Reported ion concentrations exhibit considerable variability, highlighting the need for a standardized composition of SNF that can accurately reflect the nasal environment. To simulate diverse conditions within the nasal cavity, the composition of a newly developed SNF should be adjustable to encompass extreme ion concentrations that may occur. In the current study, ions with a pivotal influence on drug delivery were identified and prioritized to determine their concentrations, followed by establishing the concentrations of other ions.

Table 1. Ion Concentrations in Nasal Fluid (mmol/L)

Source	Sodium	Potassium	Calcium	Magnesium	Chloride	Phosphate
(*6*)	128–150	17–41	4	5	139	ND
(*7*)	98–225	23–68	3–14	ND	ND	3–7
(*8*)	≈ 110	≈ 30	ND	ND	≈ 125	ND
(*9*)	138–189	31–40	1.0–1.85	ND	156–217	0.72–1.31
(*10*)	127 ± 6	27 ± 3	5 ± 1	ND	140 ± 7	ND
(*10*)	142 ± 28	43 ± 10	ND	ND	150 ± 36	ND
(*11*)	141 ± 8	61 ± 8	ND	ND	170 ± 12	ND
(*12*)	85 ± 10	ND	ND	ND	108 ± 5	ND
Developed SNF-I	145	35	5	0	188	1.12 (Glycerophosphate)

ND: not detected; SNF-I: fundamental ionic simulated nasal fluid.

Calcium, magnesium, and phosphate were prioritized owing to their susceptibility to compatibility issues with drugs. Given that both calcium phosphate and magnesium phosphate are insoluble compounds, and that the solution must mimic the nasal pH of 6.4, it is essential to prevent the formation of insoluble precipitates. Calcium glycerophosphate was used to introduce an organic phosphate group in place of the inorganic phosphate group, preventing precipitation while supplying calcium ions. To achieve a balance between physiological relevance and composition stability, the calcium concentration was set at 5 mmol/L, the mid-point of the reported range, and the phosphate concentration was determined to be 1.12 mmol/L (*9*). Magnesium was excluded from the fundamental composition due to limited data, but it can be introduced via mucin reagent. The sodium concentration in nasal fluid is reported to range from 75–225 mmol/L, with a maximum plasma reference concentration of 145 mmol/L (*7, 12*). The developed SNFs have the same sodium ion concentration as that of plasma. Similarly, potassium, known for its high concentration in nasal mucus owing to bacteriostatic properties, was standardized at 35 mmol/L based on most reported values (*7, 9, 10*). Chloride ions were used to balance the charge in the final composition. By integrating both robust literature data and practical considerations, the developed SNF composition supports more accurate assessment and development of nasal drug delivery systems.

The in vitro performance testing of nasal products, along with the associated methodological approaches and challenges, has been recently reviewed by a USP Expert Panel, although no official recommendations for performance testing of nasal drug gels or ointments have been established (*13, 14*). Electrolyte solutions have been used in in vitro release experiments for nasal formulations, with one study demonstrating that the concentration of potassium ions in the release medium significantly influences the erosion and release rate of carrageenan-poloxamer 407 hydrogel; however, no studies specifically mention the use of biorelevant nasal fluids (*15–17*). The development of biorelevant methods has been suggested as a clear path forward for future research (*13*). Several drug delivery routes, including the nasal route, currently lack a standardized biorelevant fluid, which is essential for future performance testing and ultimately for achieving an in vitro-in vivo correlation (IVIVC).

It has been demonstrated that porcine nasal mucosa can be used as a model for in vitro assessment of nasal drug delivery, and porcine stomach mucin (type II mucin) has been used to prepare simulated airway or nasal mucus (*18–23*). Higher mucin concentrations significantly decrease particle mobility, with a 44-fold reduction in the particle diffusion rate observed with 0.5% mucin and a 2570-fold reduction with 5% mucin (20). Even a 1% mucin concentration in mucin-hydrogels can lead to a 2500-fold decrease in particle mobility compared to the rate of free diffusion (*24*). A 2% concentration of mucin, which is near physiological concentrations, was used in the developed SNFs to enable more accurate characterization of nasal spray formulation performance.

HNF contains a high concentration of lipids, similar to the lipid composition found in secretions from human respiratory epithelial cells (*25*). Removing some of these lipids decreases the fluid's antimicrobial activity, which can be restored by adding lipids back into the fluid (*25*). In another study, saturated and polyunsaturated fatty acids accounted for 45% and 29% of the nasal total fatty acids, respectively (*26*). Omega-6 fatty acids were predominant in the polyunsaturated fatty acids subgroup, and linoleic acid and arachidonic acid were incorporated in the main nasal phospholipid classes (*26*).

Although nasal mucus contains a variety of lipid categories, integrating lipids into ionic solutions for nasal drug formulations presents challenges. Typically, this integration requires the preparation of lipids either as liposomes or emulsions, which are then capable of dispersing within the aqueous phase. Similar techniques have been employed in the development of simulated lung fluids. For example, liposomes were prepared with phosphatidylcholine to ensure uniform dispersion of lipids and to evaluate in vitro release of itraconazole from nebulized nanoparticle dispersions (*27, 28*). In parenteral nutrition emulsions (e.g., Intralipid), the components contain triglycerides (fatty acid composition containing myristic, palmitic, palmitoleic, stearic, oleic, and linoleic acids) and egg yolk lecithin (mixture of several phospholipids), and the emulsion is a fairly stable liquid system that allows for a ready-to-use composition (*29*). In the developed SNFs, Intralipid was used to simulate the lipid content of nasal mucus at a dosage of 10 mL/L (equivalent to 2 g lipid/L).

METHODS

Chemicals and Reagent Kits

Commercially available SNF products used in the study, referred to as CP1 and CP2, were obtained from Chemazone, Inc (Canada). HNF from a single human donor was purchased from MYBioSource (USA, lot 20-11-598), and pooled HNF (PHNF) was purchased from Innovative Research, Inc (USA, lot 48147).

Sodium chloride (Caledon, Canada, lot 40091), potassium chloride (Merck KGaA, Germany, lot K51693109004), calcium chloride (Aldrich Chemical Company, USA, lot 06924A1), calcium glycerophosphate (TCI America, USA, lot ZQUFB-YM$N), Intralipid 20% (Fresenius Kabi Canada Ltd, lot 10QL3207), mucin from porcine stomach type II (Sigma-Aldrich, USA, lot 0000329256), were used for preparation of the SNF solutions. All other chemicals used were analytical grade.

Melatonin was purchased from Medisca Canada (lot 198251/A). Triamcinolone acetonide was purchased from Thermo Fisher Scientific (lot P251013).

Preparation of SNF Solutions

As shown in Table 2, composition of the developed SNF solutions included sodium, potassium, calcium, and glycerophosphate, with total chloride at 187.76 mmol/L (i.e., sodium chloride 145 mmol/L, potassium chloride 35 mmol/L, calcium chloride 3.88 mmol/L, calcium glycerophosphate 1.12 mmol/L).

Three variations of the developed SNF were prepared according to the quantities specified in Table 3.

SNF-I

The fundamental ionic solution of SNF (SNF-I) was prepared by sequentially adding sodium chloride, potassium chloride, calcium chloride, and calcium glycerophosphate into a 1-L volumetric flask. All reagents were dissolved thoroughly in an appropriate amount of water before adjusting the volume to 1 L. The pH of the solution was adjusted to 6.4 using an appropriately diluted hydrochloride solution.

SNF-IL

For the preparation of the lipid-containing SNF solution (SNF-IL), 100 mL of the SNF-I solution was mixed with 1 mL of Intralipid 20% (an intravenous lipid emulsion). This solution was freshly prepared daily and used within 24 hours; any remaining solution after this period was discarded. The volume of the solution was scaled up or down proportionally as required for experimental needs.

SNF-ILM

To prepare the SNF solution containing both lipid and mucin (SNF-ILM), 100 mL of the SNF-IL solution was mixed with 2 g of mucin. The mixture was thoroughly stirred until the mucin was completely dissolved. The pH was then adjusted to 6.4 using an appropriately diluted sodium hydroxide solution. This solution was freshly prepared and used within 24 hours. The volume of the solution was scaled up or down proportionally as needed.

Table 2. Ion Concentration Conversion for Composition of Developed Simulated Nasal Fluid

Compound	Molecular Weight (g/mol)	Concentration (mmol/L)	Amount (g/L)	Ion Concentrations (mmol/L)
NaCl	58.44	145.00	8.47	Na: 145
KCl	74.55	35.00	2.61	K: 35
$CaCl_2$	110.98	3.88	0.43	Ca: 5
Calcium glycerophosphate	210.14	1.12	0.24	Glycerophosphate: 1.12 Total Cl: 187.76

NaCl: sodium chloride; KCl: potassium chloride; CaCl2: calcium chloride.

Table 3. Compositions of Developed Simulated Nasal Fluid (SNF) Solutions

Category	Compound	SNF-I	SNF-IL	SNF-ILM
Ion composition	NaCl	8.47 g/L	8.47 g/L	8.47 g/L
	KCl	2.61 g/L	2.61 g/L	2.61 g/L
	$CaCl_2$	0.43 g/L	0.43 g/L	0.43 g/L
	Calcium glycerophosphate	0.24 g/L	0.24 g/L	0.24 g/L
Lipid (0.2%, w/v)	Intralipid 20%	-	10 mL (≈ 2 g lipid)	10 mL (≈ 2 g lipid)
Protein (2%, w/v)	Mucin	-	-	20 g/L
		Add water to 1 L		
		Adjust pH to 6.4		

Dash (-) indicates not applicable.
SNF-I: fundamental ionic simulated nasal fluid; SNF-IL: SNF-I with lipids; SNF-ILM: SNF-I with lipids and mucin; NaCl: sodium chloride; KCl: potassium chloride; CaCl2: calcium chloride.

Analysis of SNF Components

Composition of the SNF-I, SNF-IL, and SNF-ILM solutions was analyzed and compared with two commercially available SNF products (CP1 and CP2) and two human nasal fluid samples (HNF, PHNF). Additionally, a 0.2% lipid solution and 2% mucin solution were analyzed as controls to study the additional components introduced by lipid emulsion Intralipid and mucin.

Chemical composition analysis of all nasal fluid solutions was performed using the Easy RA reagent kit and Easy RA clinical chemistry analyzer (Medica, USA). This instrument was used to detect the concentrations of sodium, potassium, calcium, magnesium, chloride, phosphorus, as well as total protein, albumin, and triglycerides. Following the standard operating procedures of the Easy RA analyzer, the probes and ion-selective electrodes were thoroughly cleaned. The instrument was then calibrated and system-checked using standard solutions. Appropriate reagents kit and blanks (purified water) were placed in the reagent rack, and 500 µL of each test sample solution was placed in the sample rack. For solutions exceeding the upper limit of the linear range, appropriate dilutions were made, and the samples were reanalyzed. The obtained results were recorded for further calculation and comparison.

The mucin content in the SNF solutions and HNFs was determined using a solid-phase sandwich enzyme-linked immunosorbent assay (ELISA) kit to detect and quantify Human MUC2 levels in biological fluids (Thermo Fisher Scientific, Canada, lot WU11J8HT0707). Following the protocol provided in the kit, the absorbance readings of the samples were obtained and compared to a standard curve to determine the concentration of MUC2 in each sample.

Analysis of SNF Properties

pH

The pH and conductivity of the fluids was measured using an Accumet AB200 meter purchased from Fisher Scientific (USA).

Density and Viscosity

The relative density of various solutions was measured using a 5-mL graduated bicapillary pycnometer (model 13377-92, Shangqiu Ruiboer Chemical Glass Instrument Co., China). The measurements were conducted according to the methods outlined in ISO 3838:2004. Calibration was performed at a constant room temperature of 22 °C to determine the density of purified water. The procedure included weighing the empty pycnometer, filling the dry pycnometer with the test solutions, allowing it to stabilize at room temperature for 30 min, then recording the liquid levels and corresponding weights to obtain at least 4 measurements. A linear regression between the height of the liquid level and the mass was established ($r^2 > 0.999$). The relative density was then determined by comparing the mass of the pycnometer filled with the test liquid to the mass of the pycnometer filled with water at the room temperature.

Viscosity of the fluids was measured using a portable field viscometer (PDVdi-120, Stony Brook Scientific, Ltd., USA). Following the setup instructions provided in the manual, 25 mL of each sample was added to the viscometer body. An extension bar was screwed into the needle, which was then inserted into the viscometer body until the needle top aligned with the viscometer body. The needle was then released to fall freely, and the time taken for the needle to pass between two pre-marked points on the extension bar was measured using a video recording. Each sample was measured three times, and the average fall time was calculated. The fall time was then substituted into the viscosity conversion formula provided with the instrument, viscosity = $9.1463 \times (\rho s - \rho f) \times t$, to obtain the viscosity results of the solutions, where ρs is needle density (2.9263 g/cm^3) and ρf is fluid density (g/cm^3), and t is time.

Surface Tension

Surface tension (dyn/cm) was measured with flexible video system (FTÅ200, First Ten Angstroms, USA) to measure the contact angle in conjunction with a 1 mL luer-lock syringe and a blunt needle. The test parameters were set as follows: pump rate 2.0009 µL/s, camera frame rate 40.0 fps, and all other parameters used the system's default settings. From the series of captured images, the photo with the largest droplet volume just before detachment was selected for analysis using the accompanying software. The measurements were taken in quadruplicate, and the average value was reported.

Zeta Potential

Zeta potential of the SNF solutions was measured using the Zetasizer Nano ZS (Malvern Instruments, UK). The zeta potential of the fluids was determined by disposable plain folded capillary zeta cells. All measurements were carried out at room temperature in triplicate.

Drug Solubility

Solubility of model drugs melatonin and triamcinolone acetonide, was determined using a 12-well plate. Each well was filled with 3 mL of various media, with three replicates for each medium. An appropriate amount of each model drug was added to the different media, and

the wells were covered with a parafilm membrane. The 12-well plate was placed on the incubated microplate shaker (model 130000, Boekel Scientific Jitterbug, USA) and shaken at 37 °C, mix level 7, for 36 hours. After the incubation period, the media were subjected to centrifugation at 10,000 g for 20 minutes or filtration using 0.45-µm Basix nylon syringe filters. For samples containing mucin, acetonitrile was used to precipitate the mucin before injection. The filtered solutions were analyzed using a high-performance liquid chromatography (HPLC) system (Shimadzu Corp., Japan) equipped with an Kinetex-C18 column (150 × 4.6 mm, 5 µm), SPD-M10A VP UV–VIS detector, LC-10AS pumps, and SIL-10A auto injector. The chromatographic conditions for melatonin and triamcinolone acetonide were employed as specified in the United States Pharmacopeia (USP) monograph for melatonin and triamcinolone acetonide (*30*).

RESULTS AND DISCUSSION

The components and properties of the developed SNF solutions were systematically compared with those of commercially available SNF solutions (CP1 and CP2) as well as human nasal fluid samples (HNF and PHNF). The comparative data are comprehensively presented in Tables 4 and 5.

Ion Composition

Comparative analysis of ion concentrations in human nasal fluid samples (HNF and PHNF) with previously reported values revealed some notable differences. Sodium, chloride, and phosphorus were within the expected range, whereas potassium and calcium levels were significantly lower. Magnesium levels were also below the expected range, but to a lesser extent. Additionally, the concentrations of albumin in HNF and PHNF were below the detection limits. These findings highlight the inherent variability in nasal fluid composition, influenced by sampling techniques, individual biological differences, health status, physiological changes, and external environmental factors (*6*, *31*).

In terms of ionic interactions, sodium, potassium, and chloride primarily contribute to the osmolarity of solutions. Due to their compatibility with drug ingredients, there is minimal evidence of these ions causing degradation or precipitation in drug formulations. Calcium, magnesium, and phosphorus, however, often lead to precipitation and degradation in sensitive drugs. Tetracycline antibiotics (including tetracycline, minocycline, and doxycycline), known chelating agents, form insoluble complexes with divalent and trivalent metal cations such as calcium and magnesium, adversely affecting drug

Table 4. Comparison of Newly Developed Simulated Nasal Fluid (SNF), Commercially Available Simulated Nasal Fluids, and Human Nasal Fluids

Components	0.2% Lipid	2% Mucin	SNF-I	SNF-IL	SNF-ILM	CP1	CP2	HNF	PHNF	Ref. Value
Na^+ (mM)	< LLQ	< LLQ	138.2 ± 0.3	137.4 ± 0.4	147.1 ± 0.6	133.8 ± 0.1	147.3 ± 0.8	106.0 ± 0.3	106.6 ± 0.1	75–225
K^+ (mM)	< LLQ	3.64 ± 0.02	35.41 ± 0.02	35.97 ± 0.20	37.45 ± 0.12	5.43 ± 0.00	6.58 ± 0.06	18.81 ± 0.02	14.32 ± 0.08	17–69
Ca^{2+} (mM)	< LLQ	0.36 ± 0.03	3.80 ± 0.11	4.05 ± 0.13	4.29 ± 0.10	1.22 ± 0.03	1.78 ± 0.03	0.44 ± 0.02	0.97 ± 0.02	1–14
Mg^{2+} (mM)	0.04 ± 0.01	2.03 ± 0.11	< LLQ	0.04 ± 0.00	2.05 ± 0.04	1.73 ± 0.01	1.77 ± 0.03	0.45 ± 0.01	0.92 ± 0.01	5
Cl^- (mM)	< LLQ	< LLQ	171.7 ± 1.8	171.6 ± 1.9	186.5 ± 0.4	147.0 ± 4.0	146.7 ± 0.7	109.0 ± 0.6	127.3 ± 0.4	103–217
P^{2-} (mM)	< LLQ	1.71 ±0.01	< LLQ	< LLQ	1.79 ± 0.01	0.80 ± 0.01	1.15 ± 0.03	0.78 ± 0.02	2.04 ± 0.01	0.72–7
Total protein (g/L)	5.3 ± 0.6	6.0 ± 0.0	< LLQ	3.0 ± 0.0	12.3 ± 0.6	< LLQ	4.0 ± 0.0	< LLQ	1.3 ± 0.6	4.14–8.95 (*7*)
Albumin (g/L)[a]	< LLQ	< LLQ	< LLQ	< LLQ	< LLQ	< LLQ	< LLQ	< LLQ	< LLQ	0.31–1.05 (*7*)
Triglycerides (mM)	4.38 ± 0.09	0.25 ± 0.01	0.43 ± 0.01	4.26 ± 0.06	4.66 ± 0.05	4.24 ± 0.19	2.63 ± 0.01	0.04 ± 0.00	0.39 ± 0.02	-
Mucin (ng/mL)[b]	-	-	-	-	< LLQ	< LLQ	< LLQ	8.94	0.89 ± 0.06	2% (*51*)

Values are expressed as mean ± SD (n = 3) or range unless otherwise noted.
[a]Albumin lower limit of quantification is 4 g/L.
[b]Due to limited sample volume, a single measurement is reported for HNF and duplicate measurements are reported for PHNF.
Dash (-) indicates not applicable; SNF-I: fundamental ionic simulated nasal fluid; SNF-IL: SNF-I with lipids; SNF-ILM: SNF-I with lipids and mucin; CP1: commercial product 1; CP2: commercial product 2; HNF: human nasal fluid; PHNF: pooled human nasal fluid; LLQ: lower limit of quantification; Na: sodium; K: potassium; Ca: calcium; Mg: magnesium; Cl: chloride; P: phosphorus.

Table 5. Properties of Simulated Nasal Fluid (SNF) Solutions

Property	Water	SNF-I	SNF-IL	SNF-ILM	CP1	CP2
pH	-	6.38 ± 0.03	6.35 ± 0.02[a]→6.4	3.54 ± 0.04[a]→6.4	7.37 ± 0.03	6.89 ± 0.05
Conductivity (ms/cm)	-	19.86 ± 0.06	19.61 ± 0.02	20.10 ± 0.02	15.14 ± 0.12	13.81 ± 0.06
Relative density[b]	-	1.0081	1.0083	1.0155	1.0101	1.0181
Viscosity, μ(cP)	-	3.33 ± 0.17	3.33 ± 0.22	4.19 ± 0.14	3.33 ± 0.29	6.46 ± 0.22
Surface tension (dyn/cm) (n = 4)	-	72.25 ± 0.62	56.65 ± 0.49	101.53 ± 2.82	70.81 ± 0.67	64.84 ± 0.44
Zeta potential (mV)	-	–11.18 ± 1.09	–2.17 ± 0.46	–3.80 ± 1.40	–19.96 ± 2.37	–34.53 ± 1.20
Melatonin solubility (mg/mL)	2.05 ± 0.08	3.00 ± 0.10	2.98 ± 0.15	1.62 ± 0.26	1.51 ± 0.11	1.39 ± 0.17
Triamcinolone acetonide solubility (μg/mL)	24.9 ± 0.6	21.7 ± 0.7	22.9 ± 0.4	25.4 ± 1.7	23.6 ± 7.1	23.5 ± 3.5

Values are expressed as mean ± SD (n = 3).
[a]pH measured after adding lipid and mucin before adjusting pH.
[b]The relative density was without replicates, thus no standard deviation was calculated. The high precision of the measurement is indicated by the linear regression coefficient ($r^2 > 0.999$).
Dash (-) indicates not applicable; SNF-I: fundamental ionic simulated nasal fluid; SNF-IL: SNF-I with lipids; SNF-ILM: SNF-I with lipids and mucin; CP1: commercial product 1; CP2: commercial product 2.

absorption and reducing bioavailability (*32, 33*). Similarly, quinolone antibiotics like ciprofloxacin and levofloxacin are incompatible with multivalent cations, forming insoluble complexes that lead to incompatibility (*34, 35*). Furthermore, reports have indicated that dicalcium phosphate dihydrate is incompatible with various drugs including ceronapril, oxprenolol, quinapril, metronidazole, parthenolide, famotidine, and temazepam (*36*). Therefore, the variability of calcium, magnesium, and phosphorus in SNF can significantly impact the evaluation of nasally administered drugs. Given the known physicochemical properties of drugs sensitive to multivalent ions, it is advisable to prepare SNF solutions using higher values of calcium, magnesium, and phosphorus than what has been reported in the literature.

Comparison of commercially available products (CP1 and CP2) with HNFs revealed that magnesium was significantly higher than both the reported values and the actual measured values, whereas calcium and phosphorus were close to the lower limits of physiological ranges. Comparison with the developed SNF-ILM solution revealed that the magnesium, calcium, and phosphorus levels more closely approximated the mid-values of physiologic ranges than CP1 and CP2. Therefore, the developed SNF-ILM more accurately reflects the physiological concentrations of ions in HNF.

Protein Content

C SNF-ILM is an artificial composition solution designed to mimic the properties of natural nasal secretions. The total protein content in SNF-ILM is three times greater than that of commercial products, which also exceeds the protein levels found in HNFs. This elevated protein concentration is especially significant due to the presence of mucins, as glycoproteins play a crucial role in maintaining the viscosity and elasticity of nasal mucus (*1, 37, 38*). Mucins, by virtue of their structure and high molecular weight, contribute extensively to the gel-like consistency of mucus, making it an effective barrier against pathogens and particulate matter (*1, 39, 40*). They bind to water molecules, thereby ensuring that the nasal passages remain moist, which is essential for the proper functioning of cilia in the respiratory epithelium (*40, 41*). This moisture retention also facilitates the trapping of airborne particles and microbes, preventing them from reaching the lungs and causing infection (*38*).

In addition to its role in maintaining nasal mucus properties, mucin interacts with drug carriers through hydrogen bonding, electrostatic interactions, and hydrophobic forces, which significantly influence drug release, retention time, and absorption within the nasal cavity. Research indicates that mucins can act as selective diffusion barriers, potentially limiting drug delivery and affecting the bioavailability and absorption of drugs (*42, 43*). In the presence of mucin, especially at higher concentrations (≥ 0.6%), the diffusion of compounds is significantly hindered (i.e., atenolol, caffeine, naproxen, and hydrocortisone) (*42*). Positively charged chitosan exhibits strong adhesion to negatively charged mucin, whereas negatively charged or neutral polymers display weaker or negligible interactions (*44*). Moreover, mucin can adhere to different polymers through various mechanisms: anionic polymers like carboxymethyl cellulose bind via electrostatic attraction; pectin and carboxymethyl chitosan form stable structures through hydrogen bonding; and hydroxypropyl methylcellulose

and hydroxypropyl cellulose enhance adhesion through molecular entanglement and van der Waals forces (*45*). Additionally, many excipients in nasal powders have demonstrated effectiveness in prolonging nasal residence time by interacting with mucin and altering mucus rheology (46). Mucin content influences the hydration state of the mucus layer, with proper hydration being crucial for maintaining the optimal viscoelasticity needed for effective ciliary clearance (*47*). Therefore, negatively charged mucin has been identified as a key target for developing in situ nasal gels. The high mucin content in SNF-ILM enhances its utility as a representative medium for evaluating the release of nasal formulations, assessing their potential for prolonged contact time, and their ability to penetrate the mucus barrier.

The ELISA results revealed that mucin levels in HNF and PHNF differed by a factor of 10. The commercial products and developed SNF solutions did not yield detectable results due to the absence of human-derived mucin in these compositions (porcine-derived mucin was used in the developed SNFs).

Albumin Content

The absence of detectable albumin in both commercial products and SNF-ILM, which deviates from the expected values of 0.31–1.05 g/L, can be attributed to the albumin levels being below the lower limit of detection (4 g/L) (*7*). Designed primarily for blood albumin level detection, the Easy RA and its reagents lack the analytical sensitivity necessary to detect minute quantities of albumin present in nasal fluids. This limitation can result in undetectable albumin levels in samples that fall below the threshold.

The presence of albumin in nasal fluids has been reported based on samples of natural secretions, which are influenced by various physiological and environmental factors, resulting in a complex and dynamic protein composition (*48*). Albumin, primarily found in plasma, is a crucial carrier for both hydrophilic and hydrophobic drugs, enhancing their solubility and systemic distribution. By forming complexes with drugs, albumin can protect them from rapid degradation or elimination, thereby extending their half-life within the circulatory system. However, the presence of albumin in nasal fluids is notably low, typically constituting only 1–2% of its concentration in blood plasma (*7*). This minimal concentration suggests that in nasal drug delivery systems, due to the limited volume of mucus within the nasal cavity (≈ 1 mL), small amounts of albumin are unlikely to significantly affect drug solubility and permeability. SNF solutions are typically designed for specific therapeutic or evaluative purposes and are not intended to replicate the complete protein spectrum of natural nasal secretions. Consequently, the composition process often focuses more on other components deemed more critical for the intended applications, excluding albumin.

Lipid Content

HNF contains a rich array of lipids. Intralipid was utilized to simulate the lipids in nasal fluid, while also accommodating the solubility of lipid particles. The triglycerides in a lipid emulsion form are capable of dispersing relatively uniformly in an aqueous solution. Both commercially available products and the newly developed SNF solutions contained triglyceride levels significantly higher than those found in HNF. This might be because lipids in nasal fluid are not exclusively in the form of triglycerides but also include diglycerides, free fatty acids, cholesterol, and phospholipids.

Based on the analysis of nasal fluid components, the high inherent variability in nasal secretion compositions suggests that using a fixed composition of SNF cannot truly represent the physiological range across a diverse population. It is necessary to determine a composition range that can cover the physiological concentration ranges under various conditions for most of the population. Therefore, a fundamental composition that allows for flexible adjustments in component composition would be more appropriate to mimic this nasal secretion inherent variability.

Introducing lipids and mucin into the SNF-I solution altered its ionic concentrations. Specifically, the addition of 0.2% lipid introduced trace amounts of magnesium, and its main contribution was triglycerides.

Compared to the minimal impact of the lipid solution on ionic concentrations, the mucin solution had a more pronounced effect. In addition to the expected contribution to detectable protein levels, the addition of mucin introduced additional trace amounts of potassium and calcium, significant quantities of magnesium and phosphorus, and trace amounts of triglycerides.

The addition of lipids and mucin together substantially enhanced the physiological relevance of the SNFs. The most notable changes were increases in sodium, calcium, magnesium, total protein, albumin, triglycerides, and mucin concentrations. These alterations bring the composition of the SNFs closer to that of human nasal fluid, making SNF-ILM particularly well-suited for studies that aim to mimic the biological environment of the nasal cavity for drug delivery evaluation.

Properties of SNF solutions

pH

The natural pH of nasal secretions generally ranges from 5.5–6.5 in adults and from 5.0–7.0 in infants (*2*). In the developed SNFs, the addition of mucin significantly lowered the pH, requiring adjustments during preparation. In contrast, the pH values for CP1 and CP2 were 7.37 and 6.89, respectively. These deviations from the pH range suggest that commercially available products may not accurately reflect the physiological pH environment.

Electrical conductivity, indicative of a solution's ionic strength, plays a crucial role in nasal fluid by ensuring effective mucociliary clearance, maintaining drug stability and solubility, and enhancing mucosal absorption. In developed SNFs, the addition of lipids and mucin did not significantly alter the conductivity. Conductivity of CP1 and CP2 was lower than that of the developed SNF solutions, which is a normal manifestation of composition differences.

Density and Viscosity

Density and viscosity characteristics significantly impact the retention time of solutions within the nasal cavity. Higher viscosity can enhance the retention of nasal drugs, but it may also affect the rate of drug dissolution and absorption. CP2 exhibited relatively higher density and viscosity compared to other SNF solutions, whereas the other SNF solutions showed no significant differences in these properties.

Surface Tension

Surface tension determines how a solution spreads over a surface. Lower surface tension enhances the spreadability of nasal formulations on mucosal surfaces. This ensures greater surface area coverage, facilitating more extensive contact between the drug and the mucosal tissue, thereby potentially improving drug absorption. In developed SNF solutions, the addition of lipids alone led to a noticeable increase in surface tension, whereas the addition of lipids and mucin decreased this parameter.

Zeta Potential

Zeta potential influences the interactions between drug delivery systems and the mucosal layer. Current developments in nasal delivery are focusing on nano and liposome carriers, where the zeta potential of nasal mucus can indicate compatibility with the ions of nasal dosage forms and potential impacts on mucosal permeability. A low zeta potential for the SNF-IL and SNF-ILM solutions suggests that both were unstable dispersion systems.

Drug Solubility

Based on reported physicochemical properties of melatonin and triamcinolone acetonide, both compounds exhibit relatively high pKa values (Table 6) (*49*). At physiological pH values (≈ 5–7.4), both drugs predominantly exist in their nonionized forms. Consequently, their solubility is not expected to be pH-dependent, and the solubility in the commercial and developed SNF solutions should remain consistent. Due to the sample preparation steps involved in the solubility determination process (i.e., filtration, acetonitrile precipitation, and centrifugation) the relative standard deviation (RSD) for the solubility measurements of melatonin and triamcinolone acetonide was as high as 30%.

The presence of mucin results in decreased solubility of melatonin. This reduction may be due to the possible formation of a complex between mucin and melatonin, which is subsequently removed by filtration, thereby reducing the detectable concentration of melatonin in the solution. Other studies have reported that mucin can delay precipitation and stabilize the supersaturation of poorly water-soluble drugs, such as carvedilol and piroxicam, without significantly affecting their solubility (*50*).

Table 6. Properties of Model Drugs (49)

	Melatonin	Triamcinolone Acetonide
Chemical structure	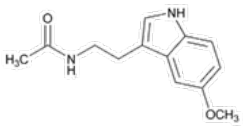	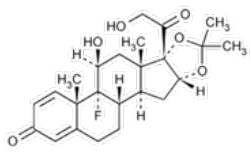
Molecular formula and weight	$C_{13}H_{16}N_2O_2$ 232.28 g/mol	$C_{24}H_{31}FO_6$ 434.5 g/mol
pKa values	0.6, 16.5	13.3
Log P Log D (pH 4–8)	1.148	1.944

Cost Advantages of the Developed SNFs

The developed SNFs provide significant advantages over commercial products and HNFs, particularly in terms of economic feasibility and practical application in vitro and ex vivo research settings. A cost analysis highlights that producing 1 L of the developed SNF solution costs approximately $50 CAD (Table 7). This is substantially lower than that of CP1 and CP2, which are priced at $975 CAD for an equivalent volume. Even more pronounced is the contrast with HNFs, which cost $710–790 CAD per milliliter and are typically available only in extremely limited volumes of 0.5 mL or 1 mL. These limitations render HNFs impractical and prohibitively expensive for routine laboratory studies.

Table 7. Cost of Newly Developed Simulated Nasal Fluid (SNF)

Component	Required amount per 1 L of SNF	Price per Unit	Cost per Liter (CAD)
NaCl	8.47 g	$155.23 / 1 kg	$1.30
KCl	2.61 g	$115.00 / 1 kg	$0.30
$CaCl_2$	0.43 g	$130.12 / 1 kg	$0.10
Calcium glycerophosphate	0.24 g	$370.05 / 1 kg	$0.10
Intralipid (20%)	10 mL	$339.91 / (10 × 100 mL)	$3.40
Mucin (2%)	20 g	$1110.00 / 500 g	$44.40
			Total: $49.60

Price sourced from Fisher Scientific (accessed May 24, 2024): https://www.fishersci.ca/ca/en/home.html
CD: Canadian Dollars; NaCl: sodium chloride; KCl: potassium chloride; $CaCl_2$: calcium chloride.

The developed SNF, costing only $50 CAD per liter, which translates to 5 cents per milliliter, emerges as an economically viable alternative (Table 8). The developed SNF offers a more accessible option for extensive experimental and pharmaceutical research, often constrained by the high costs and scarcity of human nasal fluid. The affordability and greater volume availability of SNF allow for broader and more diverse applications, facilitating comprehensive research that natural nasal fluids cannot support due to their high cost and limited supply.

Table 8. Cost Comparisons of Simulated Nasal Fluid (SNF)

	Developed SNF	CP1	CP2	HNF	PHNF
Volume	1 mL	1 mL	1 mL	1 mL	1 mL
Cost (CAD)	$0.05	$0.975	$0.975	$790.00	$710.00

CP1: commercial product 1; CP2: commercial product 2; HNF: human nasal fluid; PHNF: pooled human nasal fluid; CAD: Canadian Dollars.

Moreover, adjustability of the SNF composition allows researchers to tailor the fluid's properties to meet specific research objectives. This flexibility is crucial for studying the solubility characteristics of nasal fluids, as it enables the simulation of various physiological conditions that may affect drug solubility and release. By understanding how different components of nasal mucus influence these properties, researchers can significantly optimize the design of potential nasal drug performance tests.

CONCLUSION

Developing a standardized SNF is crucial for accurately assessing the solubility and uptake of drugs intended for nasal delivery and for the development of future standardized performance tests. Current alternatives, including limited human donor nasal fluids and commercial products, fail to consistently replicate the complex environment of the nasal mucosa and may be cost-prohibitive. The novel composition of SNF described herein addresses these shortcomings by incorporating mucin and lipid components to mimic the natural conditions of the nasal cavity more closely. The developed SNF provides a more reliable medium for evaluating nasal drug formulations, thereby enhancing the accuracy of performance assessments. Such advancements are vital for optimizing nasal drug delivery systems, ultimately improving therapeutic outcomes and expanding the potential for nasal administration of various pharmaceuticals.

ACKNOWLEDGEMENT

The authors thank the graduate students and post-doctoral fellows in the faculty for their invaluable support and helpful collaboration.

DISCLOSURES

Shengnan Zhao is supported by the China Scholarship Council. The authors have no conflicts of interest.

REFERENCES

1. Leal, J.; Smyth, H. D. C.; Ghosh, D. Physicochemical properties of mucus and their impact on transmucosal drug delivery. *Int. J. Pharm.* **2017**, *532* (1), 555–572. DOI: 10.1016/j.ijpharm.2017.09.018.
2. Mittal, S.; Jobin, J.; Kawale, S. *Review on nasal drug delivery system*; World Journal of Pharmaceutical Sciences; 2014; pp 1058–1070.
3. Washington, N.; Steele, R. J.; Jackson, S. J.; Bush, D.; Mason, J.; Gill, D. A.; Pitt, K.; Rawlins, D. A. Determination of baseline human nasal pH and the effect of intranasally administered buffers. *Int. J. Pharm.* **2000**, *198* (2), 139–146. DOI: 10.1016/S0378-5173(99)00442-1.

4. McShane, D.; Davies, J. C.; Davies, M. G.; Bush, A.; Geddes, D. M.; Alton, E. W. Airway surface pH in subjects with cystic fibrosis. *Eur. Respir. J.* **2003**, *21* (1), 37–42. DOI: 10.1183/09031936.03.00027603.
5. Kim, B. G.; Kim, J. H.; Kim, S. W.; Kim, S. W.; Jin, K. S.; Cho, J. H.; Kang, J. M.; Park, S. Y. Nasal pH in patients with chronic rhinosinusitis before and after endoscopic sinus surgery. *Am. J. Otolaryngol.* **2013**, *34* (5), 505–507. DOI: 10.1016/j.amjoto.2013.04.015.
6. Beule, A. G. Physiology and pathophysiology of respiratory mucosa of the nose and the paranasal sinuses. *GMS Curr. Top. Otorhinolaryngol. Head Neck Surg*. **2010**, *9*, Doc07. DOI: 10.3205/cto000071.
7. Lorin, M. I.; Gaerlan, P. F.; Mandel, I. D. Quantitative composition of nasal secretions in normal subjects. *J. Lab. Clin. Med*. **1972**, *80* (2), 275–281. .
8. Knowles, M. R.; Robinson, J. M.; Wood, R. E.; Pue, C. A.; Mentz, W. M.; Wager, G. C.; Gatzy, J. T.; Boucher, R. C. Ion composition of airway surface liquid of patients with cystic fibrosis as compared with normal and disease-control subjects. *J. Clin. Invest*. **1997**, *100* (10), 2588–2595. DOI: 10.1172/JCI119802.
9. Burke, W. The ionic composition of nasal fluid and its function. *Health*. **2014**, *6* (8), 720–728. DOI: 10.4236/health.2014.68093
10. Vanthanouvong, V.; Roomans, G. M. Methods for determining the composition of nasal fluid by x-ray microanalysis. *Microsc. Res. Tech*. **2004**, *63* (2), 122–128. DOI: 10.1002/jemt.20020.
11. Vanthanouvong, V.; Kozlova, I.; Johannesson, M.; Nääs, E.; Nordvall, S. L.; Dragomir, A.; Roomans, G. M. Composition of nasal airway surface liquid in cystic fibrosis and other airway diseases determined by x-ray microanalysis. *Microsc. Res. Tech*. **2006**, *69* (4), 271–276. DOI: 10.1002/jemt.20310.
12. Hull, J.; Skinner, W.; Robertson, C.; Phelan, P. Elemental content of airway surface liquid from infants with cystic fibrosis. *Am. J. Respir. Crit. Care Med*. **1998**, *157* (1), 10–14. DOI: 10.1164/ajrccm.157.1.9703045.
13. Klein, S.; Sakagami, M.; Li, S. K.; Warner, K. Testing the in vitro product performance of mucosal drug products: view of the USP Expert Panel. *Dissolut. Technol*. **2023**, *30* (4), 202–223. DOI: 10.14227/DT300423P202
14. Sakagami, M.; Fotaki, N. Testing the in vitro product performance of inhalation and nasal drug products: Views of the USP Expert Panel. *Dissolut. Technol*. **2024**, *31* (4), 162–172. DOI: 10.14227/DT310424P162.
15. Maiti, S.; Chakravorty, A.; Chowdhury, M. Gellan co-polysaccharide micellar solution of budesonide for allergic anti-rhinitis: an in vitro appraisal. *Int. J. Biol. Macromol*. **2014**, *68*, 241–246. DOI: 10.1016/j.ijbiomac.2014.05.003.
16. Li, C.; Li, C.; Liu, Z.; Li, Q.; Yan, X.; Liu, Y.; Lu, W. Enhancement in bioavailability of ketorolac tromethamine via intranasal in situ hydrogel based on poloxamer 407 and carrageenan. *Int. J. Pharm*. **2014**, *474* (1-2), 123–133. DOI: 10.1016/j.ijpharm.2014.08.023.
17. Karavasili, C.; Bouropoulos, N.; Sygellou, L.; Amanatiadou, E. P.; Vizirianakis, I. S.; Fatouros, D. G. PLGA/DPPC/ trimethylchitosan spray-dried microparticles for the nasal delivery of ropinirole hydrochloride: in vitro, ex vivo and cytocompatibility assessment. *Mater. Sci. Eng. C* **2016**, *59*, 1053–1062. DOI: 10.1016/j.msec.2015.11.028.
18. Wadell, C.; Björk, E.; Camber, O. Nasal drug delivery-evaluation of an in vitro model using porcine nasal mucosa. *Eur. J. Pharm. Sci*. **1999**, *7* (3), 197–206. DOI: 10.1016/S0928-0987(98)00023-2.
19. Wadell, C.; Björk, E.; Camber, O. Permeability of porcine nasal mucosa correlated with human nasal absorption. *Eur. J. Pharm. Sci*. **2003**, *18* (1), 47–53. DOI: 10.1016/S0928-0987(02)00240-3.
20. Huck, B. C.; Hartwig, O.; Biehl, A.; Schwarzkopf, K.; Wagner, C.; Loretz, B.; Murgia, X.; Lehr, C.-M. Macro-and microrheological properties of mucus surrogates in comparison to native intestinal and pulmonary mucus. *Biomacromolecules* **2019**, *20* (9), 3504–3512. DOI: 10.1021/acs.biomac.9b00780.
21. Nafee, N.; Forier, K.; Braeckmans, K.; Schneider, M. Mucus-penetrating solid lipid nanoparticles for the treatment of cystic fibrosis: Proof of concept, challenges and pitfalls. *Eur. J. Pharm. Biopharm*. **2018**, *124*, 125–137. DOI: 10.1016/j.ejpb.2017.12.017.
22. Leal, J.; Dong, T.; Taylor, A.; Siegrist, E.; Gao, F.; Smyth, H. D. C.; Ghosh, D. Mucus-penetrating phage-displayed peptides for improved transport across a mucus-like model. *Int. J. Pharm*. **2018**, *553* (1-2), 57–64. DOI: 10.1016/j.ijpharm.2018.09.055.
23. YYang, Y.; Tsifansky, M. D.; Wu, C.-J.; Yang, H. I.; Schmidt, G.; Yeo, Y. Inhalable antibiotic delivery using a dry powder co-delivering recombinant deoxyribonuclease and ciprofloxacin for treatment of cystic fibrosis. *Pharm. Res*. **2010**, *27* (1), 151–160. DOI: 10.1007/s11095-009-9991-2.
24. Lieleg, O.; Vladescu, I.; Ribbeck, K. Characterization of particle translocation through mucin hydrogels. *Biophys. J*. **2010**, *98* (9), 1782–1789. DOI: 10.1016/j.bpj.2010.01.012.
25. Do, T. Q.; Moshkani, S.; Castillo, P.; Anunta, S.; Pogosyan, A.; Cheung, A.; Marbois, B.; Faull, K. F.; Ernst, W.; Chiang, S. M.; et al. Lipids including cholesteryl linoleate and cholesteryl arachidonate contribute to the inherent antibacterial activity of human nasal fluid. *J. Immunol*. **2008**, *181* (6), 4177–4187. DOI: 10.4049/jimmunol.181.6.4177.
26. Khoury, S.; Gudziol, V.; Grégoire, S.; Cabaret, S.; Menzel, S.; Martine, L.; Mézière, E.; Soubeyre, V.; Thomas-Danguin, T.; Grosmaitre, X.; et al. Lipidomic profile of human nasal mucosa and associations with circulating fatty acids and olfactory deficiency. *Sci. Rep*. **2021**, *11* (1), 16771. DOI: 10.1038/S41598-021-93.
27. Son, Y. J.; McConville, J. T. Development of a standardized dissolution test method for inhaled pharmaceutical formulations. *Int. J. Pharm*. **2009**, *382* (1-2), 15–22. DOI: 10.1016/j.ijpharm.2009.07.034.
28. YYang, W.; Tam, J.; Miller, D. A.; Zhou, J.; McConville, J. T.; Johnston, K. P.; Williams, R. O., III. High bioavailability from nebulized itraconazole nanoparticle dispersions with

biocompatible stabilizers. *Int. J. Pharm*. **2008**, *361* (1-2), 177–188. DOI: 10.1016/j.ijpharm.2008.05.003.
29. Fell, G. L.; Nandivada, P.; Gura, K. M.; Puder, M. Intravenous lipid emulsions in parenteral nutrition. *Adv. Nutr*. **2015**, *6* (5), 600–610. DOI: 10.3945/an.115.009084.
30. *USP 43–38*. United States Pharmacopeia, 2020.
31. Riechelmann, H.; Deutschle, T.; Friemel, E.; Gross, H. J.; Bachem, M. Biological markers in nasal secretions. *Eur. Respir. J*. **2003**, *21* (4), 600–605. DOI: 10.1183/09031936.03.00072003.
32. Pulicharla, R.; Hegde, K.; Brar, S. K.; Surampalli, R. Y. Tetracyclines metal complexation: Significance and fate of mutual existence in the environment. *Environ. Pollut*. **2017**, *221*, 1–14. DOI: 10.1016/j.envpol.2016.12.017.
33. Rusu, A.; Buta, E. L. The development of third-generation tetracycline antibiotics and new perspectives. *Pharmaceutics* **2021**, *13* (12), 2085. DOI: 10.3390/pharmaceutics13122085.
34. Walden, D. M.; Khotimchenko, M.; Hou, H.; Chakravarty, K.; Varshney, J. Effects of magnesium, calcium, and aluminum chelation on fluoroquinolone absorption rate and bioavailability: a computational study. *Pharmaceutics* **2021**, *13* (5), 594. DOI: 10.3390/pharmaceutics13050594
35. Pitman, S. K.; Hoang, U. T. P.; Wi, C. H.; Alsheikh, M.; Hiner, D. A.; Percival, K. M. Revisiting oral fluoroquinolone and multivalent cation drug-drug interactions: are they still relevant? *Antibiotics* **2019**, *8* (3), 108. DOI: 10.3390/antibiotics8030108
36. Bharate, S. S.; Bharate, S. B.; Bajaj, A. N. Interactions and incompatibilities of pharmaceutical excipients with active pharmaceutical ingredients: a comprehensive review. *Int. J. Pharm. Excip*. **2010**, *1* (3).
37. Corfield, A. P. Mucins: a biologically relevant glycan barrier in mucosal protection. *Biochim. Biophys. Acta* **2015**, *1850* (1), 236–252. DOI: 10.1016/j.bbagen.2014.05.003.
38. Kaliner, M.; Marom, Z.; Patow, C.; Shelhamer, J. Human respiratory mucus. *J. Allergy Clin. Immunol*. **1984**, *73* (3), 318–323. DOI: 10.1016/0091-6749(84)90403-2.
39. Girod, S.; Zahm, J. M.; Plotkowski, C.; Beck, G.; Puchelle, E. Role of the physiochemical properties of mucus in the protection of the respiratory epithelium. *Eur. Respir. J*. **1992**, *5* (4), 477–487. DOI: 10.1183/09031936.93.05040477.
40. Song, D.; Cahn, D.; Duncan, G. A. Mucin biopolymers and their barrier function at airway surfaces. *Langmuir* **2020**, *36* (43), 12773–12783. DOI: 10.1021/acs.langmuir.0c02410.
41. Bej, R.; Haag, R. Mucus-inspired dynamic hydrogels: synthesis and future perspectives. *J. Am. Chem. Soc*. **2022**, *144* (44), 20137–20152. DOI: 10.1021/jacs.1c13547.
42. Falavigna, M.; Stein, P. C.; Flaten, G. E.; di Cagno, M. P. Impact of mucin on drug diffusion: development of a straightforward in vitro method for the determination of drug diffusivity in the presence of mucin. *Pharmaceutics* **2020**, *12* (2), 168. DOI: 10.3390/pharmaceutics12020168.
43. LLock, J. Y.; Carlson, T. L.; Carrier, R. L. Mucus models to evaluate the diffusion of drugs and particles. *Adv. Drug Deliv. Rev*. **2018**, *124*, 34–49. DOI: 10.1016/j.addr.2017.11.001.
44. Harding, S. E. Trends in muco-adhesive analysis. *Trends Food Sci. Technol*. **2006**, *17* (5), 255–262. DOI: 10.1016/j.tifs.2005.12.007.
45. Bayer, I. S. Recent advances in mucoadhesive interface materials, mucoadhesion characterization, and technologies. *Adv. Mater. Interfaces* **2022**, *9* (18), 2200211. DOI: 10.1002/admi.202200211.
46. Trenkel, M.; Scherließ, R. Nasal powder formulations: in-vitro characterisation of the impact of powders on nasal residence time and sensory effects. *Pharmaceutics* **2021**, *13* (3), 385. DOI: 10.3390/pharmaceutics13030385.
47. Gizurarson, S. The effect of cilia and the mucociliary clearance on successful drug delivery. *Biol. Pharm. Bull*. **2015**, *38* (4), 497–506. DOI: 10.1248/bpb.b14-00398.
48. Mardikasari, S. A.; Katona, G.; Csoka, I. Serum albumin in nasal drug delivery systems: exploring the role and application. *Pharmaceutics* **2024**, *16* (10), 1322. DOI: 10.3390/pharmaceutics16101322.
49. Chemicalize website. Chemaxon. Accessed Jul 5, 2024. chemicalize.com/welcome.
50. Yeap, Y. Y.; Lock, J.; Lerkvikarn, S.; Semin, T.; Nguyen, N.; Carrier, R. L. Intestinal mucus is capable of stabilizing supersaturation of poorly water-soluble drugs. *J. Control. Release* **2019**, *296*, 107–113. DOI: 10.1016/j.jconrel.2018.11.023.
51. Ugwoke, M. I.; Agu, R. U.; Verbeke, N.; Kinget, R. Nasal mucoadhesive drug delivery: background, applications, trends and future perspectives. *Adv. Drug Deliv. Rev*. **2005**, *57* (11), 1640–1665. DOI: 10.1016/j.addr.2005.07.009.

dx.doi.org/10.14227/DT320125P32

Investigation of Dissolution Failures of Metformin Delayed-Release Tablets During Formulation Design

Anumol Joseph[1], Sideequl Akbar Thencheeri[1], Rajkumar Malayandi[1*], Subramanian Natesan[2], and Ravichandiran Velayutham[1,2]

[1]Department of Pharmaceutics, National Institute of Pharmaceutical Education and Research Hajipur, Export Promotion Industrial Park, Hajipur, Bihar, India.
[2]Advanced Formulation Laboratory, Department of Pharmaceutics, National Institute of Pharmaceutical Education and Research Kolkata, Kolkata, India.

e-mail: rajkumar.ceutics@niperhajipur.ac.in

ABSTRACT

Introduction: Metformin HCl (MET) is widely used as an oral hypoglycemic agent for the management of type 2 diabetes mellitus. MET is contraindicated for renal compromised patients, so low-dose formulations are recommended for renal failure patients. The alternative approach is to minimize systemic exposure without compromising the therapeutic efficacy using novel site-targeted delayed-release (DR) MET tablets with low bioavailability. Proof-of-concept studies were conducted to achieve the desired targeted dissolution profile. The manufactured batches failed to attain the desired targeted drug release profile in both acidic as well as buffer media. **Methods:** MET DR tablets were manufactured using the wet granulation method and subjected to pharmaceutical characterization. The investigation of the dissolution failures was conducted using different orthogonal analytical techniques including Fourier transform-infrared spectroscopy (FT-IR), differential scanning calorimetry (DSC), scanning electron microscopy (SEM), and rheological studies. **Results:** DSC results revealed reduction in enthalpy values of the drug/polymer physical mixtures and subsequent change in peak transition time of a melting endothermic event. The rheological study results confirmed the loss of viscosity of the rate-controlling polymer in the presence of the drug. There could be a possible interaction between the free acid functional group of the polymer and cationic group of MET. **Conclusion:** Thermal and rheological analyses were useful analytical tools for investigating dissolution failures during formulation design, submission, and post-approval commercial manufacturing.

KEYWORDS: Metformin, diabetes, kidney failure, delayed release, tablets, dissolution

INTRODUCTION

Metformin HCl (MET) is the first-line agent for management of type 2 diabetes mellitus (T2DM), and it has been used for many decades (*1*). It gained approval from the United States Food and Drug Administration (US FDA) in 1994 and remains the most frequently prescribed medication, owing to its favorable risk-benefit ratio (*2*). MET was thought to exert its pharmacological effects by inhibiting hepatic gluconeogenesis and reducing glucose absorption from the intestine. Additionally, it enhances insulin sensitivity by promoting glucose uptake and utilization in peripheral tissues. The key benefits of MET therapy include its affordability, absence of weight gain and hypoglycemia, and reductions in triglycerides and low-density lipoprotein (LDL) levels (*3*).

MET therapy can be started with a low dose of 500 mg twice daily, and the maximum daily dose should not exceed 2000 mg. The marketed solid dosage forms of MET are immediate-release and extended-release tablets (*4*). Even though MET is the primary medication for treating T2DM, adhering to the therapy remains a clinical bottleneck. The predominant reasons for MET noncompliance include gastrointestinal (GI) side effects, such as nausea, vomiting, abdominal discomfort, and diarrhea, as well as deficiencies in vitamin B12 and folic acid (*5, 6*).

Use of MET is limited in conditions that lead to elevated blood drug concentration, such as chronic kidney disease (CKD), liver diseases, and cardiac/respiratory insufficiency. Elevated MET levels in the bloodstream can give rise to

*Corresponding author

a condition known as lactic acidosis; although rare, the high mortality rate is a clinical concern (*7, 8*). In those patients, the US FDA advises cautious use of MET at low doses. Before initiating therapy, the patient's glomerular filtration rate should be assessed because MET is contraindicated in those with a glomerular filtration rate below 30 mL/min/1.73 m^2; the maximum recommended dose of MET for these patients is 250–500 mg (*9*). The existing MET formulations, including immediate-release and extended-release tablets, release MET in the upper portion of the intestine, resulting in higher systemic exposure, increased GI side effects, and reduced tolerance in patients with CKD (*10*).

MET delayed-release (DR) tablets are designed to deliver the drug onto the site of action with low systemic exposure, which is suitable for patients with CKD. The design of MET DR tablets increases the drug concentration in the intestine region, so intestinal targeting of MET from DR tablets reduces systemic exposure without compromising therapeutic efficacy. MET DR tablets may offer lower bioavailability, fewer GI side effects, and increased tolerability in such patients (*10*). MET DR has been used in several clinical trials, including phase 1 and 2 studies (*11–13*). The DR formulations are designed and developed as enteric-coated tablets or multi-unit particulate systems with pH-dependent polymers (*14*). The drug release mechanism for these systems is the erosion of polymeric coating upon contact with intestinal pH (*15*). However, these drug delivery systems are classified as inconsistently highly variable dosage forms due to pharmacokinetic (PK) variability with unpredicted clinical outcomes (*16, 17*).

To address the PK variability, DR matrix tablets were designed and developed for initial proof-of-concept (POC) feasibility assessment. The POC formulations failed to attain the targeted dissolution profiles. This study aims to investigate the dissolution failures of prototype formulations using different orthogonal techniques.

METHODS

Materials

MET was purchased from Exmed Pharmaceuticals (Gujarat, India). Eudragit L 100 (EL 100) and eudragit S 100 (ES 100) were obtained from Central Drug House (P) Ltd. (Delhi, India). Carbopol 934 (CP 934) and magnesium stearate (MgS) were obtained from Sisco Research Laboratories Pvt. Ltd. (Mumbai, India). Microcrystalline cellulose (MCC) was supplied by Sigma Aldrich Chemicals Pvt. Ltd. (Bangalore, India). Aerosil 200 and isopropyl alcohol were purchased from Otto Chemie Pvt. Ltd. (Mumbai, India) and TCI Chemicals (Hyderabad, India), respectively. All other solvents and reagents were analytical grade purchased from Merck (India).

Ultraviolet Method for Estimation of Drug

Ultraviolet (UV) calibration curves for MET were generated in various media, including 0.1 N HCl, pH 6.8 phosphate buffer (PB), and water (*18*). Sample solutions were prepared through a serial dilution method using the appropriate solvents. The UV absorbance of these solutions was measured using a UV-visible spectrophotometer (model 1900i, Shimadzu, Kyoto, Japan) at 233 nm, and the designated λ_{max} and calibration curves were subsequently plotted.

Quality Target Product Profiles

Quality target product profiles (QTPPs) were synthesized for POC batches to get good physical, chemical, and microbial stability of both drug substances and drug products throughout their shelf life. Drug dissolution studies are one of the predictive tools used to understand the in-vivo drug release behavior as well as absorption of the formulations being developed. PK data and dissolution data for the drug products were obtained from the literature, and physiologically based PK models were developed for intravenous and oral formulations (*19*). The developed models were validated and convoluted to obtain the in-vitro release profile (unpublished data), which was set as the target drug profile for POC establishment.

Manufacturing of Metformin Delayed-Release (MET DR) Matrix Tablets

A 2^3-factorial design was used for the formulation of MET DR tablets. The concentration of EL 100/ES 100 (X_1), CP 934 (X_2), and MCC (X_3) were taken as independent variables. A total of 22 formulations (F1–F22) including six center batches were obtained using Microsoft Excel-based software. The composition details for all batches are provided in Table 1, and independent variables are listed in Table 2.

All MET DR matrix tablet formulations were prepared using the wet granulation technique. A total target batch size of 200 tablets was used for manufacturing of POC batches. An accurately weighed quantity of MET and other excipients were sifted through a no. 40 sieve and thoroughly mixed in a polybag for 10 min. This mixture was then wet-granulated with isopropyl alcohol as the granulating solvent. The time for granulation was 15 min, and granulating solvent was poured into the powder bed after 5 min. The obtained wet granules were milled using a mini multimill (Rimek, Karnavathi, Amdavad, India). The wet granules were passed through a no. 8 sieve and dried at 60 °C in a tray dryer (Bio SB Equipments, Kalyani, India)

Table 1. Composition of Metformin Delayed-Release Matrix Tablets

Batch	MET (mg)	EL 100 (mg)	ES 100 (mg)	CP 934 (mg)	MCC (mg)	MgS (mg)	Aerosil 200 (mg)	Total Weight (mg)
F1	600	233.33	-	233.33	133.33	6.66	3.33	1209.98
F2	600	233.33	-	233.33	0	6.66	3.33	1076.65
F3	600	166.66	-	166.66	0	6.66	3.33	943.31
F4	600	200	-	200.00	66.66	6.66	3.33	1076.65
F5	600	166.66	-	233.33	133.33	6.66	3.33	1143.31
F6	600	200	-	200.00	66.66	6.66	3.33	1076.65
F7	600	166.66	-	233.33	0	6.66	3.33	1009.98
F8	600	200	-	200.00	66.66	6.66	3.33	1076.65
F9	600	166.66	-	166.66	133.33	6.66	3.33	1076.64
F10	600	233.33	-	166.66	0	6.66	3.33	1009.98
F11	600	233.33	-	166.66	133.33	6.66	3.33	1143.31
F12	600	-	233.33	233.33	133.33	6.66	3.33	1209.98
F13	600	-	233.33	233.33	0	6.66	3.33	1076.65
F14	600	-	166.66	166.66	0	6.66	3.33	943.31
F15	600	-	200.00	200.00	66.66	6.66	3.33	1076.65
F16	600	-	166.66	233.33	133.33	6.66	3.33	1143.31
F17	600	-	200.00	200.00	66.66	6.66	3.33	1076.65
F18	600	-	166.66	233.33	0	6.66	3.33	1009.98
F19	600	-	200.00	200.00	66.66	6.66	3.33	1076.65
F20	600	-	166.66	166.66	133.33	6.66	3.33	1076.64
F21	600	-	233.33	166.66	0	6.66	3.33	1009.98
F22	600	-	233.33.	166.66	133.33	6.66	3.33	1143.31

Dash (-) indicates not applicable. MET: Metformin HCl; EL 100: eudragit L 100; ES 100: eudragit S 100; CP 934: carbopol 934; MCC: microcrystalline cellulose; MgS: magnesium stearate

for 2 h. The dried blend was passed through sieve no. 16 and lubricated with MgS and Aerosil 200. The resulting granules were compressed using an 8-station rotary tablet press (Proton Engineers, Ahmedabad, India).

Table 2. Independent Variables and Their Levels Affecting Metformin Dissolution

Variable	Level		
	+1	0	-1
EL 100/ES 100 (X_1) (mg)	233.33	200	166.66
CP 934 (X_2) (mg)	233.33	200	166.66
MCC (X_3) (mg)	133.33	66.66	0

EL 100: eudragit L 100; ES 100: eudragit S 100; CP 934: carbopol 934; MCC: microcrystalline cellulose.

Evaluation of Physical Properties

All MET DR matrix tablet formulations were evaluated for dimensions, weight variation, hardness, friability, and drug content. Weight variation and hardness were assessed using a tablet tester (Labindia, Mumbai, India), and friability testing was conducted using a Roche friabilator (Labindia). The drug content of all batches was determined using the developed UV-spectrophotometric method. All evaluation procedures for physical parameters and drug content were performed in accordance with the *Indian Pharmacopoeia* (*20*).

In-Vitro Drug Release Study

Given that MET is a pH-dependent high soluble drug, media composition, volume, and hydrodynamics have insignificant roles in establishing a biorelevant dissolution method. Two dissolution studies were carried out using a United States Pharmacopeia (USP) type 1 dissolution apparatus (Labindia).

The first dissolution test was performed in two stages (acid stage and buffer stage) with 900 mL of 0.1 N HCl and pH 6.8 PB, respectively, at 50 rpm and 37 ± 0.5 °C. Sampling occurred at 30, 60, and 120 min during the acid stage, with 5 mL samples collected and replaced with an equal volume of fresh medium to maintain sink conditions. Following the acid stage, the tablets were transferred to the buffer stage, and samples were collected at 3, 4, 6, 10, and 14 h. Collected samples were appropriately diluted and analyzed using a UV-visible spectrophotometer at λmax of 233 nm. The percentage of drug release was calculated and reported.

The second dissolution test was performed for all center point batches (F4, F6, F8, F15, F17, and F19) using pH 6.8 PB as the medium. Sampling intervals were 0.5, 1, 2, 3, 4, 5, and 6 h, and all other dissolution parameters were the same. These samples were similarly diluted as needed and assessed using a UV-visible spectrophotometer at 233 nm to determine the MET content.

Both dissolution procedures were carefully chosen based on the previous literature (*21*). The two-stage method was used to ensure the acid-resistant nature of the DR formulations as a fasting biopredictive tool. The second method was used as a quality control (QC) tool for routine current good manufacturing practices (cGMPs) in addition to the acid-resistant test stated in the pharmacopeia (*22*).

Investigation of Dissolution Failures

Dissolution failures of POC batches were investigated in the solid state as well as the solution state using different orthogonal analytical techniques. The physical composition of the drug and excipients were prepared using the reported method (*23*). Fourier transform-infrared spectroscopy (FT-IR), differential scanning calorimetry (DSC), and scanning electron microscopy (SEM) studies were performed to explore solid-state incompatibilities, and rheological studies were performed to explore solution-state incompatibilities that resulted in the dissolution failures.

Fourier Transform Infrared Spectroscopy (FT-IR)

The compatibility of MET with excipients was evaluated using FT-IR spectroscopy. MET and polymers were blended in a 3:1 ratio, resulting in various combinations: MET + EL 100, MET + ES 100, MET + CP 934, MET + CP 934 + EL 100, and MET + CP 934 + ES 100. For FT-IR analysis, each sample was divided into three portions for estimations on day 0, 15, and 30 and scanned using the FT-IR spectrometer (Spectrum Two with $LiTaO_3$ detector and UATR Two, Perkin Elmer, USA). The spectra of each sample were collected in 2-min intervals immediately after placing the sample on the diamond crystal (range of 400–4000 cm^{-1}, single scan mode, resolution of 4 cm^{-1}). A comparative analysis of all spectra was conducted to identify potential solid-state incompatibilities, focusing on principal drug peaks and presence or absence of peaks indicative of any polymer interactions.

Differential Scanning Calorimetry (DSC)

DSC studies were conducted on various samples including MET, CP 934, EL 100, ES 100, and combinations such as MET + CP 934, MET + EL 100, MET + ES 100, MET + CP 934 + EL 100, and MET + CP 934 + ES 100. The DSC instrument (DSC 2500, TA instruments, USA) consists of a finer air-cooling system, autosampler, and discover liquid nitrogen pump. Aluminium pans were used for DSC analysis (Tzero Pan model T 210503, Lot 160141; Tzero lid model T 210830, lot 170048). The samples were weighed in an aluminium pan, and the samples contained 3.0 mg equivalent of MET. DSC samples were analyzed with an analytical heating rate of 10 °C·min^{-1} at a nitrogen flow rate of 50 mL·min^{-1}. The temperature range of the experiments was kept between 25 °C and 250 °C. Differences in heat flow rate were measured against an empty pan as a reference.

Scanning Electron Microscopy (SEM)

The SEM analysis (GeminiSEM 360, ZEISS Microscopy, Jena, Germany) was performed on samples comprising individual drugs and excipients, as well as their physical mixtures. The physical mixtures included MET + EL 100, MET + ES 100, MET + CP 934, MET + CP 934 + EL 100, and MET + CP 934 + ES 100. These samples were affixed to carbon double-sided tape, subjected to gold-coating via sputtering, then analyzed using a 15-kV excitation voltage under a vacuum of 5–10 Torr.

Rheological Studies

The rheological studies characteristics of EL 100, ES 100, and CP 934 in matrix tablets and their impact on drug release were investigated using a modular compact rheometer (MCR 302e, cone plate CP40-1, Anton Paar, Hofheim, Germany) The study involved individual samples of MET, CP 934, EL 100, and ES 100, as well as their various mixtures in water and 0.1 N HCl. Viscosity was measured using a cone-plate system with a 40-mm diameter and 1° cone angle. The measurements were performed at both 25 °C and 37 °C, maintaining a constant shear rate of 20 s^{-1}. Over a duration of 0–600 s, a total of 20 measuring points were recorded to generate a viscosity versus time curve, and mean viscosity was used to evaluate the samples.

RESULTS AND DISCUSSION

The calibration curves obtained from UV-visible spectra, which were used for the quantification of the drug, are provided as supplemental material (Supplemental Figure 1).

All physical parameters were well within the acceptable regulatory limits, except drug content. Physical characteristics and drug content for all MET DR tablet formulations are also provided as supplemental material (Supplemental Table 1).

In-Vitro Drug Release Study

The target dissolution profile for the two-stage method was no more than 10% drug release in 2 h (acid stage),

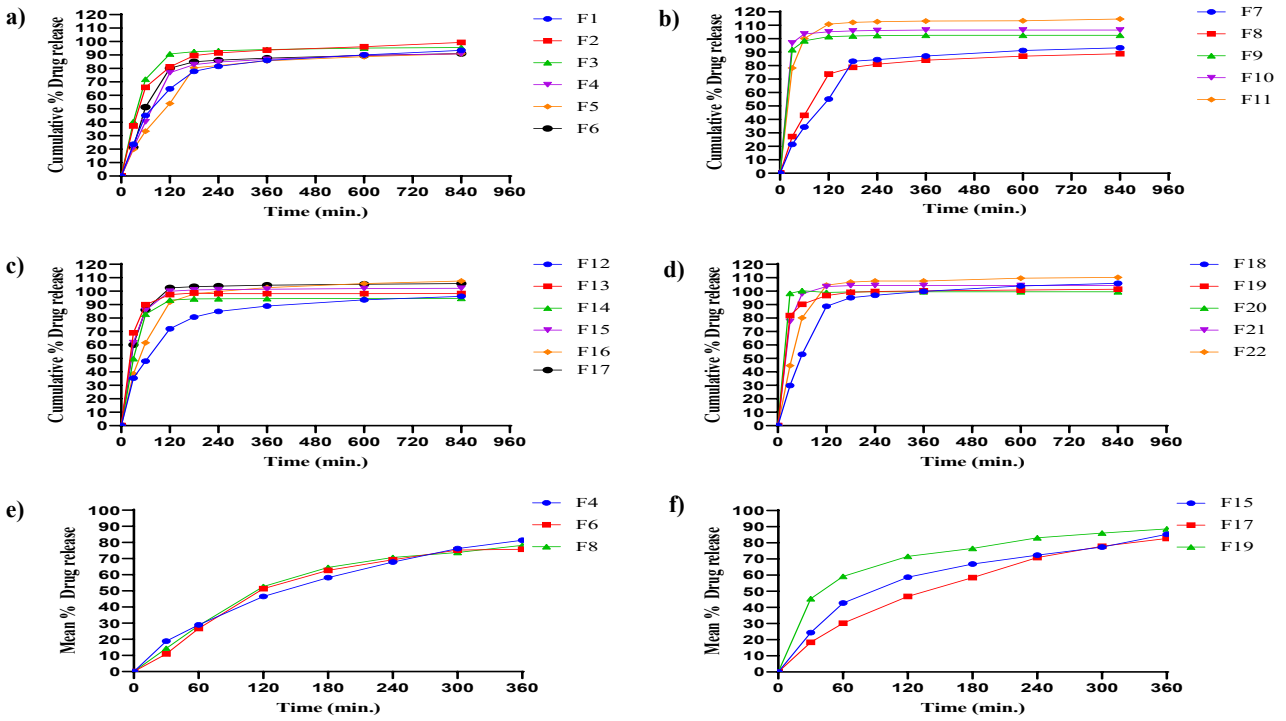

Figure 1 . Comparative in vitro dissolution profiles of Metformin delayed-release tablets; a–d: Formulations F1–F22 in acid and buffer stages; e and f: quality control batches (F4, F6, F8, F15, F17, F19) in 6.8 phosphate buffer alone.

40–60% in 3.5 h (buffer stage), and 90% in 4 h (*24*). The QC dissolution method specifications were obtained from USP (*22*). All MET DR tablet formulations were expected to exhibit no more than 10% drug release in the acid stage, followed by an immediate or controlled release in the buffer stage.

Figure 1 depicts the in-vitro drug release profiles of all batches with both dissolution methods. All batches failed to meet the target dissolution profile, exhibiting more than 10% drug release in 2 h. Specifically, batches with high concentrations of EL 100 (F10 and F11) showed 90% drug release, ES 100 showed more than 90% drug release, and high concentrations of CP 934 (F5 and F7) showed around 50% drug release in 2 h. MET is a strong base HCl salt, so the pH of the saturated solution is 6.9. This neutral pH is sufficient to form enough gelation for controlling drug release from the matrix, thus high CP 934 content in the formulation results in a slower release rate. Surprisingly, batches with EL 100 as a polymer exhibited a relatively slower release profile compared to those with ES 100.

The critical threshold pH for solubility is 6.0 and 7.0 for EL 100 and ES 100, respectively. Both EL 100 and ES 100 are anionic polymers; however, the free acid functional group is 50% for EL 100 and 33% for ES 100. In an enteric-coated system, the drug-polymer interaction is minimal due to the physical protection of seal coating. In a matrix system, the free acidic group in eudragit polymer creates the acidic microenvironment that facilitates faster drug release for basic drugs like MET. Hence, the faster drug release profile of ES 100 compared with EL 100 is due to pH of the acidic microenvironment. Moreover, the pH-dependent nature of enteric polymers results in low swelling and erosion in an acidic environment, thus resulting in poor matrix integrity. The critical dissolution pH of eudragit polymers has minimal impact on drug release. Therefore, alteration of the tablet matrix microenvironment pH should be considered when selecting rate-controlling polymers.

In the buffer stage alone (QC method), less than 50% of the drug was released within the initial 2 h. Notably, 90% drug release only occurred after 6 h, regardless of whether the batches contained EL 100 or ES 100. Differences in drug release profiles between acid-treated vs buffer-alone dissolution could be due to buffering capacity of dissolution media, which did not alter the microenvironmental pH significantly and hence had no meaningful impact on dissolution in the first 2 h. CP 934 was used as a rate-controlling polymer to control drug release in acidic conditions owing to favorable physicochemical properties such as ionization, pKa, and pH-dependent solubility (pKa of CP 934 is reported as

6.0, and an acidic polymer gets ionized and swells at a pH above 6.0). In acidic pH, these acrylic polymers are unionized and have low solubility and poor gel formation. In acidic pH, MET has relatively high solubility and CP 934 has poor gel formation, so the matrix erodes rapidly and fails to control drug release. However, in buffer-only dissolution studies, the extent of gel formation inside the matrix was relatively high due to buffering capacity, thus drug release was controlled better than in acid-stage dissolution studies.

Investigation of Dissolution Failures

FT-IR Study

Analysis of the spectra revealed that the peaks corresponding to the major functional groups of MET remained unchanged even in the presence of excipients (Table 3). This observation confirms the absence of solid-state interaction between the drug and polymers in the formulation without any physical and chemical instability issues during their shelf life. Results of the FT-IR study are provided in the supplemental material (Supplemental Figures 2–4).

Table 3. Peaks and Corresponding Functional Groups of MET HCl

Functional Group	Reported Wave Number Range	Observed Wave Number
N-H stretching	3100–3400	3370.2
N-H in-plane deformation	1530–1590	1556.97
N-H wagging	660–910	938.0
C=N stretching	1580–1685	1623.2
C-N stretching	1020–1220	1060.4
C-H	3095–3010	3146.5
CH_3 asymmetric deformation	1445–1475	1446.46

MET: metformin HCl; N: nitrogen; H: hydrogen; C: carbon.

DSC Study

DSC experiments are widely used in pre-formulation research (*25*). The DSC parameters for MET and its various formulations are detailed in Table 4, and DSC thermograms are provided in the supplemental material (Supplemental Figure 5). For MET, a peak transition temperature of 233.3 °C was recorded with an enthalpy of 324.2 J/g. The peak transition temperature decreased in all formulations, notably with the CP 934 + EL100 mixture. The enthalpy of MET for melting was significantly lower with all formulations. The CP 934 mixture had a low enthalpy value of 111.9 J/g compared with eudragit polymers. The formulation of MET with EL 100 resulted in the lowest enthalpy of 91.3 J/g. This observation agrees with results obtained from the dissolution studies. EL 100 formulations have a comparatively low extent of dissolution when compared with ES 100 formulations. This could be due to the relationship between melting enthalpy and free energy, and the associated free energy used for dissolution of the drug from the matrix.

The significant reduction in enthalpy of the granules might reveal the thermodynamic characteristics of the granules, which may be used to investigate dissolution failures during POC selection and life-cycle management.

Table 4. Parameters from DSC Thermogram Studies

Sample	Onset of MET (°C)	Peak of MET (°C)	Enthalpy of MET (J/g)
MET	231.26	233.23	324.24
MET + CP 934	228.08	231.21	111.86
MET + EL 100	224.34	231.11	194.73
MET + ES 100	229.74	232.85	161.00
MET + CP 934 + EL 100	228.20	228.84	91.27
MET + CP 934 + ES 100	226.84	231.34	98.45

DSC: differential scanning calorimetry; MET: Metformin HCl; CP 934: carbopol 934; EL 100: eudragit L 100; ES 100: eudragit S 100.

SEM Study

Figure 2 displays the photomicrographs of MET, CP 934, EL 100, ES 100, and their physical mixtures. The results indicate that both MET and the excipients maintain their distinct morphologies, with no evidence of morphological changes in the MET crystals and excipients. This observation reconfirms the solid-state stability of the physical mixtures.

Results obtained from FTIR and SEM confirmed the absence of solid-state interaction. Therefore, interactions between the drug and polymer are solution-state mediated, and the pH plays an important role in the matrix integrity.

Rheological Studies

Viscosity studies were carried out in the solution state, whereas dissolution studies were performed in saturated conditions. Swelling of the polymer during the initial stage of dissolution restricts the entry of dissolution media inside the tablet matrix core, thereby retaining the matrix integrity. Viscosity measurements are useful for the initial assessment of dissolution behavior of the formulation during the design stage and for retrospective investigation of batch failures.

Table 5 presents the viscosity values for all MET DR formulation samples. The results confirmed that the viscosity of CP 934 in 0.1 N HCl is lower than that in water. This is due to the higher degree of ionization and swelling of CP 934 in the presence of water when compared with 0.1 N HCl.

Temperature has a significant effect on the viscosity of the

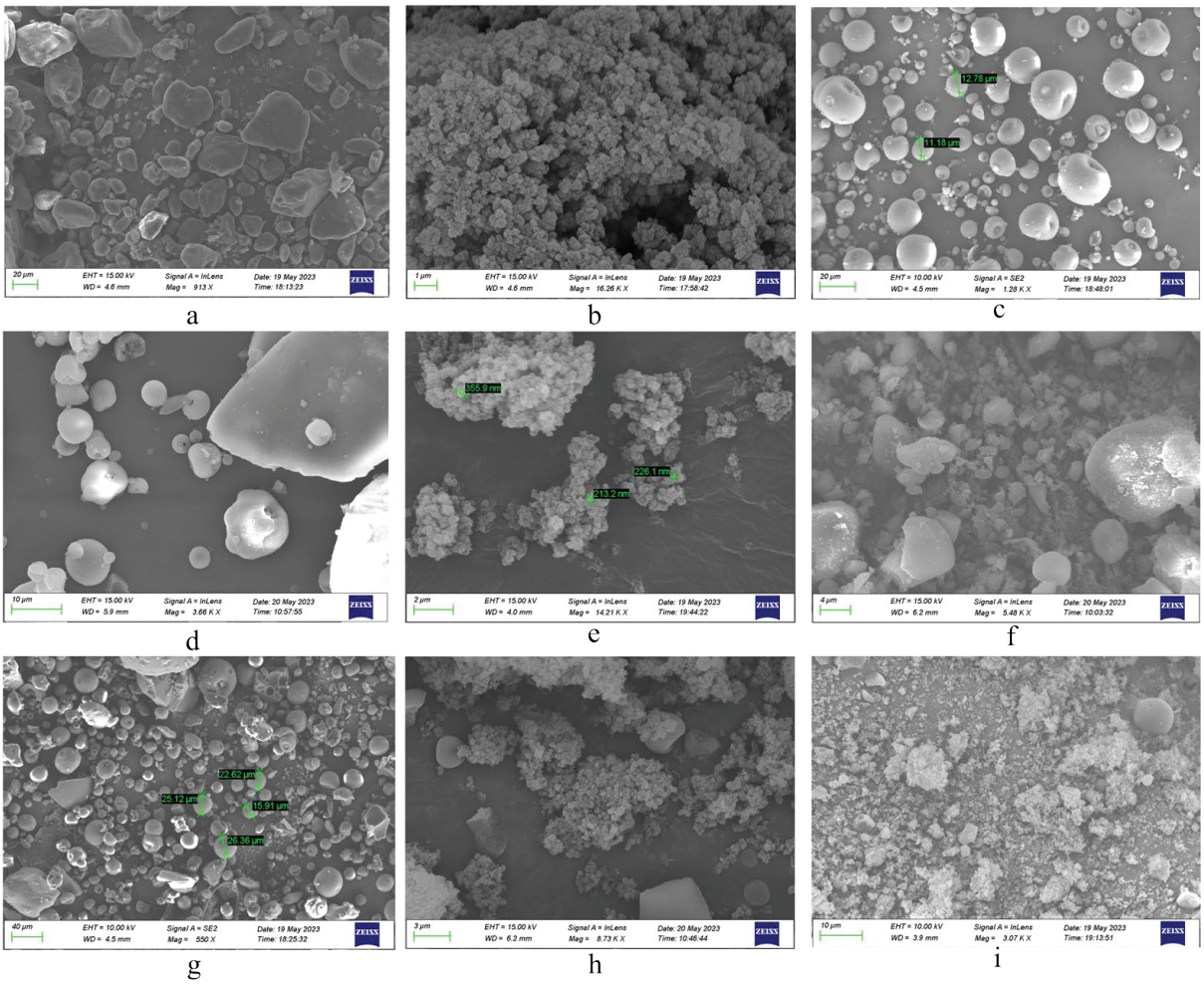

*Figure 2. Scanning electron microscopy images of Metformin delayed-release tablets; (**a**) MET, (**b**) CP 934, (**c**) EL 100, (**d**) ES 100, (**e**) MET + CP 934, (**f**) MET + EL 100, (**g**) MET + ES 100, (**h**) MET + CP 934 + EL 100, and (**i**) MET + CP 934 + ES 100.*
MET: Metformin HCl; EL 100: eudragit L 100; ES 100: eudragit S 100; CP 934: carbopol 934.

Table 5. Viscosity of MET formulations in Water and 0.1 N HCl

Sample	Viscosity (mPaS)			
	Water		0.1 N HCl	
	25 °C	37 °C	25 °C	37 °C
0.3% MET	0.9 ± 0.045	0.7 ± 0.005	0.74 ± 0.05	0.78 ± 0.05
0.3% CP 934	23.7 ± 1.6	38.0 ± 1.6	1.4 ± 0.09	3.9 ± 0.36
0.1% EL 100	0.8 ± 0.02	0.7 ± 0.05	0.82 ± 0.006	0.82 ± 0.03
0.1% ES 100	0.76 ± 0.02	0.78 ± 0.01	-	-
0.3% MET + 0.3% CP 934	1.7 ± 0.09	1.9 ± 0.07	2.4 ± 0.78	5.4 ± 1.18
0.3% MET + 0.1% EL 100	1.7 ± 0.29	1.8 ± 0.29	0.85 ± 0.04	0.72 ± 0.04
0.3% MET + 0.3% CP 934 + 0.1% EL 100	5.0 ± 0.38	4.6 ± 0.7	5.8 ± 1.25	12.9 ± 3.06
0.3% MET + 0.3% CP 934 + 0.1% ES 100	4.5 ± 0.02	3.5 ± 0.4	-	-
0.3% CP 934 + 0.1% EL 100	19.4 ± 1.5	13.5 ± 0.52	1.8 ± 0.12	4.2 ± 1.6
0.3% CP 934 + 0.1% ES 100	27.6 ± 1.16	30.03 ± 1.8	1.53 ± 0.06	1.6 ± 0.43

Values are expressed at mean ± SD.
Dash (-) indicates not applicable; MET: Metformin HCl; CP 934: Carbopol 934; EL 100: Eudragit L 100; ES 100: Eudragit S 100.

solution. The viscosity of CP 934 gel in a physiologically relevant temperature of 37 °C is higher than the ambient conditions. Although there is an insignificant difference in the pH of water vs saturated solution of MET (6.4 vs 6.9), the presence of MET has a significant reduction in the viscosity of CP 934 due to the presence of a cationic reactive functional group of MET. Hence, the use of CP 934 as a rate-limiting polymer in matrix tablets is questionable.

The data obtained from viscosity measurement of eudragit polymers revealed that there was no role of these polymers in gelation. The probable mechanism for controlling drug release could be their pH-dependent erosion pattern; however, the free acidic group might influence drug release rather than pH-dependent ionization and erosion. A key observation from this investigation was that EL 100 reduced viscosity of the CP 934 polymer, whereas ES 100 increased viscosity. Although the CP 934 + EL 100 mixture had less viscosity than the CP 934 + ES 100 mixture, the rate of dissolution was faster with ES 100 than with EL 100. This indicates that rather than viscosity, the free acid function group plays an important role in the faster dissolution profile of ES 100 compared with EL 100.

The presence of MET in the polymeric system reduced viscosity to a greater extent (i.e., 27.6 vs 4.5 cps). These data reveal that the solution-state physical interaction between the drug and excipients reduced viscosity of the polymeric formulations. This could be due to the presence of a strong cation, which interacts with the free anionic group in both eudragit and CP 934 polymers. This interaction resulted in lowering of not only viscosity but also gelation of polymer, subsequently reducing matrix integrity.

Moreover, MET has high aqueous solubility and ionization. The solubility of MET is high in acidic pH, which favors dissolution. The presence of free acidic functional groups and their influence on microenvironmental matrix pH further enhances the solubility of MET in a matrix, hence causing the observed dissolution failures in DR tablets.

CONCLUSION

This study aimed to investigate observed dissolution failures of POC batches of MET DR tablets. DSC studies revealed a difference in peak endothermic transition temperature and associated enthalpy, indicating a possible interaction between the drug and polymers, which may have caused dissolution failure. Polymers such as CP 934, EL 100, and ES 100 have free acidic functional groups that interact with MET in the solution state, resulting in lower enthalpy values, which may be linked with higher free energy for solubilization and lack of controlled drug release. Rheological studies revealed reduced viscosity of these polymers in the presence of MET, indicating failure to provide sufficient gel strength to control the release profile. This study demonstrated that DSC and rheological studies are useful for the investigation of dissolution failures in design stage optimization as well as commercial manufacturing.

SUPPLEMENTAL MATERIAL

Supplemental material is available for this article and may be requested by contacting the corresponding author.

ACKNOWLEDGMENTS

The authors acknowledge the contribution of Dr. Lalit Kumar (Assistant Professor, National Institute of Pharmaceutical Education and Research Hajipur) for his critical review and comments and support from the Department of Pharmaceuticals, Ministry of Chemicals and Fertilizers, Government of India.

DISCLOSURES

The authors received no financial support for this work and have no conflicts of interest.

REFERENCES

1. Abutaleb, M. H. Diabetes mellitus-an overview. *Pharm. Pharmacol. Int. J.* **2016**, *4* (5), 406–411. DOI: 10.15406/ppij.2016.04.00087.
2. Singh, N.; Kesherwani, R.; Tiwari, A. K.; Patel, D. K. A review on diabetes mellitus. *Pharma Innov. J.* **2016**, *5* (7), 36–40.
3. Brunetti, L.; Kalabalik, J. Management of type-2 diabetes mellitus in adults: focus on individualizing non-insulin therapies. *P&T* **2012**, *37* (12), 687–696.
4. Luna, B.; Feinglos, M. N. Oral agents in the management of type 2 diabetes mellitus. *Am. Fam. Physician* **2001**, *63* (9), 1747–1756.
5. Christofides, E. A. Practical insights into improving adherence to metformin therapy in patients with type 2 diabetes. *Clin. Diabetes* **2019**, *37* (3), 234–241. DOI: 10.2337/cd18-0063.
6. Bailey, C. J.; Turner, R. C. Metformin. *N. Engl. J. Med*. **1996**, *334* (9), 574–579. DOI: 10.1056/NEJM199602293340906.
7. Nasri, H.; Rafieian-Kopaei, M. Metformin: Current knowledge. *J. Res. Med. Sci*. **2014**, *19* (7), 658–664.
8. Shurrab, N. T.; Arafa, E. S. A. Metformin: A review of its therapeutic efficacy and adverse effects. *Obes. Med*. **2020**, *17*, 100186. DOI: 10.1016/j.obmed.2020.100186.
9. FDA Drug Safety Communication: FDA revises warnings regarding use of the diabetes medicine metformin in certain patients with reduced kidney function. United States Food and Drug Administration, April 8, 2016.
10. Scheen, A. J. Will delayed release metformin provide better management of diabetes type 2? *Expert Opin. Pharmacother*.

2016, *17* (5), 627–630. DOI: 10.1517/14656566.2016.1149166.

11. Buse, J. B.; DeFronzo, R. A.; Rosenstock, J.; Kim, T.; Burns, C.; Skare, S.; Baron, A.; Fineman, M. The primary glucose-lowering effect of metformin resides in the gut, not the circulation: Results from short-term pharmacokinetic and 12-week dose-ranging studies. *Diabetes Care* **2016**, *39* (2), 198–205. DOI: 10.2337/dc15-0488.
12. Henry, R. R.; Frias, J. P.; Walsh, B.; Skare, S.; Hemming, J.; Burns, C.; Bicsak, T. A.; Baron, A.; Fineman, M. Improved glycemic control with minimal systemic metformin exposure: Effects of metformin delayed-release (metformin DR) targeting the lower bowel over 16 weeks in a randomized trial in subjects with type 2 diabetes. *PLoS One* **2018**, *13* (9), e0203946. DOI: 10.1371/journal.pone.0203946.
13. DeFronzo, R. A.; Buse, J. B.; Kim, T.; Burns, C.; Skare, S.; Baron, A.; Fineman, M. Once-daily delayed-release metformin lowers plasma glucose and enhances fasting and postprandial GLP-1 and PYY: results from two randomised trials. *Diabetologia* **2016**, *59* (8), 1645–1654. DOI: 10.1007/s00125-016-3992-6.
14. Singh, B. N. Modified-release solid formulations for colonic delivery. *Recent Pat. Drug Deliv. Formul*. **2007**, *1* (1), 53–63. DOI: 10.2174/187221107779814122.
15. Wathoni, N.; Nguyen, A. N.; Rusdin, A.; Umar, A. K.; Mohammed, A. F. A.; Motoyama, K.; Joni, I. M.; Muchtaridi, M. Enteric-coated strategies in colorectal cancer nanoparticle drug delivery system. *Drug Des. Devel. Ther*. **2020**, *14*, 4387–4405. DOI: 10.2147/DDDT.S273612.
16. Asghar, L. F. A.; Chandran, S. Design and evaluation of matrix base with sigmoidal release profile for colon-specific delivery using a combination of Eudragit and non-ionic cellulose ether polymers. *Drug Deliv. Transl. Res*. **2011**, *1* (2), 132–146. DOI: 10.1007/s13346-011-0016-4.
17. Asghar, L. F. A.; Chandran, S. Design and evaluation of matrices of Eudragit with polycarbophil and carbopol for colon-specific delivery. *J. Drug Target*. **2008**, *16* (10), 741–757. DOI: 10.1080/10611860802473345.
18. Dange, Y. D.; Honmane, S. M.; Bhinge, S. D.; Salunkhe, V. R.; Jadge, D. R. Development and validation of uv-spectrophotometric method for estimation of metformin in bulk and tablet dosage form. *Indian J Pharm Educ Res*. **2017**, *51* (4S), S754–S760. DOI: 10.5530/ijper.51.4s.109.
19. Malayandi, R.; Joseph, A.; Akbar, S.; Natesan, S.; Velayutham, R. Application of mechanistic pharmacokinetic model for the optimization of metformin delayed release dosage form for intestinal targeting. *Ind. J. Pharm. Edu. Res*. **2024**, *58* (3), 991–1001.
20. Metformin hydrochloride prolonged release tablets. In *Indian Pharmacopoeia, 9th ed. 2022*; pp. 2876–2878.
21. Eaga, C.; Mantri, S.; Malayandi, R.; Kondamudi, P. K.; Chakraborty, S.; Raju, S. V. N.; Aggarwal, D. Establishing postprandial bio-equivalency and IVIVC for generic metformin sustained release small sized tablets. *J. Pharm. Investig*. **2014**, *44* (3), 197–204. DOI: 10.1007/s40005-013-0115-y.
22. Metformin hydrochloride extended-release tablets. The United States Pharmacopoeial Convention, Sep 1, 2010.
23. Bhise, S.; Rajkumar, M. Effect of HPMC on solubility and dissolution of carbamazepine form III in simulated gastrointestinal fluids. *Asian J. Pharm*. **2008**, *2* (1), 38. DOI: 10.4103/0973-8398.41564.
24. Baron, A. D.; Fineman, M. S.; Beeley, N. R. A. Compositions and methods for treating metabolic disorders. U.S. Patent 20150065578A1, Jan 5, 2013. patents.google.com/patent/US20150065578A1/en (accessed Jan 20, 2025).
25. Malayandi, R.; Malgave, A.; Gaikwad, V.; Peraman, R.; Aishwarya, D.; Ravichandiran, V. Understanding the influence of thermal cycles on the stability of metformin HCl in presence of sitagliptin phosphate monohydrate and polyvinyl alcohol. *J. Therm. Anal. Calorim*. **2023**, *148* (2023), 13321–13335. DOI: 10.1007/s10973-023-12639-7.

ERWEKA

Live online demos:
sales@erweka.com

www.erweka.com

Dissolution Online System

Disso.NET controlled dissolution online testing with precise UV-Vis analysis

- IPC or PVP pump
- Several available photometers
- Full Disso.NET control
- Extensive report functionalities
- Upgradeable at any time
- User management with Active Directory connection

ERWEKA GmbH
Pittlerstraße 45
Langen
Germany

sales@erweka.com
+49 6103 92426-200

part of VERDER scientific

dx.doi.org/10.14227/DT320125P42

Hypothetical Plasma Concentration-Time Profiles of Amiodarone-HCl From In Vitro Release Data

José Raúl Medina-López[1*] and Felipe Dino Reyes-Ramírez[1]
[1]*Departamento Sistemas Biológicos, Metropolitan Automomous University-Xochimilco, Mexico City, Mexico.*

e-mail: rmlopez@correo.xoc.uam.mx

ABSTRACT

Introduction: This study aimed to determine the hypothetical plasma concentrations of amiodarone-HCl (AMD) formulations from in vitro release data. **Methods**: The dissolution method used a United States Pharmacopeia paddle apparatus at 75 rpm. The dissolution medium was 0.1 N hydrochloric acid (pH 1.2) with 1% sodium dodecyl sulfate (SDS), pH 4.5 acetate buffer with 1% SDS, and pH 6.8 phosphate buffer with 1% SDS. The reference and a generic tablet formulation (200 mg) were studied. Dissolution parameters were compared and analyzed for statistically significant differences (e.g., mean dissolution time, cumulative drug release, dissolution efficiency, and others). Hypothetical plasma concentration-time profiles were calculated with dissolution data and reported pharmacokinetic information for AMD using a convolution approach. **Results**: Similarity factor (f_2) analysis indicated that all dissolution profiles were similar; however, some statistically significant differences ($p < 0.05$) were noted in the dissolution parameters. According to established criteria of $R^2_{adjusted}$ and AIC values, AMD dissolution behavior was best explained by the Weibull model. **Conclusion**: Dissolution data for the reference formulation at pH 4.5 gave an acceptable prediction error for C_{max} and $AUC_{0\text{-}inf}$.

KEYWORDS: Amiodarone-HCl (AMD), plasma concentrations, prediction error, dissolution

INTRODUCTION

Amiodarone-HCl (AMD) tablets are suggested for the treatment of life-threating ventricular and supraventricular arrhythmias and atrial fibrillation (*1*, *2*). AMD is a compound with low solubility (0.35 mg/mL), high permeability, high protein binding (> 96%), and moderate bioavailability (35–65%) (*1*). Food promotes drug absorption, which improves bioavailability (*3*). AMD is classified by the Biopharmaceutic Classification System (BCS) as a class 2 drug (*2*, *4*).

Dissolution studies are an important tool to establish the release performance of poorly soluble drugs. Compendial quality control tests for AMD tablets are performed using United States Pharmacopeia (USP) apparatus 2 (paddle) at an agitation rate of 100 rpm with 1000 mL of 1% sodium dodecyl sulfate (SDS); and no less than 80% of the dose should dissolve in 60 min (*5*).

In vitro release of AMD formulations has been studied by some authors. For context, in Brazil, Rubim et al reported increased solubility and dissolution of AMD with a solid dispersion technique using an inclusion complex containing a hydrophilic carrier (dissolution media were distilled water and aqueous solution of pH 1.2, 4.5, and 6.8 in USP apparatus 2 at 50 rpm for 90 min) (*6*). In Australia, Ngo et al compared different commercially available AMD tablets using a high-performance liquid chromatography (HPLC) method (USP apparatus 2 at 100 rpm for 90 min with 1000 mL 1% SDS in water); however, only the innovator and two out of three generic (multisource) drug

*Corresponding author

products achieved the pharmacopeial criterion (Q ≥ 80% in 30 min) (*4*).

Considering the variability observed in bioequivalence studies, the narrow therapeutic ratio, and diversity in dissolution results, the objective of the present study was to determine the release behavior of AMD tablets available to the Mexican population, considering biowaiver conditions, and to estimate the hypothetical plasma concentration-time profiles (*3*, *7*).

METHODS

AMD tablets of the reference formulation (Cordarone 200 mg, Sanofi-Aventis de México, S.A. de C.V. Ocoyoacac, Mexico; lot no. BMXA002; expiration October 2023) and a generic formulation (Braxan 200 mg, Armstrong Laboratorios de México, S.A. de C.V. Mexico City, Mexico; lot no. 21080057; expiration Oct 2023) were tested. HCl, methanol, acetic acid, sodium acetate, sodium hydroxide pellets, and sodium phosphate monobasic crystals were supplied by J.T.Baker-Mexico. AMD reference substance was provided by Sigma-Aldrich Co. (St. Louis, MO, USA).

Dissolution Test

Dissolution of AMD tablets was tested under biowaiver conditions using a paddle apparatus (Sotax, AT7-Smart) at 75 rpm with 900 mL of 0.1 N hydrochloric acid (pH 1.2) and 1% SDS, pH 4.5 acetate buffer with 1% SDS, and pH 6.8 phosphate buffer with 1% SDS at 37.0 ± 0.5 °C. Automatic samples were taken every 5 min over 60 min (n = 12) and filtered with glass fiber prefilters (Millipore, Ireland). Dissolution medium was recirculated after each sample was taken. AMD was identified spectrophotometrically at 243 nm (Lambda 25, PerkinElmer, USA) with the support of solutions with known concentrations ranging from 1.87–30 µg/mL.

Data Analysis

To compare AMD dissolution curves for the reference and generic product, the difference (f_1) and similarity (f_2) factors at each pH level were calculated. Acceptable f_1 values are 0–15, and f_2 values are 50 – 100 (*8*).

The cumulative amount of drug released at the last sampling time (Q_{60}), mean dissolution time (MDT), and dissolution efficiency (DE) were computed and compared using the Student's t-test. AMD release behavior was studied with following mathematical models: Makoid-Banakar, Weibull, Korsmeyer-Peppas, Peppas-Sahlin, and logistic. The adjusted determination coefficient ($R^2_{adjusted}$) and Akaike Information Criterion (AIC) were used to determine the best fitting model (*9*).

The f_1, f_2, DE, and MDT values were computed by the Excel add-in DDSolver (*10*). Time to dissolve 50% of dose ($t_{50\%}$) was calculated with a hyperbola model.

Simulation of Plasma Concentrations

AMD plasma levels were calculated with a convolution method as follows (*11*). Pharmacokinetic parameters were used to build drug levels in function of time, including elimination rate (k_e), bioavailability factor (F), and volume of distribution (V_d) (*12*, *13*). Peak plasmatic level (C_{max}) and area under the plasma concentration-time curve from zero time to infinity ($AUC_{0\text{-}inf}$) were computed using the Excel add-in PKSolver (*14*).

Data for the reference AMD formulation in humans were then used to calculate prediction error (%PE; < 10% is optimal) for pharmacokinetic parameters C_{max} and $AUC_{0\text{-}inf}$ according to the following equation (*3*, *15*):

$$\%\mathrm{PE} = \frac{(observed\ value - predicted\ value)}{observed\ value} \times 100.$$

RESULTS AND DISCUSSION

Dissolution profiles for reference and generic AMD formulations are shown in Figure 1. Despite addition of SDS in all dissolution media, less than 50% was released from both formulations at pH 6.8 after 60 min. As shown in Table 1, both formulations had similar dissolution profiles based on f_2 values. Statistical differences (p < 0.05) in Q_{60} and DE values were noted at all pH levels, but MDT significant differences were only found at pH 1.2. Comparison of dissolution profiles by DE and MDT was made to facilitate results comparison; the differences had no physiological meaning (*16*).

These findings agree with results reported by others. Awan et al studied dissolution profiles of AMD powder, a commercial product (Cordarone 200 mg), and a test formulation (AMD nanocrystals equivalent to 200 mg) using the paddle apparatus at 100 rpm with 900 mL of distilled water and pH 1.2 and pH 6.8 buffer solutions. In all dissolution media, less than 60% of the AMD marketed product dissolved after 90 min (*17*).

Wang et al carried out an in vitro study of commercial tablets (Cordarone 200 mg) and AMD inside an inclusion complex using the paddle apparatus at 50 rpm with 900 mL of distilled water, pH 1.0 HCl, and pH 4.5 and 6.8 buffer solutions. After 90 min with the commercial formulation, limited release (< 10%) was observed at pH 1.0 and 6.8 ,

and less than 50% was released with distilled water; at pH 4.5, 84.2% of dissolved drug was released (*18*).

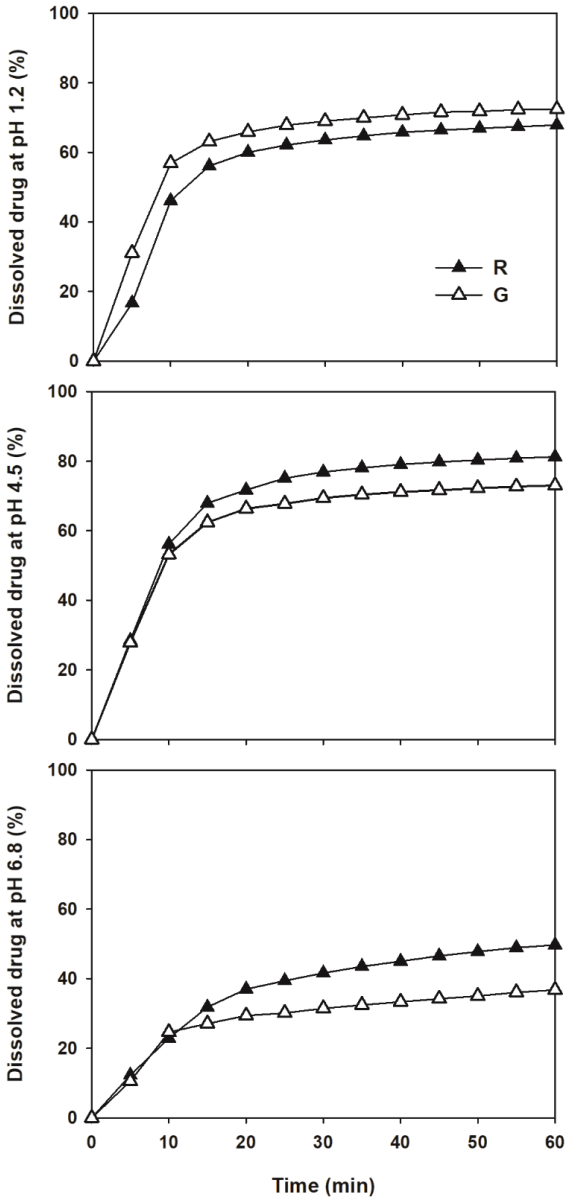

Figure 1. Dissolution profiles (mean values, n = 12) of reference and generic AMD tablet formulations using the paddle apparatus at 75 rpm with 900 mL of 0.1 N HCl (pH 1.2) + 1% SDS; acetate buffer + 1% SDS (pH 4.5); and phosphate buffer + 1% SDS (pH 6.8).
AMD: amiodarone-HCl; G: generic; HCl: hydrochloric acid; R: reference; SDS: sodium dodecyl sulfate.

Kinetic modeling of in vitro drug release for the reference and generic AMD formulations is shown in Table 2. According to established criteria of $R^2_{adjusted}$ and AIC values, AMD dissolution behavior was best explained by the Weibull model, which emphasizes the S-shaped profile (*19*). The $R^2_{adjusted}$ and AIC values were selected due observed differences in other parameters (*20*). The model-dependent parameter $t_{50\%}$ (derived from adjustment to hyperbola model) and Td (derived from Weibull function) are listed in Table 1; statistical differences ($p < 0.05$) were noted for $t_{50\%}$ but not Td. Because a low Q_{60} value (< 50%) was observed for AMD at pH 6.8, the $t_{50\%}$ and Td values were not calculated.

After applying the convolution methodology and adjusting the predicted AMD plasma levels to a compartment model, the main pharmacokinetic parameter values were calculated. The hypothetical C_{max} and $AUC_{0\text{-}inf}$ were associated with human data to calculate prediction error (*3*). As shown in Table 3, prediction error was less than 10% for both parameters of the reference formulation only at pH 4.5. Therefore, using the paddle apparatus at 75 rpm with pH 4.5 acetate buffer and 1% SDS was suitable to predict AMD plasma concentrations similar to those reported in an in vivo study. The predicted dissolution profiles obtained with in vitro release data at pH 4.5 are shown in Figure 2. The convolution method was validated, as PE < 10% was found (*15*).

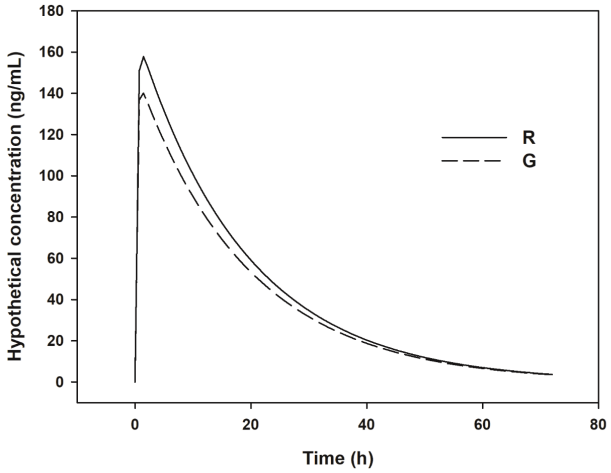

Figure 2. Hypothetical plasma concentration-time profiles of reference and generic AMD tablet formulations calculated with dissolution data at pH 4.5.
AMD: amiodarone-HCl; G: generic; HCl: hydrochloric acid; R: reference; SDS: sodium dodecyl sulfate.

It is preferable to establish an in vitro-in vivo correlation (IVIVC) for formulations with absorption limited by the dissolution rate (*21*). Two studies of IVIVC using AMD tablets have been reported (*2, 22*). The first was a recompilation of three bioequivalence studies of a reference and three commercial generic products using the paddle apparatus at 75 rpm with 0.1 M pH 5.0 acetate buffer and 1% SDS for 120 min; a poor level B correlation was found ($p = 0.033$) (*2*). The authors concluded that bioequivalence studies should be carried out to ensure the interchangeability of AMD multi-source formulations (*2*). The second IVIVC study estimated

Table 1. Dissolution Parameters of Reference and Generic AMD Tablet Formulations

pH[a]	Product	f_1	f_2	Q_{60} (%)[b]	DE (%)[b]	MDT (min) [b]	$t_{50\%}$ (min) [b]	Td (min) [b]
1.2	R	-	-	67.85 ± 0.89	55.80 ± 0.68	10.62 ± 0.36	14.70 ± 0.55	17.41 ± 7.25
	G	11.20	57.91	72.42 ± 0.29*	62.18 ± 0.58*	8.48 ± 0.44*	9.15 ± 0.59*	8.60 ± 1.12
4.5	R	-	-	81.25 ± 0.68	67.90 ± 0.77	9.85 ± 0.37	8.55 ± 0.37	9.23 ± 0.34
	G	9.05	58.83	73.03 ± 0.78*	61.79 ± 0.72*	9.23 ± 0.25	10.33 ± 0.54*	8.64 ± 0.31
6.8	R	-	-	49.67 ± 0.05	36.78 ± 0.54	15.44 ± 0.72	†	†
	G	23.34	50.94	36.73 ± 0.47*	28.54 ± 0.46*	13.38 ± 0.36	†	†

[a]Dissolution media: 0.1 N HCl (pH 1.2) + 1% SDS; acetate buffer + 1% SDS (pH 4.5); phosphate buffer + 1% SDS (pH 6.8).
[b]Values are expressed as mean ± standard error (n = 12).
**p < 0.05; †Less than 50% of dissolved drug was found at 60 min, so no $t_{50\%}$ and Td data were calculated.*
AMD: amiodarone-HCl; DE: dissolution efficiency; f_1: dissimilarity factor; f_2: similarity factor; G: generic; HCl: hydrochloric acid; MDT: mean dissolution time; R: reference, SDS: sodium dodecyl sulfate; Td: derived from the Weibull model.

Table 2. Kinetic Release Parameters of Reference and Generic AMD Tablet Formulations (n = 12).

pH[a]	Parameter	Product	Makoid-Banakar	Peppas-Sahlin	Korsmeyer-Peppas	Logistic	Weibull
1.2	$R^2_{adjusted}$	R	0.8941	0.8709	0.7268	0.8226	0.9977
		G	0.8986	0.8901	0.7350	0.8289	0.9974
	AIC	R	68.94	71.40	79.97	74.32	17.38
		G	62.83	63.78	73.79	67.77	17.88
4.5	$R^2_{adjusted}$	R	0.9270	0.9143	0.7692	0.8226	0.9953
		G	0.9142	0.9050	0.7521	0.8559	0.9954
	AIC	R	65.06	67.32	79.16	74.32	33.24
		G	63.42	65.22	76.12	69.44	16.01
6.8	$R^2_{adjusted}$	R	0.9756	0.9700	0.9412	0.9096	0.9901
		G	0.9017	0.8978	0.8455	0.8667	0.9906
	AIC	R	42.86	45.20	58.97	51.46	30.95
		G	51.19	51.66	55.95	54.08	22.27

[a]Dissolution media: 0.1 N HCl (pH 1.2) + 1% SDS; acetate buffer + 1% SDS (pH 4.5); phosphate buffer + 1% SDS (pH 6.8).
AIC: Akaike Information Criterion; AMD: amiodarone-HCl; G: generic; HCl: hydrochloric acid; R: reference; SDS: sodium dodecyl sulfate.

AMD in vivo release from the pharmacokinetics of desethylamiodarone (active metabolite) using reference tablets (200 mg) and a test formulation and the paddle apparatus at 100 rpm with 1000 mL of SDS (10 mg/mL) in ultrapure water (*22*). After 60 min, both formulations released the complete dose. The authors proposed the correlation of in vitro drug release with pharmacokinetics of the active metabolite (*22*).

Given the variability with AMD's in vitro and in vivo performance, more research is needed to establish an IVIVC for AMD tablets. This work simulated AMD plasma levels from dissolution data obtained under biowaiver conditions. The proposed methodology is an option to facilitate biopharmaceutical evaluation of AMD oral dosage forms and ensure interchangeability between different formulations.

Table 3. Prediction Error Parameters of Reference and Generic AMD Tablet Formulations.

Product	Parameter	pH[a]		
		1.2	4.5	6.8
R	C_{max}	21.75%	7.02%	41.06%
	$AUC_{0\text{-}inf}$	20.94%	4.96%	43.31%
G	C_{max}	18.64%	17.14%	57.18%
	$AUC_{0\text{-}inf}$	14.49%	14.21%	57.65%

[a]Dissolution media: 0.1 N HCl (pH 1.2) + 1% SDS; acetate buffer + 1% SDS (pH 4.5); phosphate buffer + 1% SDS (pH 6.8).
AMD: amiodarone-HCl; G: generic; HCl: hydrochloric acid; SDS: sodium dodecyl sulfate; R: reference.

CONCLUSION

The present study proposes hypothetical AMD plasma concentration-time profiles on the basis of in vitro release data for the reference and a generic formulation obtained

under biowaiver conditions. The best conditions to simulate in vivo behavior were obtained with data from the reference formulation using USP apparatus 2 at 75 rpm with 900 mL of pH 4.5 acetate buffer and 1% SDS. At this pH, significant differences in model-independent parameters Q_{60} and DE as well as the model-dependent parameter $t_{50\%}$ reflected differences in the proposed in vivo behavior of the generic formulation. The dissolution conditions and proposed predictions can be used to support better design of AMD formulations.

DISCLOSURES

The authors received no financial support for this work and have no conflicts of interest.

REFERENCES

1. Rodríguez-Fernández, K.; Gras-Colomer, E.; Climente-Martí, M.; Mangas-Sanjuán, V.; Merino-Sanjuán, M. Pharmacometric characterization of entero-hepatic circulation processes of orally administered formulations of amiodarone under complex binding kinetics. *Eur. J. Pharm. Sci*. **2022**, *174*, 106198. DOI: 10.1016/j.ejps.2022.106198
2. Emami, J. Comparative in vitro and in vivo evaluation of three tablet formulations of amiodarone in healthy subjects. *Daru J. Pharm. Sci*. **2010**, *18* (3), 193–199.
3. dos Santos Filho, H. O.; Ilha, J. O.; Silva, L. C.; Borges, A.; Mendes, G. D.; De Nucci, G. Comparative bioavailability study with two amiodarone tablet formulations administered with and without food in healthy subjects. *Arzneimittelforschung* **2007**, *57* (9), 582–590. DOI: 10.1055/s-0031-1296653.
4. Ngo, S. N. T.; Barnes, T. Is there variability in drug release and physical characteristics of amiodarone chloride from different commercially available tablets? Possible therapeutic implications. *Int. J. Pharm. Pract*. **2010**, *18* (4), 245–248. DOI: 10.1111/j.2042-7174.2010.00037.x.
5. Amiodarone Tablets Monograph. In *USP 43-NF 38*. The United States Pharmacopeial Convention, Inc., 2021.
6. Rubim, A. M.; Rubenick, J. B.; Gregolin, E.; Laporta, L. V.; Leitenberg, R.; Rolim, C. M. B. Amiodarone hydrochloride: enhancement of solubility and dissolution rate by solid dispersion technique. *Braz. J. Pharm. Sci*. **2015**, *51* (4), 957–966. DOI: 10.1590/S1984-82502015000400021.
7. Atanasova, I.; Terziivanov, D. Evaluation of average bioequivalence of two oral formulations of amiodarone hydrochloride after single administration to healthy volunteers. *Clin. Drug Investig*. **2001**, *21* (6), 423–428. DOI: 10.2165/00044011-200121060-00005.
8. Moore, J. W.; Flanner, H. H. Mathematical comparison of dissolution profiles. *Pharm. Technol*. **1996**, *20* (6), 64–74.
9. Yuksel, N.; Kanik, A. E.; Baykara, T. Comparison of in vitro dissolution profiles by ANOVA-based, model-dependent and -independent methods. *Int. J. Pharm*. **2000**, *209* (1-2), 57–67. DOI: 10.1016/S0378-5173(00)00554-8.
10. Zhang, Y.; Huo, M.; Zhou, J.; Zou, A.; Li, W.; Yao, C.; Xie, S. DDSolver: an add-in program for modeling and comparison of drug dissolution profiles. *AAPS J*. **2010**, *12* (3), 263–271. DOI: 10.1208/s12248-010-9185-1.
11. Qureshi, S. A. In vitro–in vivo correlation (IVIVC) and determining drug concentrations in blood from dissolution testing – a simple and practical approach. *Open Drug Deliv. J*. **2010**, *4*, 38–47. DOI: 10.2174/1874126601004010038.
12. Mujović, N.; Dobrev, D.; Marinković, M.; Russo, V.; Potpara, T. S. The role of amiodarone in contemporary management of complex cardiac arrhythmias. *Pharmacol. Res*. **2020**, *151*, 104521. DOI: 10.1016/j.phrs.2019.104521.
13. Marrafa, J. M. Amiodarone. In *Encyclopedia of Toxicology*; Wexler, P., Ed.; Academic Press, 2014; pp 197–199. DOI: 10.1016/B978-0-12-386454-3.00691-6
14. Zhang, Y.; Huo, M.; Zhou, J.; Xie, S. PKSolver: An add-in program for pharmacokinetic and pharmacodynamic data analysis in Microsoft Excel. *Comput. Methods Programs Biomed*. **2010**, *99* (3), 306–314. DOI: 10.1016/j.cmpb.2010.01.007.
15. Rastogi, V.; Yadav, P.; Lal, N.; Rastogi, P.; Singh, B. K.; Verma, N.; Verma, A. Mathematical prediction of pharmacokinetic parameters-an in-vitro approach for investigating pharmaceutical products for IVIVC. *Future J. Pharm. Sci*. **2018**, *4* (2), 175–184. DOI: 10.1016/j.fjps.2018.03.001.
16. Adams, E.; Coomans, D.; Smeyers-Verbeke, J.; Massart, D. L. Non-linear mixed effects models for the evaluation of dissolution profiles. *Int. J. Pharm*. **2002**, *240* (1-2), 37–53. DOI: 10.1016/S0378-5173(02)00127-8.
17. Awan, A. M.; Farid, A.; Shah, S. U.; Khan, D.; Ur Rehman, F.; Dar, M. J.; Iftikhar, T.; Ghazanfar, S.; Galanakis, C. M.; Alamri, A. S.; et al. Nanocrystals-mediated oral drug delivery: enhanced bioavailability of amiodarone. *Pharmaceutics* **2022**, *14* (6), 1300. DOI: 10.3390/pharmaceutics14061300.
18. Wang, D.; Chen, G.; Ren, L. Preparation and characterization of the sulfobutylether-β-cyclodextrin inclusion complex of amiodarone hydrochloride with enhanced oral bioavailability in fasted state. *AAPS PharmSciTech* **2017**, *18* (5), 1526–1535. DOI: 10.1208/s12249-016-0646-4.
19. Ilango, K. B.; Kavimani, S. A systematic review of mathematical models of pharmaceutical dosage forms. *Int. J. Curr. Pharm. Rev. Res* **2015**, *6* (1), 59–70.
20. Das, S. K.; Chakraborty, S.; Bose, A.; Rajabalaya, R.; Khanam, J. Effects of the preparation technique on the physicochemical characteristics and dissolution improvement of ketoprofen-SDE7-β-CD binary inclusion complexes. *Colloids Surf. A Physicochem. Eng. Asp*. **2021**, *611* (2), 125775. DOI: 10.1016/j.colsurfa.2020.125775.
21. Tuszyński, P. K.; Szlęk, J.; Polak, S.; Jachowicz, R.; Mendyk, A. In vitro-in vivo correlation (IVIVC): from current achievements

towards the future. *Dissolut. Technol*. **2018**, *25* (3), 20–27. DOI: 10.14227/DT250318P20.

22. Shleghm, M. R.; Mircioiu, C.; Voicu, V. A.; Mircioiu, I.; Anuta, V. Estimation of the in vivo release of amiodarone from the pharmacokinetics of its active metabolite and correlation with its in vitro release. *Front. Pharmacol*. **2021**, *11*, 621667. DOI: 10.3389/fphar.2020.621667.

The Handbook of DISSOLUTION TESTING

Industry experts Bryan Crist, Vivian Gray and Royal Hanson have completely updated the *Handbook of Dissolution Testing* for today's pharmaceutical executive, laboratory manager, and bench chemist.

The 4th edition builds on the teachings of the first three editions (1982, 1991, and 2004), with everything you need to know about modern dissolution testing, including:

- Updates on USP, FDA, and international compendial requirements; method development and challenges; testing of special dosage forms; controlling variables and apparatus qualification; automation; treatment of aberrant data; sources of errors and failures, and more!
- Three new chapters on compendial and regulatory guidances, method validation, and Good Manufacturing Practices in the dissolution laboratory.
- Extensive reference notes on hundreds of topics for further insight.
- Handy comprehensive appendix of dissolution resources and websites.
- Foreword by Jennifer B. Dressman, PhD, preeminent researcher and teacher in the field of pharmaceutics and dissolution.
- The go-to reference for the working practitioner, the 4th edition *Handbook of Dissolution Testing* is a must-have for every dissolution lab worldwide!

Available April 15, 2025! Order online at www.dissolutiontech.com.

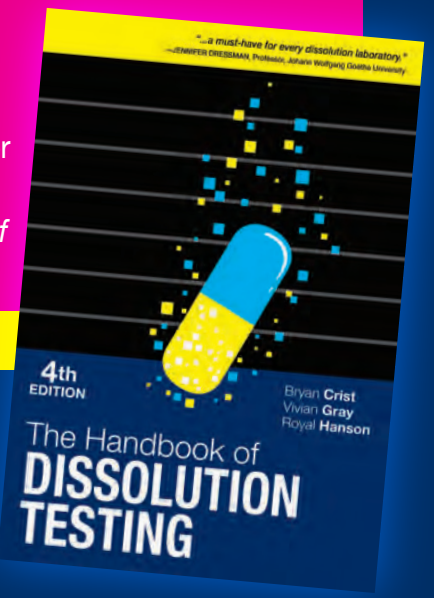

4th EDITION

Bryan **Crist**
President of DissoAssist Consulting based in Wilmington, NC

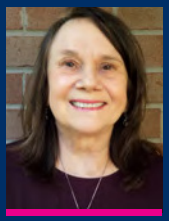

Vivian **Gray**
President of V.A. Gray Consulting based in Hockessin, DE

Royal **Hanson**
Former Chairman, President, and CEO of Hanson Research Corp.

AVAILABLE APRIL 15, 2025

Dissolution Technologies, Incorporated
9 Yorkridge Trail • Hockessin, DE 19707 USA

© 2024 Royal A. Hanson • All rights reserved.

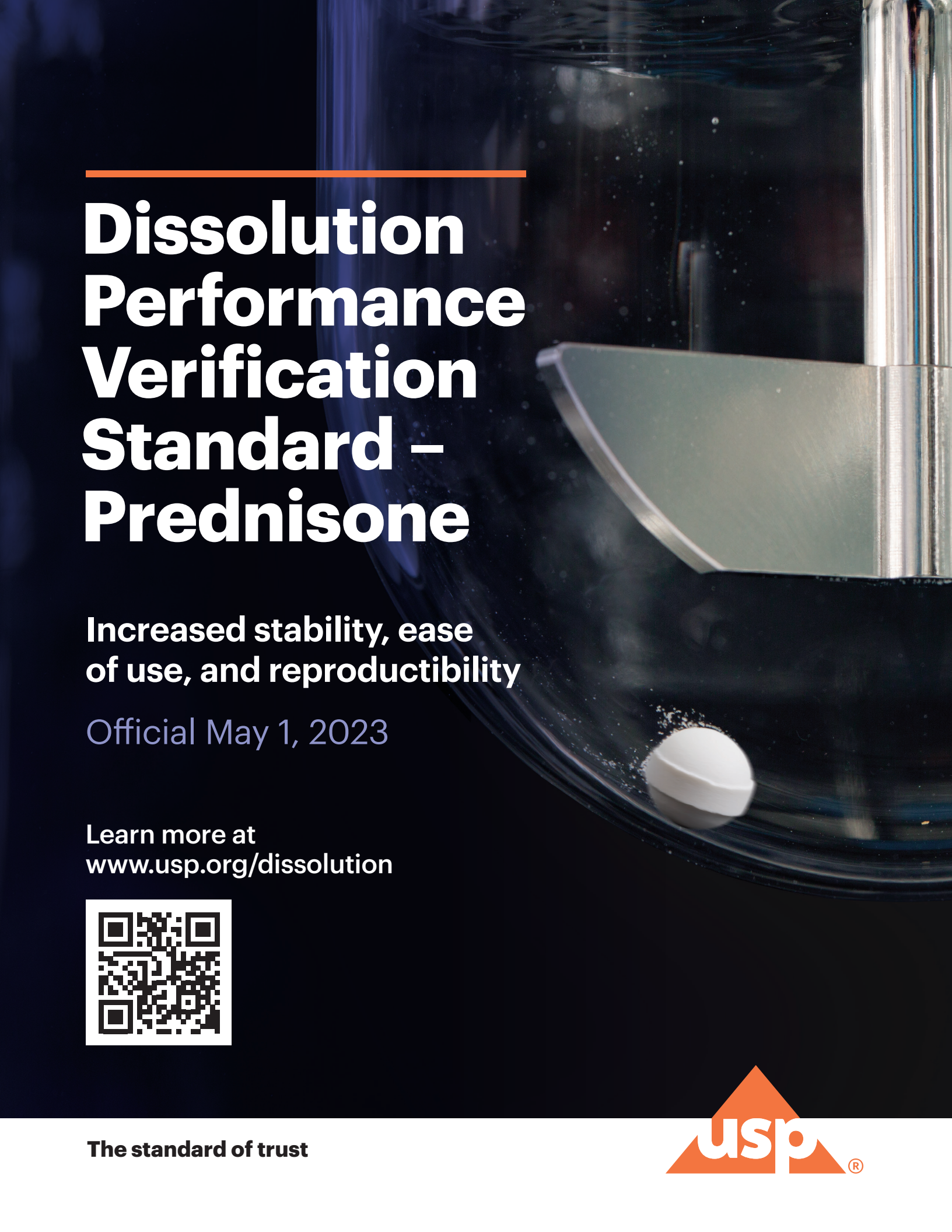

Dissolution Performance Verification Standard – Prednisone

Increased stability, ease of use, and reproductibility

Official May 1, 2023

Learn more at
www.usp.org/dissolution

The standard of trust

usp®

dx.doi.org/10.14227/DT320125P50

Q+A Question & Answer Section

*The following questions have been submitted by readers of Dissolution Technologies. Margareth R. Marques, Ph.D., and Mark Liddell, Ph.D., United States Pharmacopeia (USP), authored responses to each of the questions. *Note: These are opinions and interpretations of the authors and are not necessarily the official viewpoints of the USP. E-mail for correspondence: mrm@usp.org.*

Q What is the definition of automated systems in dissolution?

A Automated systems in dissolution are considered where any of the test steps, i.e., sampling, tablet drop, filtration, etc., are performed by programable robotic or motorized equipment and not manually. Although there are fully automated dissolution systems available, in practice, most automated dissolution systems are actually semi-automated, that is, some portion of the dissolution test is performed by an analyst or technician. There are some automated systems where only the sampling (removal of the appropriate volume of the solution under test from the dissolution vessel) is done by automation. This situation is very useful when collecting dissolution profiles and when sampling is done with high frequency. There are also some automated systems where all the steps are done by programmable equipment, including introduction of the sample, sample collection, filtration, transfer to the analytical instrument to perform the quantitative determination (e.g., spectrophotometer, HPLC, etc.), calculating the percent drug release, and reporting the data. For more information see the USP general chapter <1092> The Dissolution Procedure – Development and Validation.

Q Does USP have any recommendations about how much time can pass from when the DPVS – Prednisone tablet is removed from the blister and sachet until it is placed in the vessel or basket to start the Performance Verification Test (PVT)?

A The intention of the push-through blister packaging is that the dosage form can be pushed directly through the foil backing and dropped into the vessel when using USP apparatus 2 (paddle). When using USP apparatus 1 (basket), the tablet should be placed in the basket and the dissolution test should be conducted as soon as possible to avoid contamination and adsorption of moisture.

Q Regarding the calculation tool for the Performance Verification Test (PVT), how many decimal places should be provided for the data that the user enters in the calculation tool?

A The calculation tool allows the inclusion of individual dissolution values with up to three decimal places. Data entered with more than three decimal places will be rounded using USP rounding rules. At the end of the calculation of the geometric mean (GM) and % coefficient of variation (%CV), the final result is rounded and expressed with the same number of decimal places as the acceptance criteria. Rounding data early, i.e., before the final calculation of the GM and %CV, may lead to failing results.

Q Regarding the disintegration test, is it correct to consider the average disintegration time from the six vessels?

A Although the acceptance criteria for disintegration is specific to the type of dosage form, in all cases the disintegration time specification is intended to be applied to each individual dosage unit.

Q Is it necessary to validate repeatability and intermediate precision when validating dissolution tests?

A Yes, repeatability and intermediate precision need to be validated. Both are key validation parameters needed to evaluate the precision of the dissolution method. To evaluate the repeatability, a single analyst will evaluate several replicate of the standard, spiked placebo, and/or standard addition solutions and use the data to calculate the standard deviation. For intermediate precision,

one approach is to have 2 or more analysts perform the dissolution procedure and use the data to estimate the magnitude of random and controlled sources of variance. This is typically done later in the dissolution method validation after other validation parameters have been confirmed for the method in question. See USP general chapter <1092> The Dissolution Procedure – Development and Validation for more details.

Q Is it possible to validate repeatability using only the finished product, running the dissolution test with six units and only one determination per vessel?

A Yes, it is possible, but it will depend on the type of data that is being collected for the dissolution method in question. According to general chapter <1092>, the ICH guidance, "Q2(R1) Validation of Analytical Procedures: Text and Methodology," recommends that repeatability should be assessed using a minimum of nine determinations covering the specified range for the procedure (i.e., three concentrations and three replicates of each concentration) or using a minimum of six determinations at 100% of the test concentration. Consequently, if collecting dissolution profile data, satisfying the minimum of nine determinations is fairly straightforward. If collecting single point dissolution data, you would most likely need to use infinity dissolution data and collect multiple samples from a single vessel to have a minimum of six determinations at 100% of the concentration.

Q With respect to the validation of intermediate precision in the dissolution testing of extended-release dosage forms, in describing the acceptance criterion as indicated in the USP general chapter <1092> The Dissolution Procedure – Development and Validation, it is stated: "A typical acceptance criterion for ruggedness is that the difference in the mean value for dissolution results between any two conditions, using the same dosage strength, does not exceed an absolute 10% at time points with < 85% dissolved and does not exceed 5% for time points NLT 85%. Acceptance criteria may be product specific, and other statistical tests and limits may be used." Does the established criterion refer to the last sampling time for extended-release pharmaceutical formulations? Is it possible to demonstrate only with the last sampling time?

A Because extended-release formulations are likely to require the percent release to be evaluated at multiple time points throughout the dissolution profile, the evaluation of intermediate precision for this type of dosage form shall be performed considering the entire dissolution profile. This is a requirement because the variability may be different at each time point and tends to decrease at later times in the dissolution profile.

Q If a stability study fails to meet the tier I specification at a specified interval due to crosslinking in the gelatin capsules (e.g., at 9 months), must the remainder of the stability study (months 12–18) be conducted for tier I specifications at each timepoint? Or can a tier II analysis be performed immediately?

A USP general chapter <1094> Capsules – Dissolution Testing and Related Quality Attributes, under Dissolution Testing During Stability Studies states: "The dissolution testing during stability studies should start with the dissolution medium stated in the original method without the enzyme. When evidence of cross-linking is found, the test should be done with the addition of the appropriate enzyme to the dissolution medium. As cross-linking does not stop even if the agent causing it is removed, from this time point forward, the dissolution testing of stability samples can be carried out with the addition of the appropriate enzyme to the dissolution medium."

Q+A

Every issue of *Dissolution Technologies* features a Question and Answer section. This section is designed to address general dissolution questions submitted by our readers.

Please send your questions to:
Attn: Q&A
9 Yorkridge Trail, Hockessin, DE 19707
Email: vagray@rcn.com
Submit via our website:
www.dissolutiontech.com

Calendar of Events

March 11–12, 2025
M-CERSI workshop "Role of In Vitro Dissolution Studies for Predictive Insight into In Vivo Performance and Biopharmaceutics Risk Mitigation"
Location: Universities at Shady Grove (USG; Rockville, Maryland), Building II
Registration: www.pharmacy.umaryland.edu/centers/cersievents/2025dissolution

March 19–20, 2025
USP Workshop: Hot Topics in Orally Inhaled and Nasal Drug Product Performance Testing
Location: USP, Rockville, MD, USA
Registration: https://www.usp.org/events-training/usp-workshop-hot-topics-in-quality-assessment-of-orally-inhaled-and-nasal-drug-products

March 27–28, 2025
Implementing FDA's IVPT Guidance Recommendations: A Step-by-Step Illustration
Location: Universities at Shady Grove (USG; Rockville, MD, USA), Building II and on Zoom
Registration: Eventbrite

May 15, 2025
Automation for Your Dissolution Workflow
Location: DDG Online Meeting at 10:30 am ET
Registration: https://www.agilent.com/chem/dissolution-webinars

July 14–18, 2025
Controlled Release Society 2024 Annual Meeting
Location: Philadelphia, PA, USA

September 18, 2025
Small-Volume and Other Specialty Accessories
Location: DDG Online Meeting at 10:30 am ET
Registration: https://www.agilent.com/chem/dissolution-webinars

November 9–12, 2025
PharmSci 360 AAPS Meeting
Location: Henry B. Gonzalez Convention Center, San Antonio, TX, USA
For information, visit https://www.aaps.org/pharmsci/annual-meeting

November 16–18, 2025
Eastern Analytical Symposium and Exhibition
Location: Crowne Plaza Princeton-Conference Center, Plainsboro, NJ, USA
For information, visit eas.org

On Demand Events

- ***Fiber Optic UV: Better Dissolution Testing On Demand***
  https://www.distekinc.com/watch/fiber-optic-uv-better-dissolution-testing/
- ***Advances in In Vitro Bioequivalence Assessment for Topical Products Part 2***
  https://youtu.be/iqphypToHZ0?feature=shared
- ***Ocular Administration (OCAT™) in GastroPlus® On Demand***
  https://www.simulations-plus.com/events/gastroplus-additional-dosage-routes-workshop-ocular-administration-ocat-virtual/

- ***Oral Cavity Administration (OCCAT™) in GastroPlus® On Demand***
  https://www.simulations-plus.com/events/gastroplus-additional-dosage-routes-workshop-oral-cavity-administration-occat-virtual/
- ***Pulmonary Administration (PCAT™) in GastroPlus® On Demand***
  https://www.simulations-plus.com/events/gastroplus-additional-dosage-routes-workshop-pulmonary-administration-pcat-virtual/
- ***GastroPlus® ADR – 4 Course Bundle (TCAT™ / OCAT™ / OCCAT™ / PCAT™)***
  https://www.simulations-plus.com/events/gastroplus-adr-4-course-bundle-tcat-ocat-occat-pcat/
- ***GastroPlus® ADR – 5 Course Bundle (TCAT™ / OCAT™ / OCCAT™ / PCAT™ / Injectables)***
  https://www.simulations-plus.com/events/gastroplus-adr-5-course-bundle-tcat-ocat-occat-pcat-injectables/
- ***Transdermal Administration (TCAT™) in GastroPlus®***
  https://www.simulations-plus.com/events/gastroplus-additional-dosage-routes-workshop-transdermal-administration-tcat-virtual/
- ***Injectables (IM, SQ, IA) in GastroPlus® Including Biologics and LAIs***
  https://www.simulations-plus.com/events/gastroplus-additional-dosage-routes-workshop-injectables-incl-lai-biologics-virtual/
- ***GastroPlus® X Tutorial Series***
  https://www.simulations-plus.com/events/gastroplus-x-tutorial-series/
- ***Complimentary Introduction to GastroPlus® for up to v.9.9***
  https://www.simulations-plus.com/events/complimentary-introduction-to-gastroplus-v-9-9/
- ***Complimentary Introduction to GPX™***
  https://www.simulations-plus.com/events/complimentary-introduction-to-gpx/

EASTERN ANALYTICAL SYMPOSIUM & EXPOSITION

Across The Analytical Spectrum: Diversity of Scientific Ideas

November 17-19, 2025

Crown Plaza Princeton - Conference Center
Plainsboro, NJ

→ 4 DAYS OF SHORT COURSES

High-quality content delivered by subject matter experts with a curriculum focus on essential laboratory skills and emerging industry trends.

→ 3 DAYS OF TECHNICAL PROGRAMMING

Platform for presenting and learning about research, innovations, and advancements in a diverse array of Analytical Chemistry specializations.

→ 3 DAYS OF EXPOSITION

Technologies, products, and services on display from a variety of vendors with time and space to find your next collaboration.

→ NETWORKING OPPORTUNITIES

Relaxed atmosphere for idea exchange. Join us and get inspired by e-Posters, Special Lectures, Mixers, Employment Bureau, and Professional Development Workshops.

CALL FOR PAPERS OPENS
MARCH 1, 2025

eas.org

Hanson Marks 50 Years of Automated Dissolution Testers

Hanson Research designed and built the world's first automated dissolution testing system, the Dissograph, in 1975. Hanson's dissolution tester models cover a multitude of methods. You can trust your results with our robust line of products, precision engineered for the utmost in accuracy, reliability, and ease of use for pharmaceutical development and manufacturing facilities worldwide.

Working closely with the United States Pharmacopeia (USP) and Food and Drug Administration, Hanson has developed innovative firsts for over 50 years. We continue to exceed regulatory specifications and surpass your laboratory's performance needs. Numerous patents for design and technology document our position as leaders in the production of dissolution testing equipment. For example, the original drawings for USP apparatus 1 (basket) and 2 (paddle) in the USP general chapter <711> Dissolution are from Hanson, and Hanson designed and manufactured the world's first six-vessel dissolution tester in 1969.

Take a quick tour of the Dissolution Testing section of our website to see the dissolution tester available options. Consider our Media-Mate Plus dissolution media prep system and our Protocol Manager software, which eliminates connectivity and storage limits by linking our Vision G2 and CD systems to a centralized protocol database.

Discover the perfect dissolution testing solution for your needs by exploring our interactive system designer tool to configure your Hanson system with just a few clicks. You will receive a quick price quote, and there is no obligation to purchase. Your are always welcome to contact our experts for advice and information to help you excel in the realm of dissolution testing. To reach us, just fill out the brief form on this page.

We look forward to assisting you and leading the next 50 years of innovation in dissolution testing.

Be sure to follow Teledyne LABS on social media

Start following us Facebook, X, and LinkedIn. We will be posting daily about upcoming webinars, tradeshows, and more for all the brands now under Teledyne LABS!

Simulations Plus and the University of Connecticut Receive New FDA Grant to Expand Mechanistic Modeling Approaches for Long-Acting Injectables

Funded collaboration will leverage current FDA partnership to include additional LAI technologies

Lancaster, CA - Simulations Plus, Inc. (Nasdaq: SLP) ("Simulations Plus"), a leading provider of biosimulation, simulation-enabled performance and intelligence solutions, and medical communications to the biopharma industry, today announced that it has been awarded a newly funded grant from the U.S. Food and Drug Administration (FDA) to use physiologically based pharmacokinetic (PBPK) approaches in GastroPlus® to build and validate mechanistic in vitro-in vivo correlations (IVIVCs) for long-acting injectable (LAI) technologies through a joint proposal with the University of Connecticut's School of Pharmacy, Department of Pharmaceutical Sciences.

This project aims to use the GastroPlus PBPK platform to investigate the intricate relationship between LAI formulation critical quality attributes (CQAs) and physiological factors at the injection site to accurately predict in vivo drug release and absorption. Dr. Diane Burgess, Board of Trustees Distinguished Professor of Pharmaceutics and Pfizer Distinguished Endowed Chair of Pharmaceutical Technology at the University of Connecticut and her lab will generate in vitro and in vivo data for marketed LAI suspension products using novel discriminatory systems. The scientific team at Simulations Plus will use this data, along with additional inputs from research collaborators, to develop PBPK models and apply them to validate mechanistic IVIVCs. This effort is expected to lay the groundwork for a practical alternative to in vivo studies in establishing bioequivalence (BE) for additional LAI product technologies.

"LAI formulations are becoming increasingly important in pharmaceutical pipelines and product portfolios due to their ability to improve patient compliance and deliver extended drug release," said Dr. Daniela Silva Ryan, Scientist II at Simulations Plus and principal investigator for this grant. "Preclinical and clinical studies to evaluate new formulation designs are lengthy and expensive. With this new grant, we expect our work within GastroPlus to demonstrate how PBPK modeling can reduce development time and costs, while streamlining regulatory processes for both innovator and generic formulations."

FDA scientific and program staff will actively collaborate with the University of Connecticut, Simulations Plus, and select industry partners. Dr. Silva Ryan, with assistance from scientists at Simulations Plus, will coordinate the contract's modeling and simulation activities.

"It is a privilege to continue combining our expertise with Simulations Plus and the FDA to advance the research on LAI formulation performance even further," added Dr. Burgess. "The agency's trust and confidence in this partnership underscores the leadership role both organizations have in our respective spaces. Together, we aim to develop models that bridge the gap between animal and human data and reveal the intricate relationships between formulation properties and injection site physiology, providing insight into virtual BE approaches for this growing drug delivery technology."

Funding for this collaboration is made possible by the FDA through grant award 1U01FD008304-01. Views expressed in this press release do not necessarily reflect the official policies of the Department of Health and Human Services; nor does any mention of trade names, commercial practices, or organizations imply endorsement by the United States Government.

Simulations Plus and Partners Awarded New FDA Grant to Validate In Vitro-In Vivo Extrapolation Methods for Complex Formulations

Collaboration to develop alternative methods to assess clinical performance of product variants under different conditions

Lancaster, CA - Simulations Plus, Inc. (Nasdaq: SLP) ("Simulations Plus"), a leading provider of biosimulation, simulation-enabled performance and intelligence solutions, and medical communications to the biopharma industry, today announced a newly funded grant from the U.S. Food and Drug Administration (FDA), secured in partnership with the University of Strathclyde and InnoGI Technologies. The project is expected to improve the understanding of amorphous solid dispersion (ASD) formulations in different conditions and predict the impact of food and pH-dependent drug-drug interactions (DDIs) through the combination of novel in vitro testing and mechanistic modeling and simulation.

For this award, Professor Hannah Batchelor, through her lab at the University of Strathclyde, will analyze ASD drug products and their respective formulation variants. InnoGI Technologies will then test the different ASD formulations under fasted, fed, and higher gastric pH conditions utilizing the tiny-TIMsg, part of the SurroGUT™ Platform, in vitro system. Next, physiologically based pharmacokinetic (PBPK) models will be developed in the GastroPlus® platform to link in vitro dissolution with in vivo pharmacokinetic data and develop in vitro-in vivo extrapolations (IVIVEs). Finally, virtual bioequivalence (VBE) trial simulations will be conducted in GastroPlus to assess the clinical performance of ASD formulation variants to validate the approaches. The resulting outcomes are anticipated to help speed up formulation adjustments, reduce costs, and accelerate time-to-market for both innovator and generic ASD products.

"We are delighted to be at the forefront of this important research, which has the potential to significantly advance PBPK science and revolutionize how we predict drug product performance," said Dr. Maxime Le Merdy, Director of PBPK Collaborations at Simulations Plus and principal investigator for this grant. "Developing a novel IVIVE methodology for ASD drug products will play a crucial role in optimizing formulation development, fine-tuning process parameters, and supporting bioequivalence assessments by offering key insights into the factors that impact in vivo performance."

FDA scientific and program staff will actively collaborate with the University of Strathclyde, InnoGI Technologies, and Simulations Plus. Dr. Le Merdy, with assistance from scientists at Simulations Plus, will coordinate the modeling and simulation activities of the contract.

"By leveraging the power of this industry-academia-regulatory collaboration, we will push the boundaries of innovation and accelerate the development of safer, more effective therapies," said Prof. Batchelor. "This unique partnership allows us to combine InnoGI's cutting-edge in vitro technologies, GastroPlus's mechanistic modeling, and real-world clinical insights, driving greater efficiency and confidence in drug development decisions."

"As oral formulation development grows increasingly complex, evaluating drug product performance while studying luminal events in real time demands the integration of advanced technologies to bridge in vitro and in vivo testing gaps, thus reducing development risks for more efficient drug development," said Susann Bellmann, CTO of InnoGI Technologies.

Introducing the Variprobe Adjustable Pathlength Dip Probe for Enhanced In-Situ Dissolution Analysis

North Brunswick, NJ - Distek, Inc., a leading manufacturer of pharmaceutical laboratory instruments, proudly announces the launch of the Variprobe Adjustable Pathlength Dip Probe, patent pending. This new technology offers multiple reproducibly selectable pathlengths—2, 5, 10, and 20 mm—in a single probe, eliminating the need for multiple probes or interchangeable tips to accommodate different concentrations. The Variprobe Dip Probe, along with the Variprobe Probe Tip and Variprobe Probe Tip Spacers, are serialized for easy tracking and quality assurance, ensuring consistent performance and streamlined management of laboratory assets.

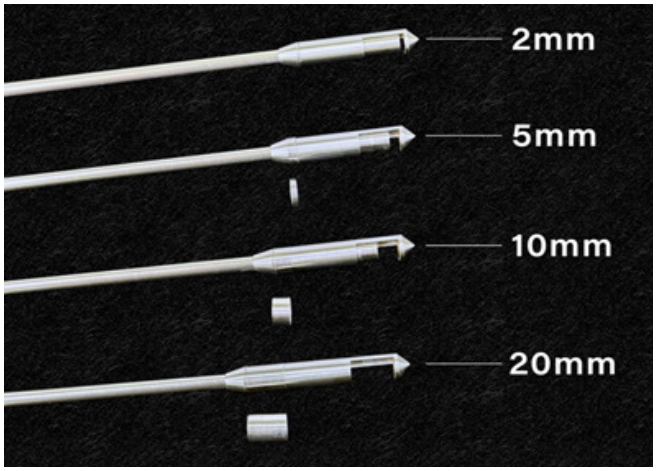

The Variprobe is designed specifically for use with Distek's Opt-Diss 410 as well as the Opt-Diss 405 In-Situ Fiber Optic UV System, enhancing in-situ dissolution testing by always allowing access to the optimum pathlength. This innovation not only improves flexibility in testing but also reduces the cost of implementing the Fiber Optic UV System for conducting varied dissolution studies.

For more information on the Variprobe Adjustable Pathlength Dip Probe and the Opt-Diss In-Situ Fiber Optic UV System, please contact Distek, Inc. at (732) 422-7585 or email sales@distekinc.com.

ABOUT DISTEK, INC.

Distek engineers innovative, user-friendly instruments with advanced features, supporting a broad range of pharmaceutical and bioprocessing applications. Our product line includes water bath and bathless dissolution systems, dissolution media preparation, in-situ fiber optic UV, bathless tablet disintegration, and dissolution autosampling. Our bioprocessing solutions include the BIOne single-use bioreactor and fermentor, as well as the BIOne 250 and 1250 bioprocess controllers for mammalian and microbial models.

Distek's core market spans brand name, generic, and biosimilar drug manufacturers, Contract Research and Manufacturing Organizations, and a variety of other industries. We work closely with producers of cultured foods, nutraceuticals, food and flavors, as well as agricultural businesses, beverage companies, government agencies, and universities. With extensive experience, Distek provides tailored support and advanced technology to meet the specific needs of each sector effectively.

CIPHER SOFTWARE

Dissolution Control for 21 CFR Part 11 Compliance

- Complete 21 CFR Part 11 and Data Integrity compliance for Distek dissolution instruments.
- Method Wizards simplify method creation.
- Remotely configure and monitor Distek instruments in real-time from your PC.
- Enable automatic export of record files for seamless integration with a LIMS package.

DISSOLUTION

FIBER OPTIC

MEDIA PREP

AUTOSAMPLER

Schedule your Free Cipher Demonstration!

Helping Science Improve Lives

DISTEK

distekinc.com • info@distekinc.com

Agilent

Trusted Answers

Elevating the Dissolution Environment

The Agilent 280-DS Mechanical Qualification System (MQS) enables the physical qualification of USP dissolution Apparatus 1 (Rotating Basket) and 2 (Rotating Paddles) using Enhanced Mechanical Qualification (EMQ) guidelines. The system's sensing technology allows hands-free measurements to be performed in seconds, while recording critical physical parameters.

A proactive approach. Easily shorten your qualification interval for more frequent insight into instrument performance, reducing the chance of failures.

Save time. Instant feedback helps the user investigate aberrant results or abnormalities at an early stage and reduce errors.

For more information about the Agilent 280-DS, visit:
www.agilent.com/chem/280-DS

DE32237991

© Agilent Technologies, Inc. 2022